A machine component monitoring system using audio acoustic signals.

NOR, Mohd Jailani Mohd.

A MACHINE COMPONENT MONITORING SYSTEM USING AUDIO ACOUSTIC SIGNALS

by:
Mohd Jailani Mohd Nor
(BSc, MSc, Oklahoma State Univ., USA)

**A thesis submitted to Sheffield Hallam University
for the degree of Doctor of Philosophy
in the School of Engineering**

December 1996

Collaborating Organisation: Universiti Kebangsaan Malaysia, Malaysia

PREFACE

This thesis is submitted in partial fulfilment of the requirements of Sheffield Hallam University for the degree of Doctor of Philosophy. It contains an account of research carried out between January 1993 and December 1996 in the School of Engineering, Sheffield Hallam University, under the supervision of Dr. R. B. W. Heng and Dr. D. Gillibrand. Except where acknowledge and reference is appropriately made, this work is to the best of my knowledge, original and has been carried out independently. No part of this thesis has been, or currently being submitted for any degree or diploma at this, or any other university.

Mohd Jailani Mohd Nor

December 1996

ACKNOWLEDGEMENTS

I would like to express my sincere gratitude to my Director of Studies Dr. R. B. W. Heng for his guidance, encouragement and support during the course of this research. I would also like to thank my second supervisor Dr. D. Gillibrand for his encouragement and invaluable advice.

I must also thank Dr. R. Saatchi for the helpful discussions and interest he has shown in this work. I am indebted to all the staff at the Caparo Merchant Bar Company, at Scunthorpe, for allowing me to carry out an industrial case study in their manufacturing plant.

My appreciation is also extended to all staff in the School of Engineering, especially to Mr. R. Wilkinson, Mr. R. Sidebottom, Mr. R. Gunson, and all technical staff in the workshop.

Many thanks to all my friends in room 4L12 for their support and encouragement especially to Mr. C. Brashaw, Mr. C. Ackroyd, Mr. S. H. Chong, Mr. F. Alhamdani, Mr. I. Elbakbakh, Mr. S. Fazel-Jahromy and Mr. Z. J. Zhao.

I am indebted to Universiti Kebangsaan Malaysia for providing the grant without which this study will not be possible.

Finally, a very sincere thanks goes to my wife, Fauziah Ishak, for her understanding and patience during the whole course of this research.

A MACHINE COMPONENT MONITORING SYSTEM USING AUDIO ACOUSTIC SIGNALS

Abstract

The main objective of this study is to develop a new type of machine-component monitoring system which is non-intrusive and non-contact in nature. Moreover, the design of the system to be developed must be robust enough for it to be implemented in an industrial environment. Therefore, this study was initiated to overcome some of the problems that were encountered using the well-established vibration method. For instance, vibration measurement of a machine component is dependent on the quality of contact between an accelerometer with a vibrating surface. Vibration measurement of a machine component is also affected by the vibration of other machine components near the vicinity, in addition to the presence of power-supply-line frequency and its harmonics. On the other hand, the application of a desirable non-intrusive and a non-contact nature of sound pressure measurement method is difficult to carry out if the background sound level is high. This is because sound pressure measurement is dependent on the characteristics of a sound field where a measurement is carried out. For these reasons, air-particle acceleration signals were utilised in the study. Air-particle acceleration is a vector quantity and measurement of vector property can improve the signal-to-noise ratio of the measured signal, even in a noisy environment.

A dedicated test rig was constructed to carry out the experiments and to test the hypothesis. Rolling element bearings were used for the experiment because of the many different types of defect that can develop in them, such as inner race, rolling element and outer race defects. Moreover, the dynamic behaviour of bearings are well understood and can be compared with experimental results obtained from the study. Several different methods of analysis were used in the study including statistical, spectral, cepstral and wavelet transform methods. The results from using air-particle acceleration signals were compared with results obtained from utilising sound pressure and vibration signals. These results showed that the performance from using air-particle acceleration signals were superior to the performance from using sound pressure signals. Results from the analysis of air-particle acceleration signals can clearly indicate the presence of a defective component in the test-bearing. This is so even when the overall background noise was 14dB higher than the overall noise level emitted by the test-bearing. Moreover, the sensitivity of the measurement of air-particle acceleration signal to indicate the presence of a defective bearing was similar to the sensitivity when using conventional vibration equipment.

Applications of artificial neural networks were also included for automatic identification of defect signals. The multilayer perceptron network was chosen and tested to classify the bearing signals because of the suitability of this type of network to be used for pattern recognition. Finally, a new type of machine-component monitoring system using air-particle acceleration signal was successfully developed and tested in industry.

TABLE OF CONTENTS

Page

List of Publications

1. R B W Heng and M. J. Mohd Nor, "Condition Monitoring of Machines Using Acoustic Signals," Proceedings of the 1996 International Congress on Noise Control Engineering (Inter-Noise '96), Liverpool, pp. 163 - 166, ISBN 1-873082-85-1.

2. R B W Heng and Mohd Jailani Mohd Nor, "Machine Health Monitoring Using Audible Acoustic Signals," Proceedings of the International Conference on Advances in Strategic Technologies: Advanced Manufacturing and Processing, Universiti Kebangsaan Malaysia, 12 - 15 June 1995, pp. 240 - 250.

3. R B W Heng and M. J. Mohd Nor, "Utilisation of Audio-Acoustic Signals for Monitoring Rolling Element Bearing Using Spectrum and Cepstrum Analysis", Proceedings of the Institute of Acoustics, Liverpool, Vol. 17, Part 4, 1995, pp. 285 - 304.

Short Course and Seminar Attended

1. Short Course "SKF Training in Condition Monitoring", 2nd - 7th. May 1993, San Diego, California, USA.

2. The UK's Exhibition and Conference for Sensors and Measurement Technology, National Exhibition Centre, Birmingham, England, 24th and 25th January, 1996.

NOMENCLATURE AND ABBREVIATIONS

ρ_o	Standard atmospheric air density (1.225 kg/m^3)
Δr	Distance between two pressure microphones
φ	Phase angle
σ	Standard deviation
$\Gamma(x)$	Gamma function
$\phi\ (x)$	Scaling function
$\psi\ (x)$	Mother wavelet
ΔF	Uncertainty in frequency calculation
Δt	Uncertainty in time-position calculation
$\beta\ (a,b)$	Beta function with variables a and b
τ	Time delay
η	Learning rate
α	Momentum coefficient
a	Beta distribution function parameter for statistical analysis, or dilation factor for wavelet analysis
$AP(f)$	Fourier transform of air-particle acceleration signal
$ap(t)$	Time variations of air-particle acceleration due to sound wave disturbance
ap_{ref}	Reference value for air-particle acceleration signals (1 x 10^{-6} g)
b	Beta distribution function parameter for statistical analysis, or shift factor for wavelet analysis
Best basis	The most efficient way of representing a signal with few large coefficients from combinations of all levels in a wavelet packet transform
Best level	The most efficient way of representing a signal with few large coefficients from a single level in a wavelet packet transform
c_n	Wavelet coefficient
$coh(n)$	Coherent component of a signal
Crest factor	Ratio of maximum peak, and rms value of a signal
d_i	Inner race diameter of a rolling element bearing

d_o	Outer race diameter of a rolling element bearing
d_p	Pitch diameter of a rolling element bearing
d_{re}	Rolling element diameter of a bearing
$E(x)$, $\bar{x}$	Statistical mean of a signal
EDM	Electro discharge machine
F_i	"Feature" which is the name of a variable used for artificial neural network input
FIR	Impulse response filter
f_{ir}	Inner race defect frequency
F_{max}	Maximum frequency
f_{or}	Outer race defect frequency
F_p	Fourier transform of sound pressure signals
f_{pm}	Pulse rate due to motor-sprocket tooth passing frequency
f_{ps}	Pulse rate due to shaft-sprocket tooth passing frequency
F_{va}	Fourier transform of air-particle velocity signals
g	Acceleration due to gravity (9.81 m/s^2)
g_n	Differencing filters
$H[x(t)]$	Hilbert transform of a function $x(t)$
$H(\omega)$	Fourier transform of the impulse response function
$h(t)$	Impulse response of a system
h_n	Summing filters
$\boldsymbol{I_a}$	Active sound intensity vector in a specified direction
I_{ref}	Reference value for sound intensity signals (10^{-12} watts/m^2)
$\boldsymbol{J_a}$	Reactive sound intensity vector
Kurtosis	Normalised fourth-order central moment of a statistical distribution
L_{ap}	Overall air-particle acceleration level
LCT	Local cosine transform
L_I	Overall sound intensity level
L_p	Overall sound pressure level
L_{vb}	Overall vibration level
L_W	Overall sound power level
M	Total number of samples in a signal

m	Wavelet level or dilation factor
MW	Magnitude of wavelet transform coefficients
n	Wavelet node number or shift factors
oh_j	Output activation function of a hidden neuron
oo_k	Output activation function of an output neuron
p	Wavelet position number
PI	Pressure-intensity index
$\tilde{p}$	Complex amplitude of sound pressure signal
$p(t)$	Variation of atmospheric pressure due to sound wave disturbance
p_o	Standard atmospheric pressure (1.013×10^5 N/m^2)
p_{ref}	Reference value for sound pressure signals (2×10^{-5} N/m^2)
QMF	Quadrature mirror filter
R	Sampling frequency
$res(n)$	Residual component of a signal
rms	Root-mean-square
$R_{xx}(\tau)$	Autocorrelation function
SI	Sound intensity
$Skew$	The ratio between the third-order central moment of a statistical distribution and the standard deviation to the power of three
STFT	Short time Fourier transform
$S_X(\omega)$, PSD	Power spectral density
v, V	Volts
$\tilde{v}$	Complex amplitude of air-particle velocity signal
v_a	Air-particle velocity vector in a specified direction
vb_{ref}	Reference value for vibration signal (0.01 g)
W_{jk}	Weight of a connection between jth and kth neurons
WPLW$^{(TM)}$	Wavelet Packet Laboratory for Windows$^{(TM)}$
$X(\omega)$	Fourier transform of a sample of signal $x(t)$

LIST OF FIGURES

LIST OF TABLES

LIST OF PLATES

CHAPTER 1
INTRODUCTION

1.1 An Overview

Maintenance of machinery in industry is carried out in several ways, namely, breakdown maintenance, preventive maintenance and predictive maintenance. In the first strategy the machine in operation will not be repaired until it fails. In the second approach a machine is scheduled for servicing at a specified time or interval of operation regardless whether the need is there or not. Because of economic reasons the third approach is becoming more popular nowadays whereby the health of a machine is continuously monitored to identify early warning of an incipient failure and appropriate maintenance action can be planned and carried out to minimise cost. This approach can also avoid catastrophic failure from occurring by scheduling remedial action at an appropriate time based on indications from the measured variables.

The need to monitor the health of machine components without degrading the performance of the machine being monitored has been established since late 1960's. In the early years, vibration signals were recorded and used to monitor the condition of machine components (Chapman 1967, Hanna 1974). The advantages of using non-contact and non-intrusive technique has encouraged the use of other types of signals for monitoring machine condition such as acoustic emission, sound pressure, temperature, eddy current, oil debris, etc.

With the development of sound intensity measurement technique sound intensity and acceleration noise signals can be used to monitor machine health. In addition to the non-contact and non-intrusive nature of the transducers, the signals measured using this technique are vector quantities which are necessary in order to achieve a high signal-to-noise ratio from the measurement. This method can be used as an alternative when and where the currently available methods fail to give good and economical solutions for monitoring machine conditions.

1.2 Research Applicability

Recent studies have shown that sound signals can be used to detect incipient damage in machine components such as motors, pumps, gears, and bearings (Igarashi and Yabe 1983, Sun et al 1991, Gargano and Bartolini 1991, Craggs 1991). In comparison sound signals are relatively easier to measure than vibration signals. Measurement of sound signals are not affected by the ground loop from the power line. In addition, the vibration measurements are also affected by the way the transducer is fixed to the measuring surface.

The variation of sound signals emitted by a machine can be detected by a person who always works with that machine. He knows if something is wrong with that machine just by listening to the sound emitted. For a more scientific approach, electronic instruments coupled with advance signal analysis methods must be used. The procedure may be a simple one such as the measurement of the overall dB level, it may also be a complex analysis such as the utilisation of simultaneous time-frequency domain analysis method. This will obviously depend on the characteristics of the sound signals to be measured.

It is only recently that the advancement in technology has made it possible to measure sound signal parameters such as sound intensity and air-particle acceleration. The advancement in computer processing power has also made it possible to analyse the signals using a more complex analysis method such as Fourier transform and wavelet transform. The advancement in computer hardware and software have also made it possible to include artificial intelligence namely, artificial neural networks in this study. This research will incorporate all these technologies to produce a robust and reliable method for detecting incipient damage in a machine component based on the measurement of audible acoustic signals.

1.3 Machine Condition Monitoring in General

Vibration signals are already used extensively in machine condition monitoring field. In the initial stage a vibration analyser and graphic recorder were used to monitor the vibration of machines and if it is above the acceptance level remedial action was scheduled prior to catastrophic failure. The signature analysis is also used to identify different types of abnormalities such as imbalance, bent shaft, defective bearings, worn gears, mechanical looseness and eccentric journals (Chapman 1967, Hanna 1974, Bannister 1985).

Other methods used in machine condition monitoring include temperature monitoring, eddy current measurement, lubricant monitoring, wear particle analysis, visual data analysis (imaging), noise monitoring, pressure monitoring, moisture or dew point monitoring, acoustic emission measurement, and ultrasonic signal monitoring. Several analysis method are also available and utilised which include spectral analysis, statistical analysis, trend or regression analysis, relative comparison, test against limits or ranges, selective frequency band analysis, and high frequency resonance technique (Bannister 1985, Kim 1984, Cory 1991). The art of condition monitoring has been described as knowing what to look for, to measure it, and to correlate the results with known a failure mechanism. Failures in machine components may start to occur during manufacturing process, during delivery, during installation, and finally during the operation. Most papers discuss the virtues of condition monitoring and trending, and very few papers discuss accurate diagnosis of machinery problems (Taylor 1992, Fuchs et al 1991, Milne and Aylett 1991).

1.3.1 Types of Signal Used For Machine Condition Monitoring

The most widely used signals in machine condition monitoring is vibration, which is usually the first by-product of a defective machine component. A machine usually starts to operate with minimal vibration level and as wear or defect starts to occur the vibration level generally increases. This makes it possible to detect incipient damage in machine components by monitoring and trending the vibration levels.

Noise signals have also been used for monitoring and diagnosing machine components mainly gearboxes and bearings. It has been shown that sound pressure signals can provide useful information with regard to the condition of the machine components (Sun et al 1991, Professional Engineer 1994, Taylor 1992, Badi et al 1990, Wilhelm and Spessert 1992). However, in case of the bearing components the sound pressure signals resulting from a defect are not measurable below a specified minimum speed. This is a result of the physics which implies that a minimum oscillatory amplitude must first be reached before a vibrating mechanical object can emit audible sound (Smith 1992). However the sound pressure signal analysis method is non-intrusive and non-contact in nature which are highly desirable features in machine condition monitoring application.

Lubricant analysis is one of the methods widely used in power generating plant. The analysis work is usually done to check that lubricants possess the proper specifications for viscosity, acid/base number, water content, and level of solid precipitates largely to prevent corrosion and abnormal wear (Nicholas 1991). Wear particle analysis involves the measurement of ferrous particles in lubricant. The relative comparison method is usually utilised to perform predictive maintenance tasks. Another method known as debris analysis provides important information about a system's internal condition. Filters or full flow strainers are placed at a strategic position to collect and monitor abnormal debris in a plant (Smith 1992). Similar to sound analysis, visual data or the visual imaging method is non-intrusive and non-contact in nature. These data are also easily interpretable by personnel with very little training in the technology. Moisture or dew point monitoring method can be used to monitor changes in moisture level which might be an indicative of an abnormal operating condition. New types of pressure and temperature monitoring systems which use fibre optics are currently being developed which is capable of indicating pressure and temperature variations in a plant at a very high resolution.

Acoustic emission monitoring is usually employed to detect metal fatigue, it detects the breakage of a metal crystalline bond which is in 100KHz to 500KHz frequency range. By trending the number of events per unit time, the indication of progressive

deterioration in metal structure can be detected (Kannatay-Asibu 1982, Diniz et al 1992, Trujillo et al 1994). The ultrasonic detection method utilises very high frequency acoustic signals usually in between 500KHz up to 5MHz. It can be used to detect crack and internal abnormalities in metals and in welded joints. Defects in the inner pipe walls due to erosion and corrosion can also be detected using this method.

1.3.2 Types of Analysis Method Used in Machine Condition Monitoring

Several analysis methods have been developed and applied to machine condition monitoring. Some of the analysis methods that are commonly encountered include monitoring of kurtosis and crest factor values, spectral analysis, cepstrum analysis, selective frequency band analysis, envelope analysis, correlation analysis, high frequency resonance technique, and wavelet transform analysis (Bannister 1985, Cory 1991, Nicholas 1991, Konig et al 1992, Geng and Qu 1994, Li and Ma 1992, Deckert at al 1992).

Statistical analysis methods used on time domain signals are capable of indicating changes in the characteristics of the signals from variations of the probability density functions. The variables used in this method are Kurtosis and Crest Factor. Kurtosis is defined as the ratio of the fourth central moment of the amplitude distribution to the second power of the second central moment (Scheithe 1992) and for a zero-mean signal the second central moment is identical to the root-mean-square (rms) variable. The Crest Factor is obtained from the ratio of the maximum peak to the rms value of the measured signals.

Time history of sound and vibration signals can be transformed and manipulated in the frequency domain with the development of Fourier transform method. Fast Fourier transform (FFT) algorithm which has been discussed in detailed by Cooley et al (1969), is currently the standard method used to perform spectral analysis for digital acoustic and vibration data. The spectral analysis method is commonly used if the impact rates

from the defect are predictable. These values can be calculated if all the required physical dimensions of the machine component are known. However, the frequency spectra obtained are dependent on the transfer function of the physical system. Direct comparison between the frequency spectrum coming from a defective component and the frequency spectrum from a normal component can indicate the presence of a defect in the machine component. If the signals are clear the impact rates are indicated from side-band and harmonic analysis of frequency peaks in the spectrum.

Cepstrum analysis is good at separating the excitation spectrum from the transfer function component. Cepstrum can also be considered as a spectrum of a logarithmic amplitude spectrum (Haddad and Parsons 1991). Therefore, it can detect any periodic component in a spectrum, such as the repetitive impact signals that have been recorded without the need to know the transfer function of the physical system.

The frequency enveloping technique exploits the ability of high frequency resonance signals from a transducer to act as an amplifier and a carrier for the low frequency defect signals. The product of this technique is a frequency spectrum of the defect signals with better signal-to-noise ratio.

In recent years, the wavelet transforms have been applied to various applications including speech, signal and image processing (Kadambe 1991, Grossman 1988, Mallat and Zhong 1989, Tuteur 1988). A wavelet transform projects a 1-D signal onto a 2-D time-scale representation which is useful for pattern identification and classification analysis (Kronland-Martinet et al 1987). Effectively, there are two variables that are used to represent the output from wavelet transform analysis namely: scale (or frequency) and position (or time). The results from wavelet transform of sound or vibration signals can be interpreted as a signature of the signals (Kronland-Martinet and Grossmann 1991) because it contains all the information carried by the signals. A more elaborate discussion on the application of wavelet transform in machine condition monitoring is presented in the next section.

1.4 The Emanation of Simultaneous Time-Frequency Domain Analysis Method

The search for an analysis method that can capture the time-frequency characteristics of signals especially ones that contain non-stationary or transient components has resulted in the emergence of new field of study known as the time-frequency distributions. The basic idea of this method is to devise a time-frequency distribution that will describe the energy density of signal simultaneously in both time and frequency domains. The initial works of Wigner (1932) and Page (1952) have encouraged other researchers to develop the time-frequency distributions field even further. A comprehensive review on this topic has been given by Cohen (1989). Boashash (1991) reviewed the developments and applications of this method in recent years.

Two of the well known distributions that have been developed are the Wigner-Ville and the Choi-Williams distributions. But because of the cross-terms effects, together with some other theoretical difficulties, these time-frequency distributions have very limited applications (Dai et al 1994).

To overcome the above problems a new method called the Short-time Fourier transform (STFT) has evolved. It started with the work done by Gabor (1946) who used a window function and sliding it over the signal in time, and then computing the Fourier transform of every portion within each window. However, the performance of the STFT method is dependent on the size of the window function. It is difficult to find a constant size window function that can be applied to signals that contain short term as well as long term variations.

The next step in the development of time-frequency distribution is the introduction of the wavelet transform method in numerous fields of science and technology. The practical application of wavelet transform started to emerge in the early 1980's when a French geophysicist, Jean Morlet (1982) applied the wavelet transform method for modelling and processing sound waves travelling through the earth's crust. The Wavelet transform has been shown to be as powerful and versatile as the Fourier transform, yet without some of its limitations (Cody 1992). For analogy, the well known oscilloscope is used to display signal as a function of voltage versus time, then with the development

of spectrum analyser the signal can be displayed as a function of voltage versus frequency and now using wavelet analyser it is capable of doing simultaneous analysis of both time and frequency of a signal (Cody 1993). Some of the properties of the wavelet analysis which makes it very promising are:

(i) linearity,

(ii) conservation of energy, and

(iii) locality.

In contrast to the Fourier transform, the wavelet transform is very efficient in identifying and representing the presence of short duration transient components in signals. However, in wavelet transform analysis, a high frequency resolution is achieved at the expense of poor time resolution and vice-versa. Thus, simultaneous high resolution in frequency and time domain is not possible in the wavelet transform analysis method (Newland 1994a). However, the significant advantage of using the wavelet transform is that it is capable of representing the temporal aspect of signals at small scales and the frequency aspect at large scales. Basically, the wavelet transform is a linear transformation that can be used to decompose an arbitrary signal into elementary contributions called wavelets which are generated from dilation and translation of a mother function called the analysing wavelet (Kronland-Martinet and Grossmann 1991). Ultimately, the wavelet transform analysis method is capable of representing the local phenomena in a signal that map a time-domain function onto a representation that is localised in both time and frequency domain. This makes the wavelet transform method to be one of the most suitable methods that can be used to analyse signals with transient components. Furthermore, the computational operations in implementing wavelet transform analysis are in general smaller than Fast Fourier Transform (FFT).

1.4.1 Applications of Wavelet Transform

In machine condition monitoring, the transient (time-varying) signals are indications of the presence of faults, such as cracks in a structure, flakes in the bearing components or broken teeth of gears (Geng and Qu 1994). The wavelet transform method can be used

to analyse the presence of transient impulsive components in sound and vibration signals and to relate such signals with the condition of the physical system that causes it.

Lopez et al (1994) applied continuous wavelet transform coupled with neural networks to real-time fault detection and classification for helicopter gear-box and Navy shipboard pumps. Newland (1994b) discussed the concept of the dilation wavelets and harmonic wavelets for analysing vibration signals in a building. The wavelet transform method has also been applied to detect fault in spur gears, in roller bearings and in gear-boxes using vibration signals (Staszewski and Tomlinson 1994). In addition, the detection of tool failure in end milling with wavelet transform and neural networks were carried out by Ibrahim Nur Tansel et al (1993) using the cutting force or torque signals created in the process.

1.5 The Role of Artificial Intelligence in Machine Condition Monitoring

Artificial intelligence encompasses many different fields such as expert systems, artificial neural networks, and pattern recognition. Artificial intelligence provides powerful techniques to manipulate a large amount of information about a particular domain as well as the expert information (Milne 1988). In recent years, artificial neural networks have started to be applied in machine condition monitoring using vibration signals (James et al 1991, Liu and Mengel 1991, O'Brien et al 1992).

1.5.1 Artificial Neural Networks

The application of artificial neural networks in machine condition monitoring is concerned with monitoring a process or operation either continuously or at intervals by appropriate sensors. Processed data are used as input to a trained networks (Steele et al 1992). The most popular neural network is the multi-layered perceptron, and the most popular algorithm to train a network is the back-propagation algorithm.

Neural networks are ideal for complex pattern recognition problems whose solution requires knowledge which is difficult to specify but which is available in the form of examples. In a limited way, neural networks operate similar to the human brain, in which they learn from experience, they generalise from examples and extract important features from noisy data. Previous studies indicate that neural networks can be used successfully in machine condition monitoring using vibration signals (O'Brien et al 1992, Harris 1993).

Another type of neural networks which has gained a lot of attention in recent years is the Kohonen Networks also known as the Kohonen Self-Organising Feature Maps (Lippman 1987). This algorithm was developed by Kohonen (1982) as a tool to transform a signal pattern of arbitrary dimension into a one- or two-dimensional discrete map, and to perform this transformation adaptively in a topological ordered fashion (Haykin 1994, Kohonen 1990). This is a very powerful algorithm that can be used to identify and to classify signal patterns from machinery noise and vibration, if no previous information is available.

1.6 Summary From Literature Review

From the literature review that has been done, a proposal for a new research study on the application of audible acoustic signals in machine condition monitoring is presented. This study is needed in order to capitalise on the strength of sound measurement for machine condition monitoring as mentioned in the previous sections. A detailed programme of study to explore the advantages and limitations of utilising audible acoustic signals would contribute towards the advancement of knowledge in this growing field.

The incorporation of other newly emerging fields such as the wavelet transform method and artificial neural networks is vital to enhance the diagnostic capability of the technique to be developed. The strength of this research is the combination of new technologies working together to produce practical and cost-effective solutions to real life problems.

1.6.1 Utilisation of Audible Acoustic Signals in Condition Monitoring

Traditionally, noise measurements are carried out in industry to identify noisy equipment in order to provide safe acoustical environment for employees and for the nearby residents (Mohd Nor 1991, and 1992). Along with a hearing conservation programme, every company can implement comprehensive acoustic monitoring of machines which is a part of predictive maintenance programme (Pelton 1993).

This research study utilised all the available parameters that can be measured from the audible acoustical signals of machine components including; sound pressure, sound intensity, and air-particle acceleration. This is a new approach in this field whereby the unwanted noise from a machine is now useful for diagnosing the condition of the machine. The research activities start with the simple measurement of the overall noise level emitted by machines followed by more complex signal processing analysis methods including statistical analysis, spectral analysis, cepstrum analysis, wavelet analysis and the incorporation of artificial neural networks.

1.7 The Research and Thesis

Recent studies have shown that sound signals can provide numerous information that can be used to find out the condition of machine components (Kim 1984, Trmal and Johnson 1993). Little work has been recorded concerning the application of sound intensity measurement technique for machine condition monitoring and diagnostic purposes. Moreover, these studies utilised straight forward application of the well established spectral analysis method without exploring the usage of other newly developed methods that are available (Tandon and Nakra 1990). So far, no work has been found regarding the application of air-particle acceleration signals in machine condition monitoring field. Therefore, a research study is proposed to capitalise on the application of sound pressure, sound intensity, and air-particle acceleration signals in machine condition monitoring incorporating newly developed technologies such as the wavelet transform and artificial neural networks.

1.7.1 Research Outline

In this study, the utilisation of air-particle acceleration signal in machine condition monitoring is implemented for the first time. The full potential and limitations of utilising this signal will be explored in detail. A comparitive study with the results obtained using vibration and sound pressure signals was also performed. On the signal processing aspect statistical, spectral, ceptral and wavelet transform methods were used to analyse the signals measured from experiments. Next, the application of artificial neural networks was included and the type of defect present in a bearing component was identified by the network. The overall scope of study is better illustrated by a schematic diagram as shown in Figure 1.1.

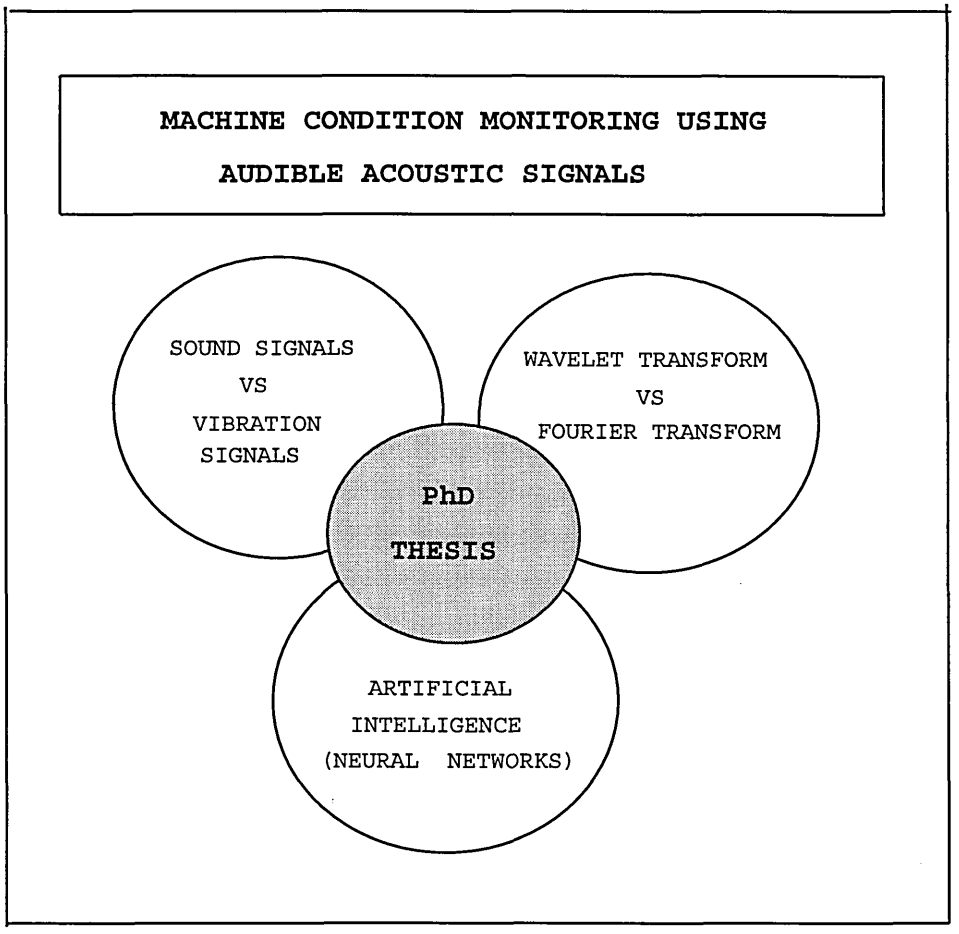

Figure 1.1 Schematic diagram indicating the scope of study.

1.7.2 Research Strategies

A test-rig was constructed to test the hypothesis that has been set. The test-rig was capable of simulating the different types of defect encountered in rolling element bearing. A compartive study utilising sound, air-particle acceleration and vibration signals was carried out. In addition, comparison studies on the performance by statistical analysis, spectral analysis, and wavelet transform analysis methods were also performed.

A feature selection algorithm was developed to process the measured signals and was fed into the artificial neural networks for pattern recognition and diagnostic purposes. Finally, a robust and efficient machine condition monitoring method utilising air-particle acceleration signals was developed and tested in an industrial case study. The overview of the research programme is shown in Figure 1.2.

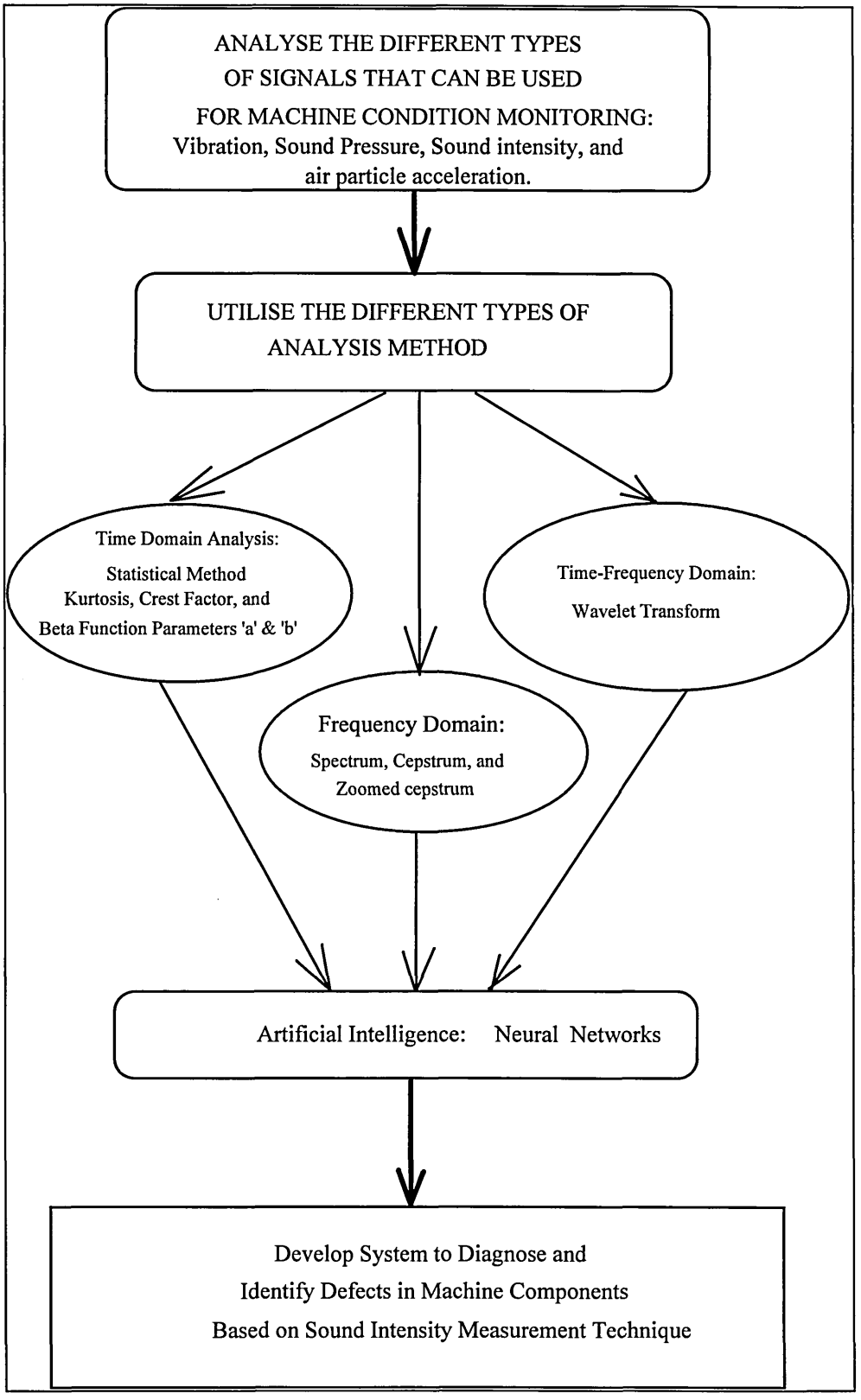

Figure 1.2 Overview of the research programme.

1.7.3 Thesis Structure

Chapter 2 presents theoretical discussion on the fundamentals of sound pressure, sound intensity, and air-particle acceleration signals. The theoretical development of sound intensity measurement technique is presented because the scope of this thesis will capitalise on the advantages that can be derived from this technique. In addition, mathematical derivations on signal processing methods that were used in this study such as statistical analysis, spectral analysis, and wavelet transform analysis are also included. A basic foundation on artificial neural networks is described at the end of the chapter.

Chapter 3 describes the initial work that was carried out including the design, fabrication, and calibration of the test-rig and the associated instrument. A summary of the procedure for selecting rolling element bearings and their dynamic characteristics are also presented in this chapter.

Chapter 4 discusses the analysis of experimental data obtained from the test-rig. A comparative study using time-domain analysis is carried in this chapter. Analysis of results obtained from using air-particle acceleration, sound pressure and vibration signals are carried out at this stage. In addition, the results of a comparison study on the performance of Kurtosis and Crest Factor with beta function parameters a and b are also presented.

Chapter 5 compares the performance of using frequency domain and simultaneous time frequency domain analysis methods in analysing bearing signals. Spectral and cepstral analysis methods were used to diagnose the condition of a test-bearing. In addition, wavelet transform and wavelet packet transform methods used for simultaneous time-frequency analysis study are presented in this chapter.

Chapter 6 presents the advantages of using air-particle acceleration signals compared to using sound pressure and vibration signals. The effect of external background noise is investigated in this chapter. The subject of defect detectability is also discussed. This chapter also presents results from an industrial case study.

Chapter 7 develops feature selection algorithms that can be used to process the measured signals and use them as input to the artificial neural networks software. Coefficients from wavelet transform analysis method are used to calculate these features to be used for artificial neural networks applications.

Chapter 8 derives the conclusion from this research study and discusses of the achievements of the research works. A summary of the findings and contribution to knowledge from the work done are presented in this chapter. Finally, this chapter presents several recommendations that can be pursued in the future.

CHAPTER 2
THEORETICAL ANALYSIS

2.1 Introduction

Sound waves can travel through any elastic medium such as gas, liquid and solid. It is a transfer of kinetic energy between molecules in the medium. In gases, only compression waves can occur due to their low viscosity, and this is the basic mechanism that transport sound signals in this medium. The oscillation of particles about their mean position in gas such as in air, caused by a disturbance will create a pressure difference at that position which can be associated to the sound waves due to the disturbance. The amplitude of most sound waves are small and it can be described using linear propagation method. In this case, the speed of the sound waves is a constant value depending on the physical properties of the medium. In air the speed of sound is about 340 m/sec and in water it is about 1500 m/sec. Audible acoustic signals are sound signals with frequencies ranging from 20Hz to 20KHz.

2.2 Fundamental of Sound Measurements

The most important parameter in sound waves is the sound pressure also known as the acoustic pressure. The sound pressure at a position in an acoustic field is the difference between the instantaneous pressure and the equilibrium pressure at that position. The variation in sound pressure can be measured using a transducer (microphone), and the parameter derived from this is called the sound pressure level (*Lp*). The other parameter used for measuring the strength of a sound wave is sound intensity level. In 1936 the American Standard Association proposed the following definition to explain this parameter, "the sound intensity of a sound field in a specified direction at a point is the sound energy transmitted per unit time in the specified direction through a unit area normal to this direction at the point". The unit of sound intensity is watts per square meter.

The term acceleration noise is used to describe the type of sound generated by the sudden movement of rigid bodies (Anderson and Anderson 1993). If collision occurs between two rigid bodies the body that is subjected to the impact will continue to accelerate and the body that causes the impact will start to decelerate. In most cases, the time period of impact is very short and is usually measured in micro-seconds (μs). Therefore, the rate of change of velocity with respect to time, which is the acceleration is very big and can be measured to represent the acceleration noise. Thus, acceleration noise can be used to detect very short metal to metal contact which happens when there is impulsive contact in machine components such as in defective bearings and gears. The easiest way to detect the strength of acceleration noise is by measuring the air-particle acceleration signals caused by a sound source.

2.2.1 Sound Pressure Level

A logarithmic scale is used to represent the sound pressure level. This is because of the very big range in pressure amplitudes that can be associated with sound waves. The unit used to describe the sound pressure level is termed the decibel or dB as defined in equation (2.1).

$$L_p = 20 \log_{10} \left(\frac{p_{rms}}{p_{ref}} \right) \quad dB \qquad (2.1)$$

where p_{rms} is the root-mean-square value of the sound pressure signals, and p_{ref} is the reference sound pressure and its value is 20 μPa. The total pressure at any time in space can be written as

$$P(t) = P_o + p(t) \qquad (2.2)$$

where $p(t)$ represents the sound wave disturbance and $P_o = 10^5 \ N/m^2$, is the mean atmospheric pressure. However, we are only interested in the strength of the fluctuating

component $p(t)$. Since energy is proportional to the square of the pressure, it is conventional to use the mean square pressure as a measurement parameter

$$p_{rms}^2 = \frac{1}{T} \int_0^T p(t)^2 \, dt . \qquad (2.3)$$

It should be noted here that the range of root-mean-square (rms) pressure fluctuations in which we are interested for audio acoustics extends from about $2 \times 10^{-5} \, N/m^2$ to $20 \, N/m^2$. These amplitudes represent a very small fluctuation of pressure about the mean atmospheric value of $10^5 \, N/m^2$, (Ford 1970).

2.2.2 Sound Intensity

Fahy (1989) presented a comprehensive discussion on the principles of sound intensity in a book entitled "Sound Intensity". It covers from the basic theoretical analysis of sound intensity, the measurement of sound intensity up to the practical applications of sound intensity technique to engineering problems such as machinery design, building acoustics, vehicle and engine technology, and workplace noise control. The fundamental development of the sound intensity measurement technique began with an effort to measure the net sound energy flow, namely the power density (W) given by the equation

$$I_a = \frac{1}{T} \int_0^T p v_a \, dt , \qquad (2.4)$$

Where I_a is the time-averaged sound intensity in any specified direction a, p is the instantaneous sound pressure at a point and v_a is the instantaneous particle velocity in the direction a in which the power density is being measured (Clapp and Firestone 1941). In order to use a two-microphone method as shown in Figure 2.1, the relation between pressure gradient and particle velocity needs to be found to carry out the integration in equation (2.4).

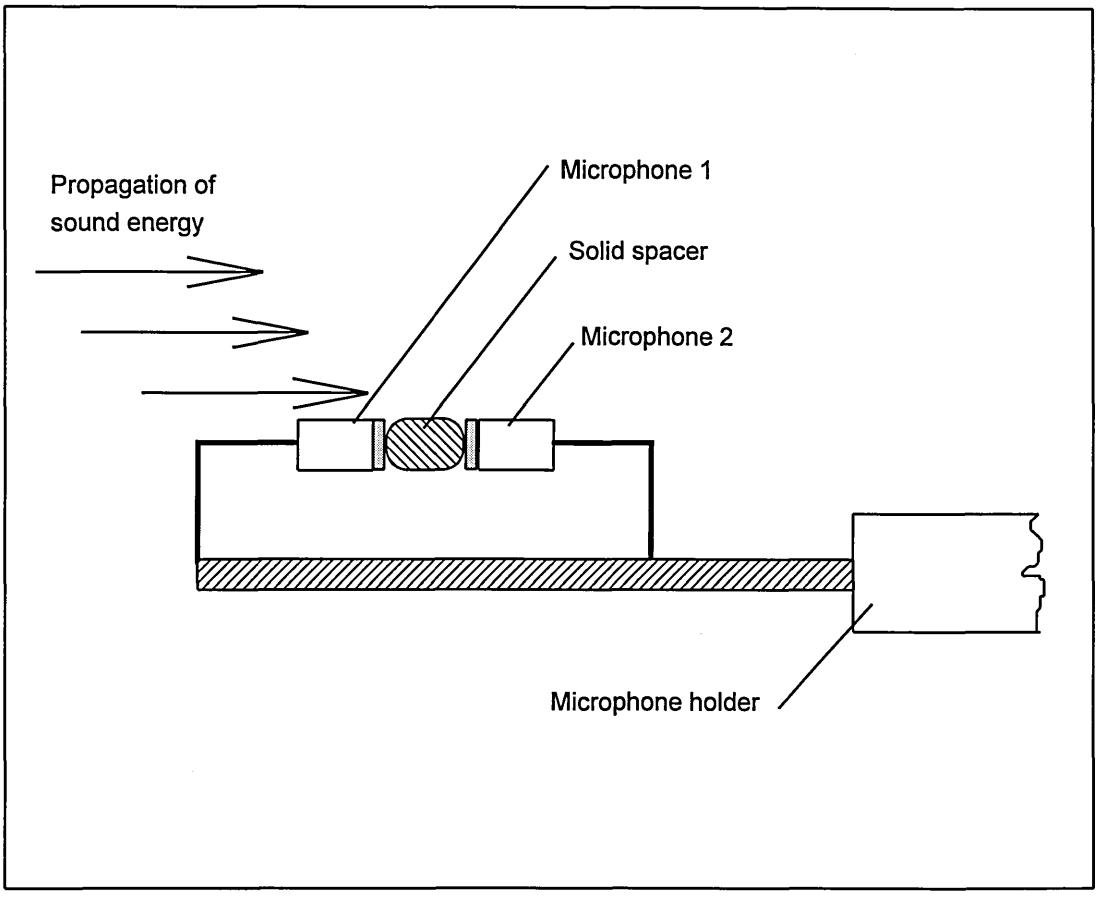

Figure 2.1 Measurement of sound intensity signals using a two-microphone method.

Newton's second law can be used to relate the pressure gradient and particle velocity at a mid-span between the two microphones

$$\rho_o \frac{dv_a}{dt} + \frac{dp}{dr} = 0 \qquad (2.5)$$

rearranging this equation, we get

$$v_a = -(\frac{1}{\rho_o}) \int \frac{dp}{dr} dt. \qquad (2.6)$$

This equation can also be obtained from the Euler equation that relates particle acceleration and pressure gradient (Lahti 1990).

$$-\nabla p = \rho_o \left[\frac{\partial v}{\partial t} + (v \cdot \nabla) v \right]. \qquad (2.7)$$

With the assumptions of small perturbation, no mean flow and neglecting higher order terms, the Euler's equation becomes

$$\frac{\partial v}{\partial t} = -\frac{1}{\rho_o} \nabla p. \qquad (2.8)$$

This equation can be simplified further to obtain equation (2.6). The average pressure at the mid-span and the pressure gradient between the two pressure microphones can be represented by the following equations:

$$p \approx (p_2 + p_1)/2, \qquad (2.9)$$

and

$$\frac{dp}{dr} = \lim_{\Delta r \to 0} \left(\frac{\Delta p}{\Delta r}\right) \approx \frac{(p_2 - p_1)}{\Delta r}, \qquad (2.10)$$

where p_1 is the pressure signal from the first microphone, p_2 is the pressure signal from the second microphone and Δr is the space between the two pressure microphones. Substituting these variables into equations (2.4) and (2.6) gives

$$I_a = -\frac{1}{T} \int_0^T \frac{(p_2 + p_1)}{2} \frac{(p_2 - p_1)}{\rho_o \Delta r} dt \qquad (2.11)$$

rearranging the variables, we get the equation for sound intensity in term of pressure from the two microphones, air density and distance between the two microphones (Baker 1955, Shultz 1956).

$$I_a = -\frac{p_2 + p_1}{2T\rho_o \Delta r} \int_0^T (p_2 - p_1)\, dt. \qquad (2.12)$$

Two approaches are used to process the signals from the two microphones for sound intensity measurement. The first approach is the digital filter method by which sound intensity is calculated in real time in the time domain. The second approach is the FFT method, by which the sound intensity is calculated in the frequency domain from the imaginary part of the cross-spectrum function. In the frequency domain, the Fourier transform of v_a at the mid-point between the pressure microphones may be approximated as

$$F_{va} \approx \frac{i\,(F_{p2} - F_{p1})}{\rho_o \Delta r \omega} \qquad (2.13)$$

where $i = (-1)^{1/2}$. In addition, Fourier transform of the pressure at the same location can be expressed as

$$F_p \approx \frac{1}{2}(F_{p1} + F_{p2}) \qquad (2.14)$$

Where F_{p1} is the Fourier transform of the pressure signal at the first microphone and F_{p2} is the Fourier transform of the pressure signal at the second microphone. For stationary and ergodic signal with zero mean (Gade 1985, Jacobsen 1989 and 1990), the active sound intensity spectrum can be represented by the following equation:

$$\begin{aligned} I_a(\omega) &= \frac{1}{2} Re\{\tilde{p}\tilde{v}_a^*\} = \frac{1}{2}|p||v_a| \cos\varphi \\ &= \frac{Im\{F_{p1}F_{p2}^*\}}{2\rho_o \Delta r \omega} = -\frac{\mathrm{Im}\{G_{12}\}}{\rho_o \Delta r \omega} \end{aligned} \qquad (2.15)$$

where $\tilde{p}$ and $\tilde{v}_a$ are complex amplitudes of the sound pressure and the particle velocity, φ is the phase angle between the two pressure signals, and

$G_{12} = \frac{1}{2}[F_{p1}{}^{*}\, F_{p2}]$ is the cross spectrum between p_1 and p_2. Note that the minus sign and the order of the conjugate asterisk is related as

$$Im\{ F_{p1}\, F_{p2}^{*} \} = - Im\{ F_{p1}^{*}\, F_{p2} \} \tag{2.16}$$

The presence of the imaginary part of the cross spectrum represents the effective integration of equation (2.4) to produce the necessary relationship between average sound pressure and the particle velocity. In addition, the reactive sound intensity can be written as follows

$$\begin{aligned} \boldsymbol{J_a}(\omega) &= \frac{1}{2} Im\{\tilde{p}\,\tilde{v}_a^{*}\} = \frac{1}{2}|p||v_a| \sin\varphi \\ &= \frac{1}{2\omega\,\rho\,\Delta r}(G_{11} - G_{22}) \end{aligned} \tag{2.17}$$

where G_{11} and G_{22} are the real auto spectra of the two microphone signals. In some cases, the velocity of the vibrating surface can be measured directly using an accelerometer. This method is widely used to find the sound power and to analyse the sound signal of a large source in-situ (Hodgson 1977, Brito 1979, Crocker 1981). It is called the surface intensity method.

Similar to sound power level the sound intensity level is represented in units of decibel with the reference intensity I_{ref} equal to $10^{-12}\ watts/m^2$. Thus the equation for sound intensity level can be written as

$$L_I = 10\log_{10}\left(\frac{Intensity}{10^{-12}\ watts/m^2}\right) dB \tag{2.18}$$

and the equation for sound power level of a sound source is

$$L_W = 10\log_{10}\left(\frac{Sound\ Power\ Output}{10^{-12}\ watts}\right) dB. \tag{2.19}$$

2.2.3 Acceleration Noise

Until recently, it has not been clear how important acceleration noise is in industrial machines (Anderson and Anderson 1993). Acceleration noise is usually associated with the sound signal that is generated by impacting bodies. It has been shown that the energy emitted as sound can never be greater than 1.5×10^{-4} times the kinetic energy produced during impact (Richards et al 1979). Fortunately, the sound pressure microphones are capable of measuring the very small variations of sound pressure signals in air. The dominating sources of sound signals emitted by a defective machine component are usually associated with acceleration noise due to impact and ringing noise from flexural vibrations of the machine component. Air-particle acceleration is an ideal variable that can be used to detect these signals. Equations (2.8), (2.9) and (2.10) can be used to derive the formula for obtaining air-particle acceleration signals using the two-microphone method.

$$ap(t) = \left(\frac{1}{\rho_o \, \Delta r}\right) (p_1 - p_2) \qquad (2.20)$$

where p_1 and p_2 are the time variation of pressure signals from the first and second microphone respectively, and Δr is the distance between the two microphones. A detailed derivation of equation (2.20) is presented in Appendix A.

2.3 Fundamental of Signal Processing Methods

In this study, the measured signals are processed in three different domains, namely; time domain, frequency domain, and simultaneous time-frequency domain. The time domain method is mostly the utilisation of statistical parameters for monitoring machine components. The frequency domain analysis capitalises on the advancement of fast Fourier transform (FFT) to analyse sampled signals. The simultaneous time-frequency domain analysis gain much momentum from the development of the wavelet transform method which is analogous to the FFT method in frequency domain analysis.

2.3.1 Statistical Analysis Methods

The application of statistical distribution moments such as kurtosis and skew using vibration and acoustic emission (high frequency sound) signals for monitoring manufacturing processes and machine conditions have been well established (Kannatay-Asibu 1982, Diniz et al 1992, Trujillo et al 1994, Daadbin and Wong 1991, Martin 1992). However, no literature has so far been found on the application of air-particle acceleration signals for such purposes.

If the probability density of the distribution of data sample exist such that

$$Prob\,[x \le x(t) \le x + dx] \;=\; p(x)\,dx\,, \tag{2.21}$$

then the expectation (*mean*) of a random function of time, *x(t)* is

$$E[x] \;=\; \frac{1}{T}\int_{-\infty}^{\infty} x(t)\,dt \;=\; \int_{-\infty}^{\infty} x\,p(x)\,dx \tag{2.22}$$

Next the *r*th-order moment about the mean $\bar{x}$, is given by

$$E\left[\{x - E(x)\}^r\right] = \int_{-\infty}^{\infty} (x-\bar{x})^r\; p(x)\; dx \tag{2.23}$$

From equation (2.23) the mean $\bar{x}$ or $E(x)$, of the random variable is the first-order moment, the *rms* value is the square root of the second-order moment and the variance σ^2 is the second-order central moment. The mean gives the average value of the variable, the rms value gives the intensity, and the variance gives the deviation from the mean. If the data available are in discrete form, equation (2.23) can be written as

$$M_r \;=\; \frac{1}{N}\sum_{k=1}^{N} (x_k - \bar{x})^r \tag{2.24}$$

where N is the number of data points, and r is the order of the moment. The following equations present the calculation for the other variables in continuous and discrete form,

$$rms = \sqrt{\int_{-\infty}^{\infty} x^2 \, p(x) \, dx} = \sqrt{\frac{1}{N} \sum_{k=1}^{N} x_k^2} \tag{2.25}$$

standard deviation,

$$\sigma = \sqrt{\int_{-\infty}^{\infty} (x-\bar{x})^2 \, p(x) \, dx} = \sqrt{\frac{1}{N} \sum_{k=1}^{N} (x_k - \bar{x})^2} \tag{2.26}$$

$$Skew = \frac{M_3}{\sigma^3} \tag{2.27}$$

$$Kurtosis = \frac{M_4}{\sigma^4} \tag{2.28}$$

and

$$Crest\ Factor = \frac{[Maximum\ Peak]}{rms} \tag{2.29}$$

The other statistical parameters used in the study were based on beta function distribution, whereby the statistical distribution is normalised based on the gamma function (Cooper and Weekes 1983):

$$\beta\ (a,b) = \frac{\Gamma(a)\Gamma(b)}{\Gamma(a+b)} x^{a-1} (1-x)^{b-1} \tag{2.30}$$

The mean of the beta function distribution can be written as,

$$Mean = \bar{x} = \frac{a}{a+b} \tag{2.31}$$

and the equation for the standard deviation is

$$\sigma = \sqrt{\frac{ab}{(a+b+1)(a+b)}}. \tag{2.32}$$

Thus, the parameters a and b can be derived from equation (2.31) and (2.32):

$$a = \frac{\bar{x}}{\sigma^2}(\bar{x} - \bar{x}^2 - \sigma^2) \tag{2.33}$$

and

$$b = \frac{(1-\bar{x})}{\sigma^2}(\bar{x} - \bar{x}^2 - \sigma^2) \tag{2.34}$$

Since the beta function algorithm requires the data to be ranged between zero to one, it is necessary to remove any dc shift, to rectify, and finally to normalise the raw data before equations (2.33) and (2.34) can be used.

The application of the beta function parameters a and b was performed by Whitehouse (1978) to classify surface texture of engineering materials using different manufacturing processes. Whitehouse presented another form of equations for calculating the beta function parameters a and b using variables borrowed from the analysis and measurement of materials' surface texture and roughness. The beta function parameters were written in the form

$$a = \frac{R_v(R_v R_p - R_q^2)}{R_t R_q^2} \tag{2.35}$$

$$b = \frac{R_p (R_v R_p - R_q^2)}{R_t R_q^2} \tag{2.36}$$

where R_p is magnitude of the highest peak, R_v is magnitude of the lowest valley, R_q is the rms value, and R_t is the maximum peak-to-valley height of the signal profile. The parameters a and b are less dependent on the extreme maxima and minima compared to the central moments variables namely skew and kurtosis. Therefore, the beta function parameters are theoretically more stable than the central moment variables. The moment of beta function distribution (Larson 1982) can be written as:

$$M_r = \frac{(a+b-1)(a+b-2)\cdots(a+1)a}{(a+b+r-1)(a+b+r-2)\cdots(a+b+1)(a+b)} \tag{2.37}$$

Odd moments, i.e., r = 1,3,5,.... etc., relate information about the position of the peak density relative to the median value. Even moments, i.e., r = 2,4,6,...., etc., indicate the spread in distribution (Dyer and Stewart 1978).

Statistical analysis is mostly applied to random signals where methods based on deterministic signals is not applicable. A random process is said to be stationary if the probability distributions obtained for an ensemble do not depend on absolute time. The term "stationary" refers to the probability distribution but not the signal samples themselves. Furthermore, a stationary process is called an ergodic process, if in addition to all the ensemble averages being stationary with respect to change of time scale, the averages taken along any single sample is the same as the ensemble averages (Newland 1993).

2.3.2 Spectral Analysis Method

Fourier-series analysis can synthesise any periodic function $x(t)$ into its sine and cosine components. For a nonperiodic function the Fourier series turns into Fourier integral and

the Fourier coefficients turn into continuous functions of frequency called Fourier transforms. The Fourier transform of a nonperiodic signal $x(t)$ is

$$X(\omega) = \frac{1}{2\pi} \int_{-\infty}^{+\infty} x(t)\, e^{-j\omega t}\, dt \qquad (2.38)$$

and the inverse Fourier integral equation is

$$x(t) = \int_{-\infty}^{+\infty} X(\omega)\, e^{j\omega t}\, d\omega \qquad (2.39)$$

where $e^{\pm j\omega t} = \cos\omega t \pm j\sin\omega t$, is the Euler's equation.

For a stationary random signal, the spectral analysis is not carried out on the function itself but on its autocorrelation function $R_{xx}(\tau)$. This autocorrelation function gives information about the frequencies present in a random process indirectly. The concept of power spectral density (PSD) is used to analyse the spectral properties of random signals, such as the characteristics of signals in the frequency domain. The plot of power spectral density function against frequency is the power spectrum (auto-spectrum) of the signal (Anderson and Anderson 1993). The Fourier transform of $R_{xx}(\tau)$ which gives the power spectral density function S_x is shown below

$$S_x(\omega) = \frac{1}{2\pi} \int_{-\infty}^{+\infty} R_{xx}(\tau)\, e^{-j\omega\tau}\, d\tau \ , \qquad (2.40)$$

and

$$R_{xx}(\tau) = \int_{-\infty}^{+\infty} x(t)\, x(t-\tau)\, dt \qquad (2.41)$$

The type of spectrum analysis used is dependent on the type of signals being measured. For deterministic signals the spectrum analysis based on the rms values can be used to detect the strength of frequency components in the signals. As an alternative, the power spectrum can also be used for this type of signals. For random signals the power spectral

density spectrum is used, and for transient signals the energy spectral density (ESD) is utilised.

2.3.3 Cepstral Analysis Method

For a linear system, the measured signal $y(t)$ is the convolution of input signal $x(t)$ and impulse response $h(t)$ of the system. Thus, the measured signal, has been obscured by the transmission medium through which it passed. Cepstrum analysis can be used to separate the excitation spectrum from the transfer function component. The Fourier transform of the output signal due to the excitation of input signal can be presented as

$$Y(\omega) = H(\omega)\, X(\omega). \tag{2.42}$$

The logarithm of the spectrum is used to separate the two components

$$\log Y(\omega) = \log H(\omega) + \log X(\omega) \tag{2.43}$$

The logarithm of the spectrum is transformed again to obtain

$$\Im[\log Y(\omega)] = \Im[\log H(\omega)] + \Im[\log X(\omega)], \tag{2.44}$$

where $\Im$ is the Fourier transform of a function.

The above process is called the cepstrum analysis which shows the signal in frequency domain, measured in units of time. Cepstrum can also be considered as a spectrum of a logarithmic amplitude spectrum. Therefore, it can be used for detection of any periodic component in a spectrum as shown by Brown and Jensen (Bruel and Kjaer Application Notes). One of the advantages of using cepstrum analysis is that it can easily reveal the

repetitive impact signals that have been recorded without the need to know the transfer function of the physical system.

2.4 Theory of Wavelet Transform Method

The wavelet transform method is based on two fundamental equations, namely, the scaling function, and the basic function. The scaling function also known as the father wavelet can be generated from the basic dilation equation and can be written as

$$\phi\ (x)\ =\ c_0\phi\ (2x) + c_1\phi\ (2x-1) + \ldots\ldots + c_n\phi\ (2x-n)\ \text{, or}$$

$$\phi\ (x)\ =\ \sum_{n\in z} c_n\,\phi\ (2x-n) \tag{2.45}$$

where z is a set of integers. The basic dilation function can be obtained either using a recursive method or using an iterative method. Once the scaling function has been established the corresponding basic function equation can be constructed from it. The basic function is sometimes called the mother wavelet, primary wavelet or analysing wavelet and can be written as

$$\psi\ (x)\ =\ \sum_{n\in z} (-1^n)\ c_{n+1}\ \phi\ (2x+n) \tag{2.46}$$

where c_n are the wavelet coefficients. The number of coefficients chosen will determine the shape of the analysing wavelet. For example, the Haar wavelet contains two coefficients, the D04 wavelet contains four coefficients and so on. This subject has been discussed in detailed by Daubechies (1988) and many different types of analysing wavelet are available today and ready to be utilised. The wavelet coefficients must satisfy three conditions for them to be eligible to be used in the analysis (Strang 1989, Strang and Fix 1973, Newland 1993). The three conditions are:

(i) conversion of area condition,

$$\sum_n c_n = 2 \qquad (2.47a)$$

(ii) accuracy conditions,

$$\sum_n (-1^n)\, n^m\, c_n = 0; \qquad (2.47b)$$

where m is a set of integer, and

(iii) orthogonality conditions.

$$\sum_n c_n\, c_{n+2m} = 0 \qquad (2.47c)$$

for all m except when $m = 0$.

A class of orthonormal basis function is derived from the dilation and translation process of the mother wavelet, usually written as

$$\psi_{a,b}(x) = \frac{1}{\sqrt{a}} \psi \left(\frac{x-b}{a} \right). \qquad (2.48)$$

For a discrete wavelet transform, the parameters a and b are discretised as follow: $a = a_o^m$, $b = nb_o 2^m$. Typical values for $a_o = 2$, and $b_o = 1$. Substitute these values into equation (2.48),

$$\psi_{m,n}(x) = 2^{-m/2} \psi\, (2^{-m} x - n). \qquad (2.49)$$

where a and m are the dilation factors, and b and n are the shift factors of the wavelet packet.

The goal of a wavelet transform is to decompose any arbitrary signal $f(x)$ into an infinite summation of wavelets at different scales. The independent variable x is assumed to be

defined in one unit interval that is for $0 \leq x \leq 1$. As an example, if the independent variable is time t and we are interested in a signal over duration T, then $x = t / T$ and x covers the range $0 \leq x < 1$, (Newland 1993). The discrete wavelet transform of a function $f(x)$ involves computation of the inner product for various values of parameters m and n as shown below (Palavajjhala et al 1994):

$$\langle f(x), \psi_{m,n}(x) \rangle = T_{m,n}(f(x)) = 2^{-m/2} \int_{-\infty}^{\infty} f(x) \psi (2^{-m} x - n) dx \qquad (2.50)$$

where $T_{m,n}(f(x))$ represents the coefficients of the wavelet transform method. Equation (2.50) shows that a time domain function $f(x)$ is mapped onto a two-dimensional time- and frequency- domain simultaneously.

2.4.1 Wavelet Packet Transform

Mallat (1989) has shown that the tree or pyramid algorithm can be applied to the wavelet transform by using wavelets as filter coefficients of the quadrature mirror filter (QMF) pairs. These are specially designed pairs of finite impulse response (FIR) filters that can separate the high-frequency and low-frequency components of the input signals. The low-pass filter coefficients are associated with the approximation components and the high-pass filter coefficients are associated with the detailed components of the input signal. Using wavelet packets analysis method, the wavelet transform is generalised to produce a library of orthonormal bases of modulated wavelet packets, and these bases are similar to adaptive windowed Fourier transforms.

Combination of $h = \{h_n\}$ defined as a summing filter and the associated differencing filter $g = \{g_n\} = (-1)^n h_{1-n}$; together known as the conjugate mirror filter can be used to construct the orthonormal bases. The coefficient sets h and g respectively define scaling and basic functions ϕ and ψ according to the relationships

$$\phi(x) = 2^{1/2} \sum_n h_n \phi (2x - n) \qquad (2.51)$$

$$\psi\ (x)\ =\ 2^{1/2} \sum_{n} g_n \psi\ (2x-n). \qquad (2.52)$$

The wavelet decomposition only keeps the detailed components of the signal whereas the approximation components are being decomposed again into the next level as indicated in Figure 2.2(a). On the other hand, the wavelet packet decompose the input signal by applying filters *H* (Low pass) and *G* (High pass) recursively to form a tree or pyramid algorithm as shown in Figure 2.2(b). Wickerhauser (1992) has developed the best basis algorithm from the wavelet packet transform method by finding the most efficient way (i.e. with minimum entropy cost function) to represent an input signal. An *M*-sample signal where $M = 2^m$, produces *m* wavelet packet bases and takes $O(M \log_2 M)$ operations, the search for the best basis uses an additional $O(M)$ operations. On the other hand, the fast Fourier transform (FFT) algorithm of an input signal with length *M* requires $O(M \log_2 M)$ operations.

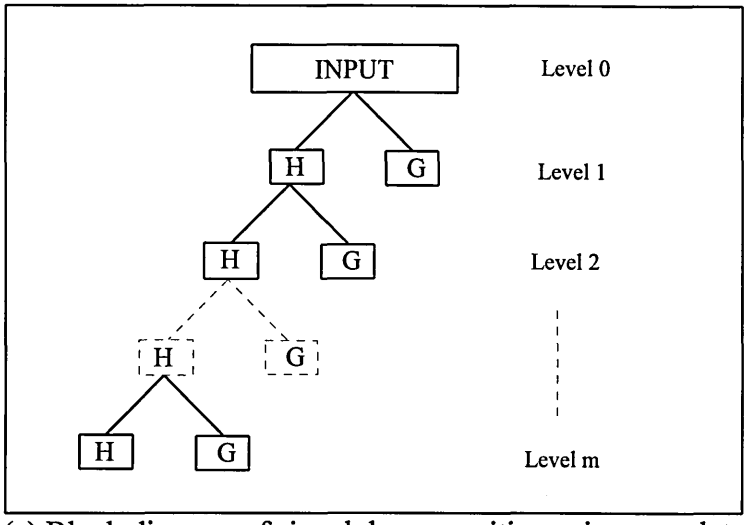

(a) Block diagram of signal decomposition using wavelet transform.

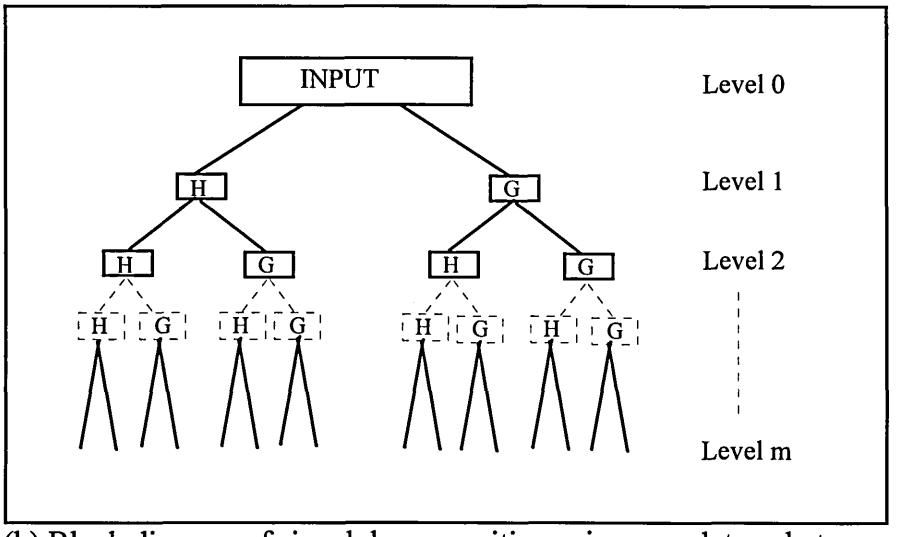

(b) Block diagram of signal decomposition using wavelet packet transform.

Figure 2.2 Signal decomposition using wavelet and wavelet packet algorithms.

The time-frequency resolutions at the different levels of the wavelet packet algorithm are best presented in Figure 2.3. It shows that at level zero the time resolution is at its best and the frequency resolution is at its worst. On the other hand, at the highest level, the frequency resolution is at its best and the time resolution is at its worst. The levels in between show compromised time-frequency resolution as shown in the diagram. The number of points, p that represents the time position of the signal at a particular level m

ranges from zero to $\frac{M}{2^m} - 1$, whereas the number of nodes, n that represents the frequency bin in the signal at a particular level m ranges from zero to $2^m - 1$. And the maximum number of levels that can represent the input signal is equal to $\log_2 M$. We can see from Figure 2.3 that each level of the time-frequency frame has its own time and frequency resolutions. Thus given a fixed level the time-frequency resolution for that level can be represented as shown in Figure 2.4.

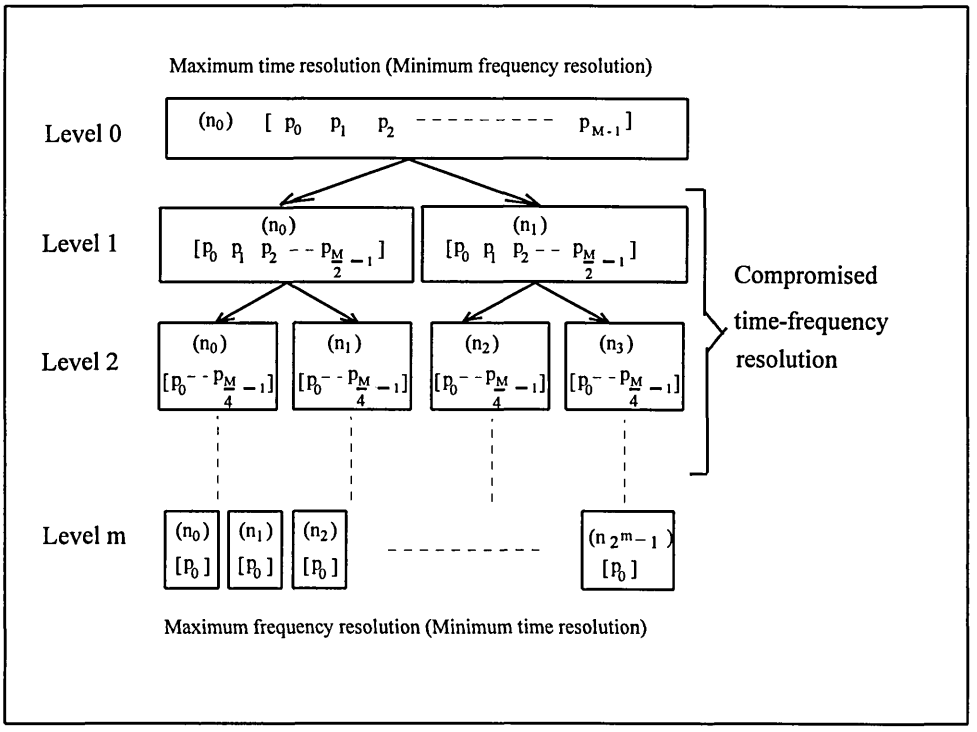

Figure 2.3 Time-frequency resolution of the wavelet packet decomposition.

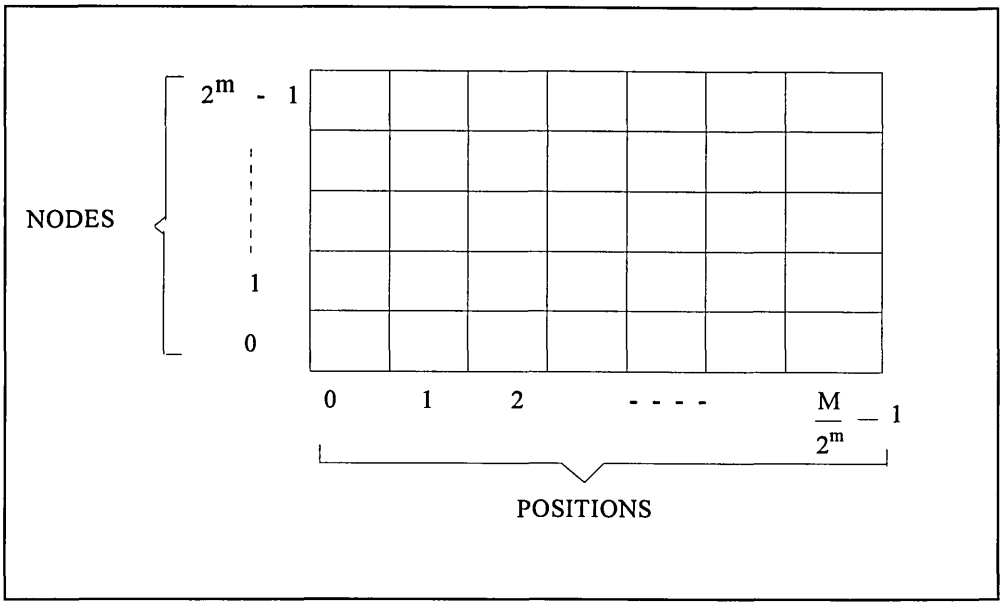

Figure 2.4 Time-frequency frame in a fixed level, *m*.

From the output of the wavelet packet transform, we can calculate back the frequency and time components of the signal. Given the sampling frequency R, wavelet level m, wavelet node number n, and the wavelet position p, the nominal centre frequency can be calculated by using the following equation:

$$F = (R/2) * (n + 0.5) / 2^m. \tag{2.53}$$

The uncertainty of the calculated frequency can be expressed as

$$\Delta F = \frac{(R/2)}{2^m}. \tag{2.54}$$

The corresponding time location of the signal is obtained from the equation

$$t = (P + 0.5) * \left(\frac{2^m}{R}\right), \tag{2.55}$$

with uncertainty of the calculated time expressed as

$$\Delta t = \frac{2^m}{R}. \tag{2.56}$$

2.5 Artificial Neural Networks

The concept of artificial neural networks was derived from basic constituents of the brain known as *neurons*. The human brain is an enormous collection of interconnected processing units known as neurons. A neuron is capable of receiving and sending signals. Each neuron can receive signals from other neurons, sum these signals, transform this sum and send the results to other neurons. A schematic diagram representation of a neuron is shown in Figure 2.5. Artificial neural networks resemble the brain in such a way that knowledge is acquired through examples and training process, and the knowledge is distributed and stored in the weights of the interneuron connection.

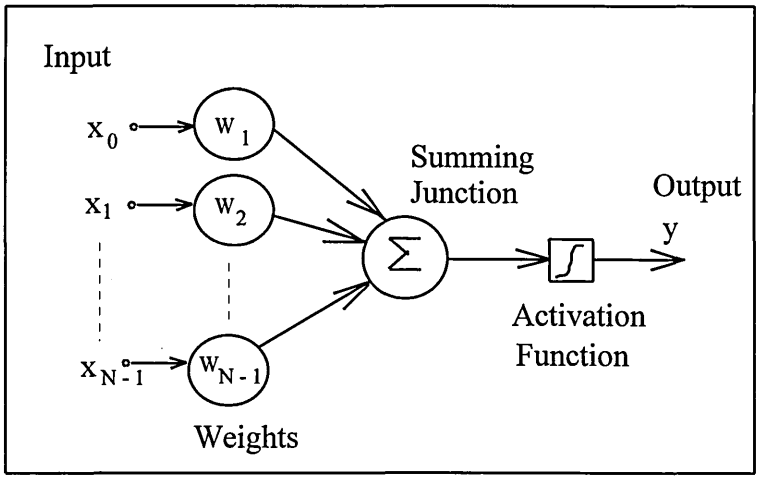

Figure 2.5 Schematic model of a neuron.

Artificial neural networks can be categorised according to the three different types of learning methods that are employed to train the networks. The first type is the

supervised learning where the output of a network is compared with the correct output and weights in the connection within the network are then adjusted to produce better output. The second type is called the reinforcement learning where the network is only told if the output produced was good or bad. And the third type is called the unsupervised learning where a network develops its own classification rules by extracting information from the examples input to the network.

2.5.1 Back Propagation Algorithm

The most popular type of algorithm for supervised learning application is back propagation. A back propagation network is a feedforward network of processing elements which can have any number of layers, such as, the input layer, hidden layer(s), and output layer. The schematic diagram showing the common feature of the back propagation network is presented in Figure 2.6. The function signals begin at the input node and propagate forward through each layer and emerge at the output layer as output signals. Whereas the error signals start at the output neurons of the network and propagate backward through each layer of the network. This type of network was used in the research study using air-particle acceleration signals to identify the type of defects induced in a test-bearing.

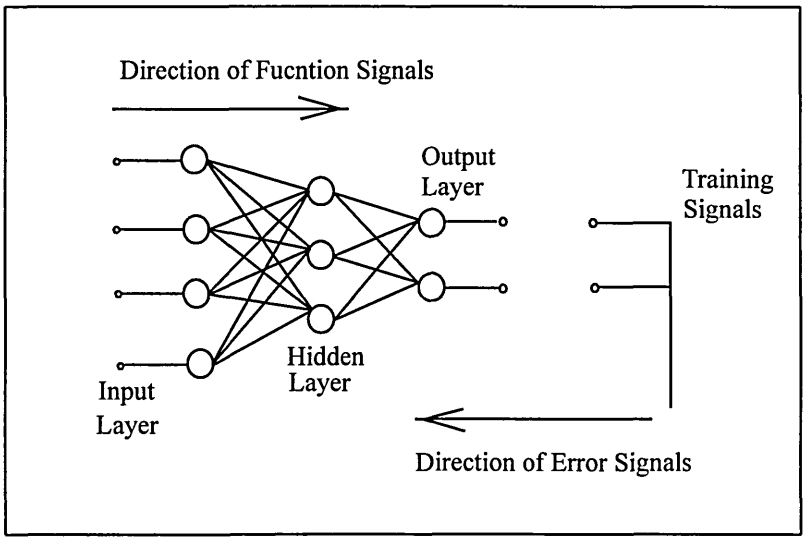

Figure 2.6 Representation of back propagation network with one hidden layer.

CHAPTER 3

DESIGN, CONSTRUCTION AND CALIBRATION OF TEST RIG

Information gathered from the literature review showed that the sound intensity measurement technique has good potential, and can offer several advantages if applied to machine condition monitoring. It is well known that excessive noise is frequently the first indication of deterioration of bearing in service. Initial studies carried out by Kim (1984) indicated that sound intensity measurement was capable of showing signs of intermediate stage of incipient failure in a rolling element bearing. Tandon and Nakra (1990) showed that a change in sound intensity frequency spectrum above 4KHz was observed due to the presence of defect in rolling element bearings. Also most of the defects in mechanical components are due to bearing failures (Daadbin and Yuen 1990). Furthermore, the mechanical behaviour of bearing component is well established which makes it convenient to compare experimental results with theoretical analysis. A test rig was constructed to carry out further experimental study on the applicability and limitations of sound intensity techniques for monitoring bearing condition.

3.1 Rig Design

A simple experimental system was designed to test the condition of rolling element bearings using vibration, sound pressure, sound intensity, and air-particle acceleration signals. A study was carried out on the rig to test the applicability of sound intensity technique for monitoring bearing condition, and to explore the advantages and limitations of this technique.

The test rig consists of a 40mm diameter shaft driven by a 2HP variable speed electric motor via a belt drive system. The speed of shaft can be varied from 500rpm up to 5000rpm. The test rig is capable of testing the different types of bearing defect such as inner race defect, rolling element defect, outer race defect, and missing

roller. In addition, the effect of shaft misalignment, loading condition, and unbalance can also be tested using the rig. Overall layout of the test rig is shown in Figure 3.1.

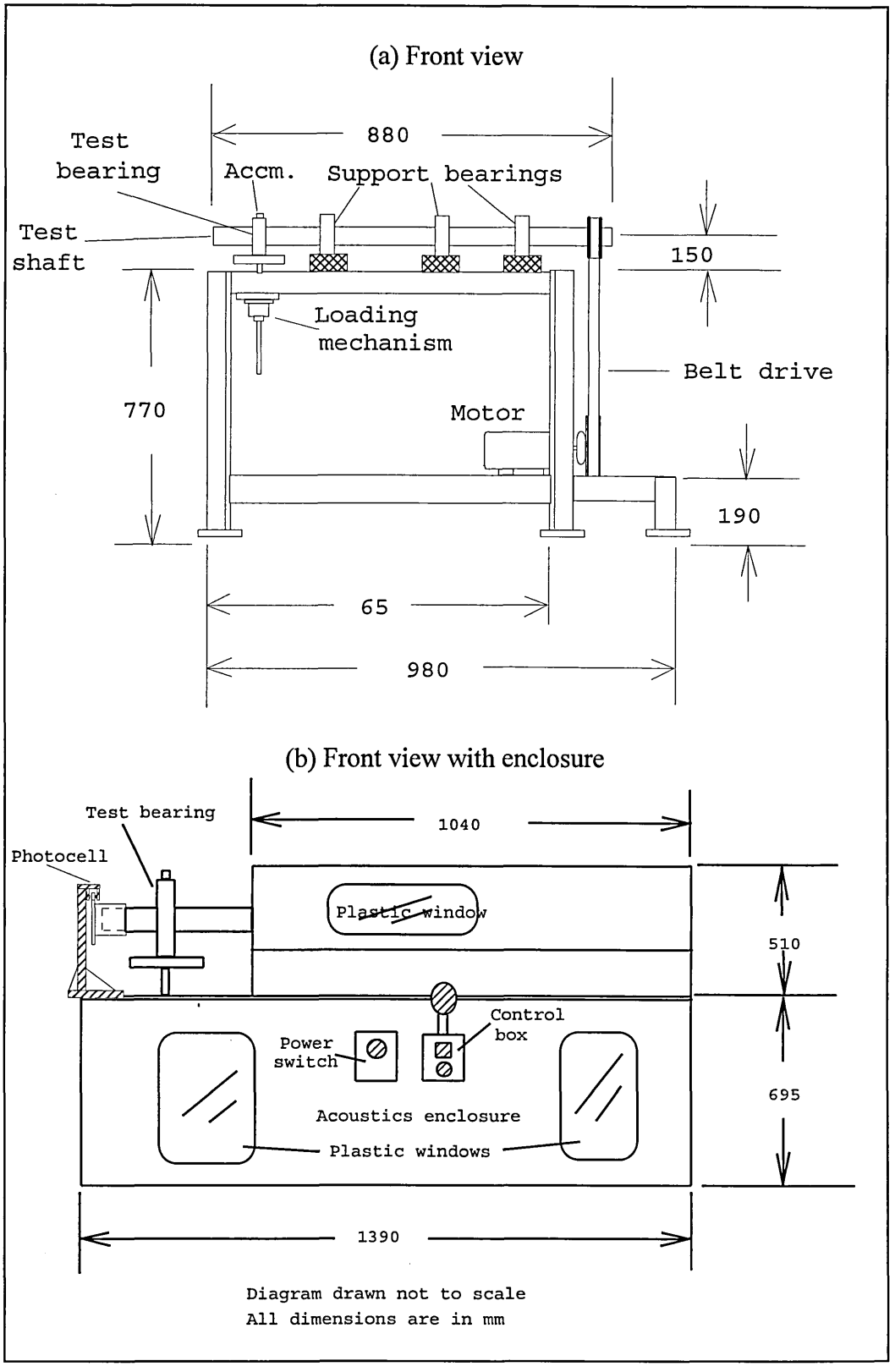

Figure 3.1 Schematic diagram of test rig.

Only the test bearing and other auxiliary equipment are exposed to the user, other moving components of the rig were enclosed in a housing. This enclosure was constructed for two purposes: first is for safety reasons, and second is for minimising the effect of noise produced by other moving components in the rig. It was built from plywood 4mm in thickness and the inside surface was coated with rubber pad 2mm in thickness. It can attenuate sound by between 16.9dB at 500Hz up to 49dB at 12KHz as indicated in Figure 3.2.

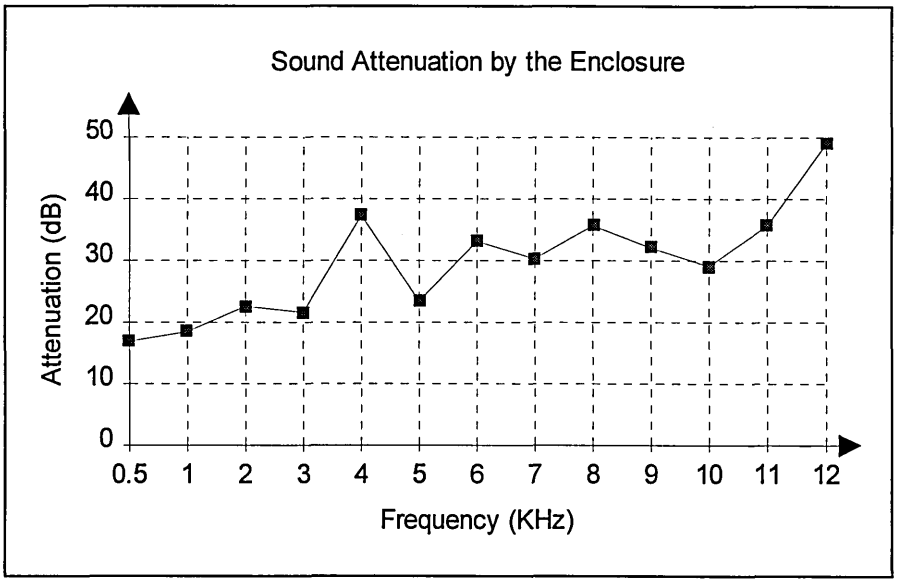

Figure 3.2 Attenuation of sound by the enclosure.

3.1.1 Ancillary Equipment

Other equipment used include Bruel and Kjaer(TM) 2032 dual-channel analyser complete with Bruel and Kjaer(TM) Type 4181 sound intensity probe, sound level meter, accelerometer, GOULD(TM) four channel oscilloscope, AMF Venner(TM) digital counter, and 80486 micro-computer with IEEE card. Signal analysis and processing softwares that were utilised include Dadisp(TM) V3.01 for data analysis and display, Wavelet Packet Laboratory for Windows, WPLW(TM) Version 1.02 for wavelet

analysis, Neudesk(TM) for artificial neural networks algorithm and Borland(TM) Turbo C++ Version 3.0 compiler for high level programming language.

3.2 Calibration of Test Rig and Ancillary Equipment

The first calibration exercise done on the test rig was to correlate the rotational speed of the shaft with the indicator at the control knob of the speed controller. These readings were also compared with results from stroboscope and hand-held tachometer. Figure 3.3 shows a linear relationship between the shaft speed and the position of control knob. The range of control knob position is from 0 to 100. Calibration of other components such as the accelerometer, charge amplifier and sound level meter were carried out regularly during the period of study to ensure that they are fully calibrated and working correctly.

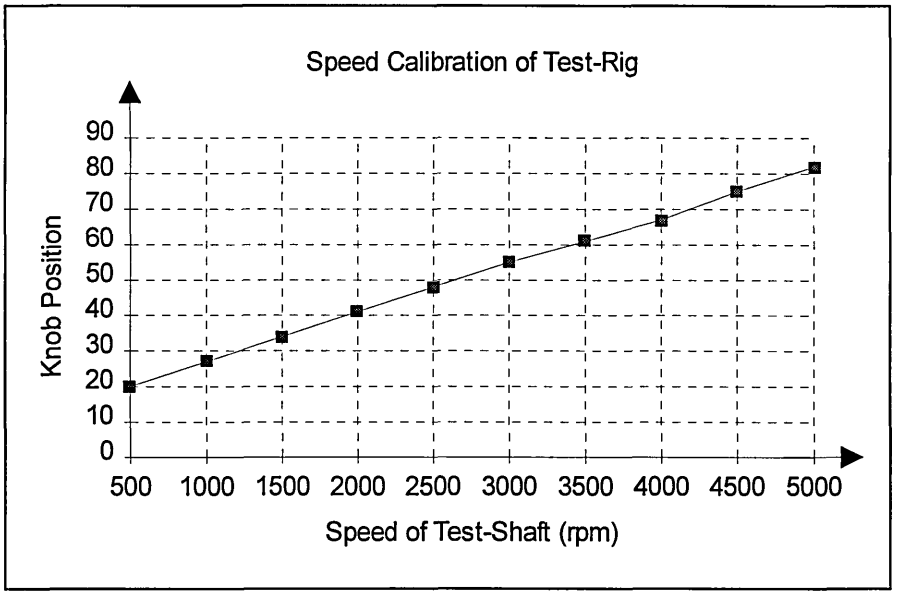

Figure 3.3 Speed calibration results from the test rig.

3.2.1 Calibration of Sound Intensity Measurement System

The measurement of sound intensity signals using the two-microphone method is very sensitive to the phase difference between the two channels of the measuring microphone and analysing instrument. Therefore, it is sensitive to the phase-mismatch error (Ren and Jacobsen 1991, Pascal and Carles 1982). However, due to the phase-corrector units specified for the Bruel and Kjaer Type 4181 microphone pair, the phase matching characteristic is retained even in sound fields with very high pressure-level gradients resulting in high accuracy of near field measurements at low frequency sound signals. Detailed analysis of phase-mismatch error was presented by Gade (1985) which utilised the indicators called the residual pressure-intensity index of the measuring system and the measured pressure-intensity index of the sound field at the microphone position. The utilisation of these indices was first introduced by Roland (1982).

The residual pressure-intensity index is defined as the difference between sound pressure and sound intensity levels when the microphones are subjected to a sound field with $0°$ phase difference between the two microphone positions. Whereas, the measured pressure-intensity index is the difference between sound pressure and sound intensity levels, at the measuring position in the field.

$$PI_{Residual} = L_{p,0} - L_{I,0} \tag{3.1a}$$

$$PI_{Measured} = L_{p,M} - L_{I,M} \tag{3.1b}$$

The criteria used to assess the accuracy of sound intensity measurement is presented by Equation (3.2),

$$PI_{Measured} \leq PI_{Residual} - K\,dB \tag{3.2}$$

if K is 7dB, then the accuracy of measurement is ±1dB, and if K is 10dB the accuracy of measurement is ±0.5dB. In addition, amplitude calibration of the two pressure microphones were also performed to ensure that their performance are identical.

Calibrations of the sound intensity measuring system were carried out regularly during the study period using Bruel and Kjaer Type 3541, Type 4226 sound intensity calibrators. Typical results for the calibration are shown in Figure 3.4. These results were consistent with the values specified by the manufacturer (Bruel and Kjaer Product Data). A quick check on the accuracy of measurement using sound intensity technique can be carried out using ordinary piston-phone calibrator and the appropriate coupler with single frequency sound source at 1KHz. The residual pressure-intensity index with 50mm and 12mm spacers should be around 30dB and 24dB respectively.

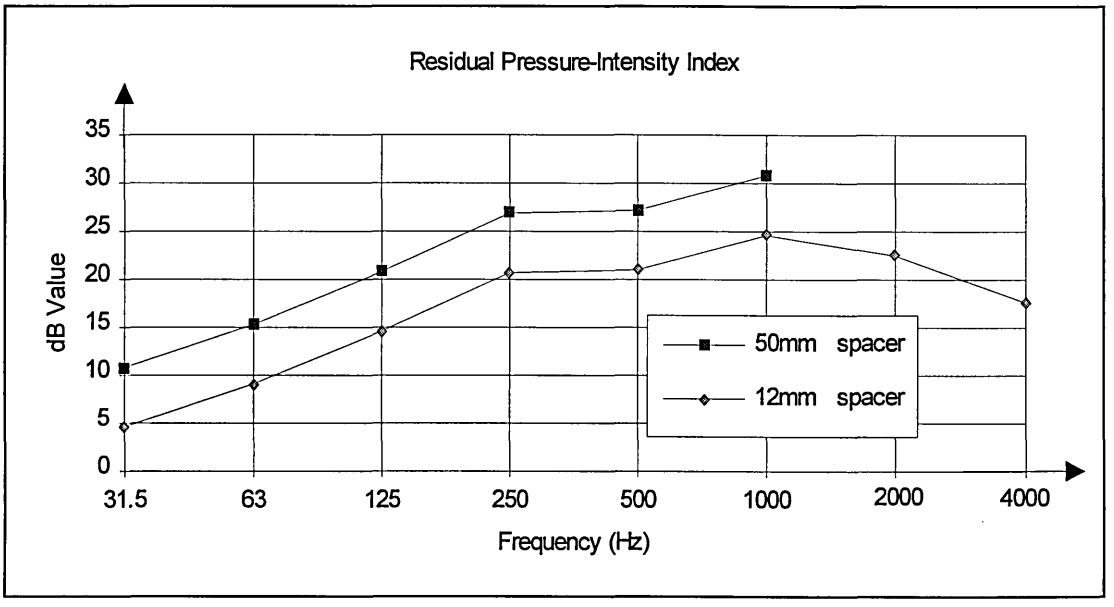

Figure 3.4 Results from calibration of sound intensity measurement system.

3.2.2 Directional Properties of the Microphone Pair

Figure 3.5 shows a typical directional properties of microphone pair when applied to measurement using sound intensity technique. The sensitivity of the microphone pair is dependent on the angle of incidence of the incoming sound signals which measures the component of the signals along the probe axis.

$$I_{measured} = I_{insident} \cos\theta \qquad (3.3)$$

The sensitivity of the microphone pair is a minimum when the angle of incidence of the sound wave propagation is equal to ninety degrees. This feature is widely used to find and to identify sound sources in the field.

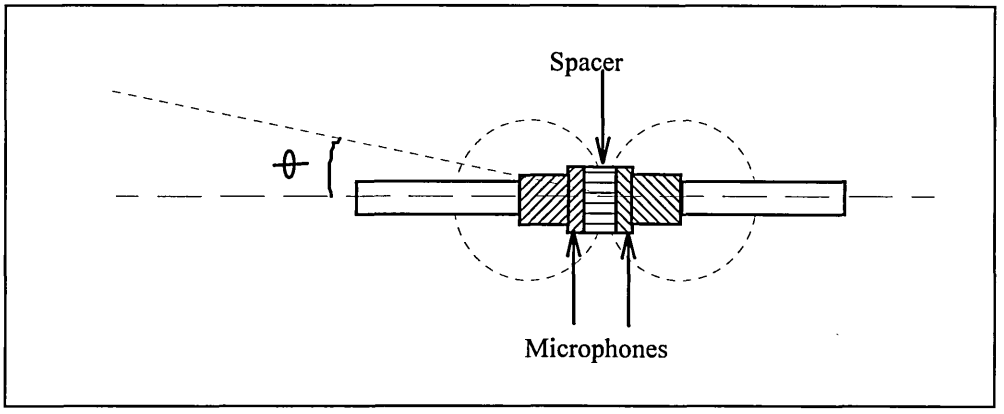

Figure 3.5 Schematic diagram showing directional properties of microphone pair.

3.2.3 Impact Test

The impact test was carried out to identify the natural frequencies at which the test rig and bearing housing were vibrating in response to external excitation force. Six different position and direction of impacts were applied as shown in Figure 3.6.

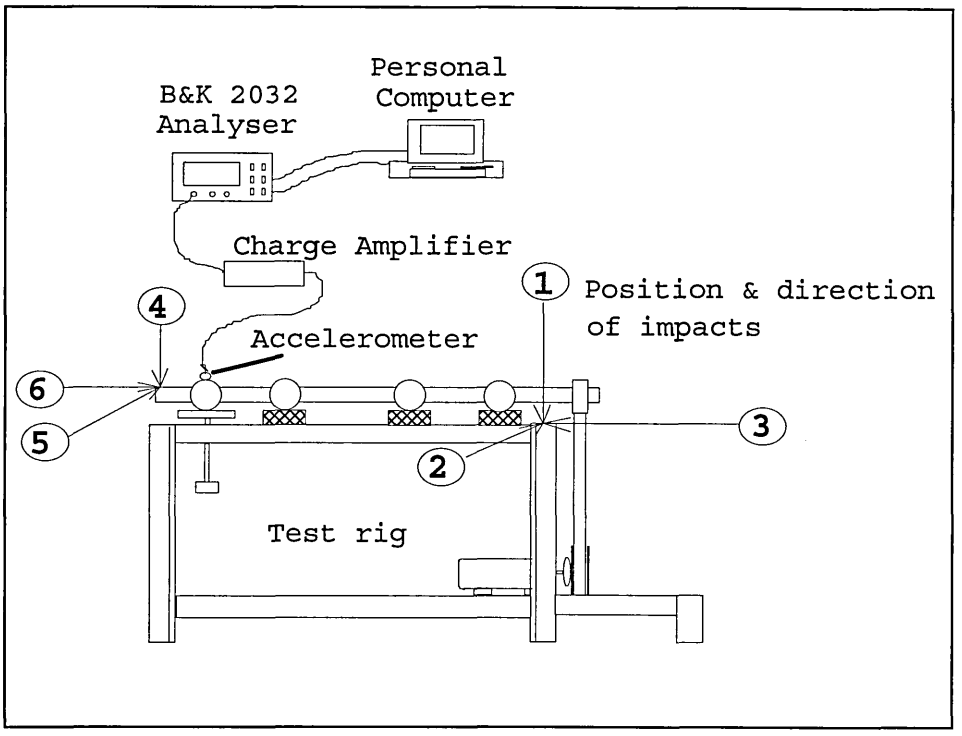

Figure 3.6 Position and direction of impacts for the test.

Three readings were recorded from each of the six impact which correspond to different set of frequency range and resolution: (a) Frequency ranging from 0 to 800Hz, with 1Hz frequency resolution, (b) Frequency ranging from 0 to 3.2KHz, with 4Hz frequency resolution and (c) Frequency ranging from 0 to 25.6KHz, with 16Hz frequency resolution. A sample of the results are shown in Figure 3.7.

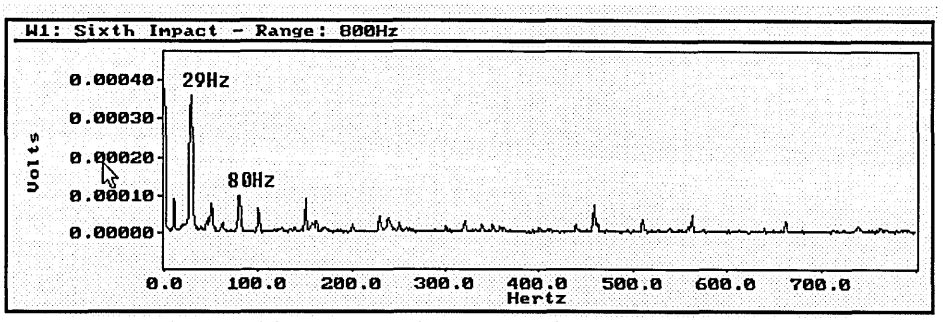

(a) Longitudinal impact on the test shaft.

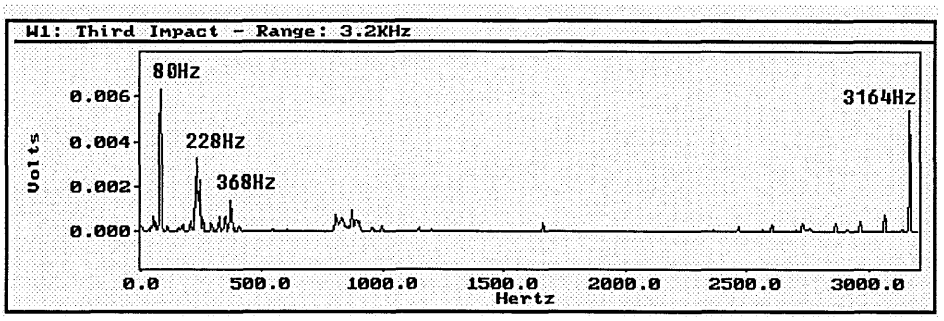

(b) Longitudinal impact on the rig structure.

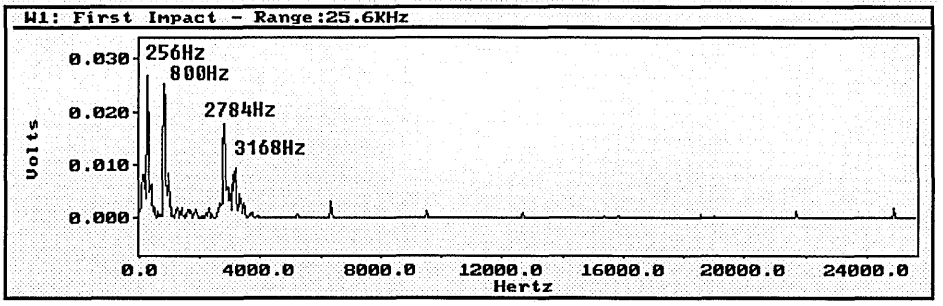

(c) Vertical impact on the rig structure.

Figure 3.7 Vibration spectrums from impact testing of the rig.

Results from the impact test indicate that natural frequencies of the support structure are mainly below 400Hz, which can be attributed to the different modes of vibration of the support structure. The natural frequencies of the bearing component and housing are measured to be from 2784Hz up to 3168Hz as shown in Table 3.1.

Table 3.1 Summary of the impact test results.

Impact Position	Frequency Component of Displayed Spectrum (Hz)
Impact on shaft (No. 1, 2 and 3)	29, 80, 156, 240, 3164, 3168, 6336
Impact on support structure (No. 4, 5 and 6)	80, 228, 240, 256, 360, 2784, 3164, 3168

3.3 Pilot Study

Experimental work for the pilot study was carried out using a self-aligning double row ball bearing (NSK 1209K) and single row cylindrical roller bearing (NSK 209K). Physical dimensions of the test bearing are presented in Table 3.2. The main objective of the pilot study was to observe changes in frequency spectrums that were obtained from the test-bearings with and without defects using sound pressure, sound intensity and vibration signals. Therefore, only frequency spectrums were measured and analysed at this stage. All defects on the roller, inner race and outer race of the test-bearings were initiated using an etching pen. The defects were made into oval shape craters with the length ranging from 1.70mm to 3.26mm, the width ranging from 1.25mm to 2.42mm and the depth ranging from 26.9μm to 160.1μm. These measurements were obtained using the Hobson Talysurf(TM) surface roughness measuring machine.

Table 3.2 Physical characteristics of the test-bearings used for the pilot study.

Bearing Type	Self-aligning ball bearing (NSK 1209K)	Single row cylindrical roller bearing (NSK NF209K)
Ball radius	4.76mm	5.01mm
Number of elements	32 (16 per row)	14
Pitch circle radius	32.75mm	33.5mm
Internal diameter	40mm	40mm

The experiments were carried out under typical laboratory conditions and the effect of background noise level was considered to be minimal. The magnitude of sound intensity and sound pressure signals were measured using the A-weighted analysis because it resemble the loudness perceived by the human ear, and at this stage the signals can also be evaluated qualitatively by the researcher. The logarithmic amplitude values were obtained for the measurement with the reference value for sound pressure signal is 20μPa and the reference value for sound intensity signal is $1x10^{-12}$ W/m^2.

3.3.1 Results From Pilot Study

The initial results obtained confirm the finding of previous researchers, and they also showed that sound intensity spectrum can be used to indicate the presence of defects in rolling element bearings (Kim 1984, Tandon and Nakra 1990). However, further detailed study needed to be carried out in order to develop and apply the sound intensity measurement technique for diagnostics and for identification of the type of defect indicated by the signals.

Figure 3.8 shows that most of the defect signals indicated from the sound intensity measurement technique were highlighted at frequencies ranging from 1KHz up to 4.6KHz when the shaft speed is 1000rpm. Similar conclusion can be derived from the sound pressure spectrum. At 500rpm the sound pressure spectrum from self-aligning bearing with defects show slight increased in level at frequencies between 1KHz to 1.4KHz as indicated in Figure 3.9.

Compared to the results obtained using vibration signals, sound intensity signals were not very effective at indicating other abnormalities in the test-rig such as the missing rollers and the presence of an unbalance rotating disk attached to the test-shaft. These results are shown in Figure 3.10(a) and (b). All of the test results obtained from the cylindrical roller bearing revealed that there were no significant differences in the frequency spectra from bearings with the presence of a defect and the frequency spectra from bearings without a defect. This is because in a cylindrical roller bearing there was line-contact occuring between the rolling elements and both the inner race and the outer race of the bearing component. Therefore, the existence of a point-defect on one of the bearing components did not have any effect on the performance of a cylindrical roller bearing. For future activities, only line defect should be used when testing a cylindrical roller bearing.

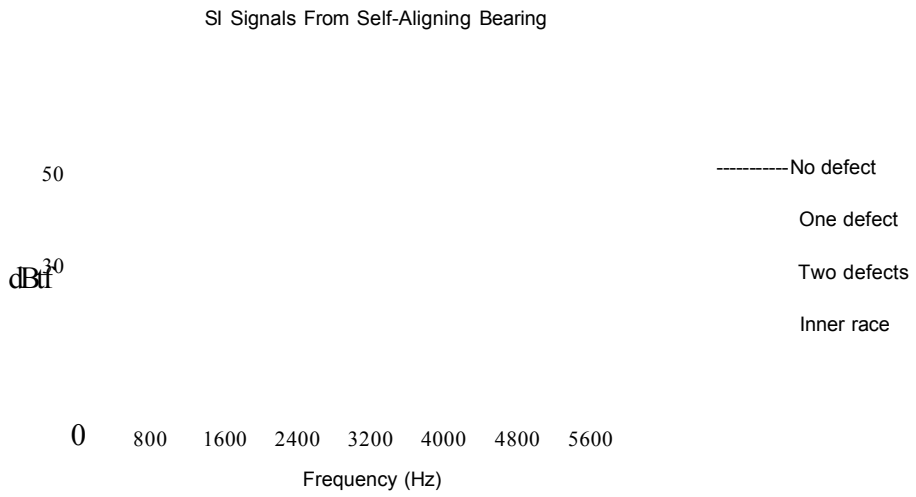

Figure 3.8 Sound intensity signals from self-aligning bearing running at lOOOrpm.

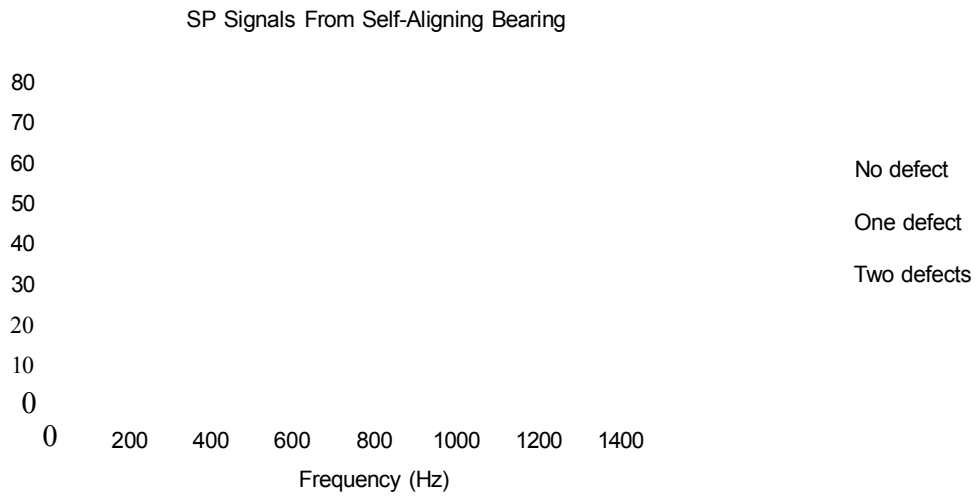

Figure 3.9 Sound pressure spectrum from self-aligning bearing running at 500rpm

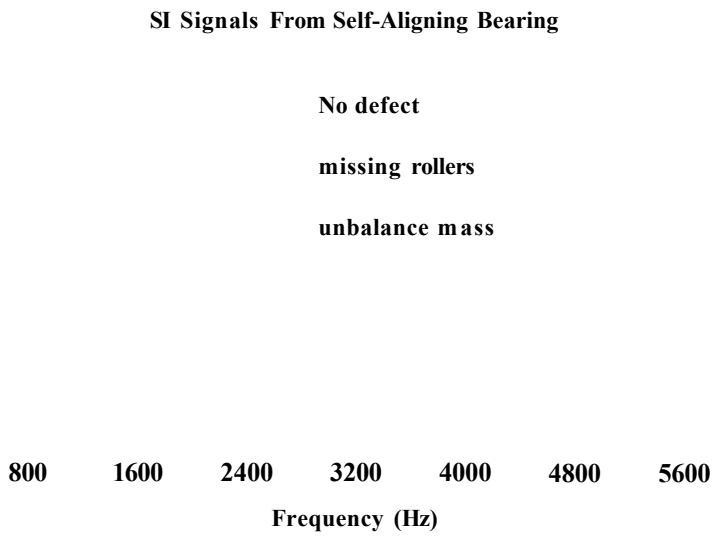

(a) Spectrums from sound intensity signals.

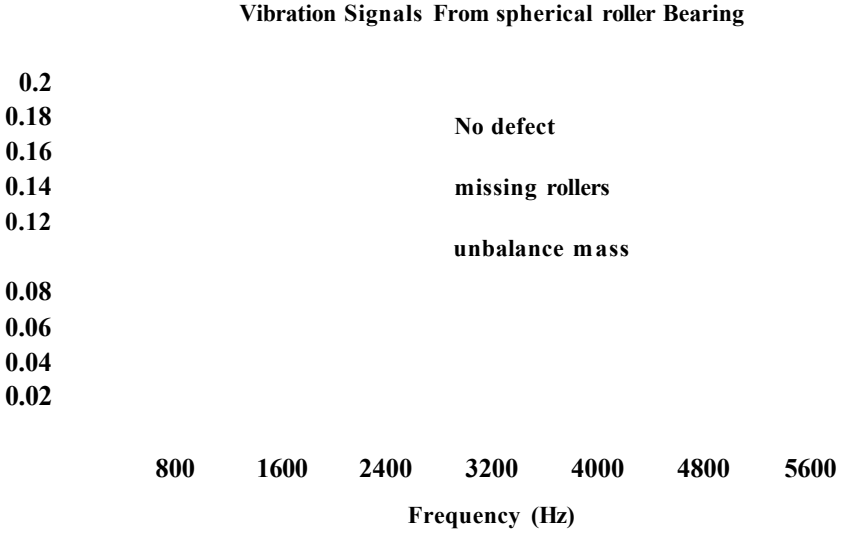

(b) Spectrums from vibration signals.

Figure 3.10 Spectrum of signals from self-aligning bearings with missing rolling elements and unbalance rotating mass running at lOOOrpm.

3.4 Conclusion From Pilot Study

The results obtained from sound intensity measurement technique showed good repeatability whereby readings taken at different time with the same conditions look very similar to each other. In general, the sound intensity spectrum can indicate the presence of abnormalities in rolling element bearing components. However, the frequency spectrum alone is not sufficient to identify the type of defect present in the bearing. Other signal processing methods need to be employed to carry out this task.

Many weaknesses in the performance of the test-rig were identified from the pilot study. The next task of the research project was to modify the test-rig, and to ensure that the performance of the test-rig is further improved. The list of tasks to be carried out were as follow:

(i) Replace the rubber isolators below the support bearing housings with mild steel support structure.

(ii) Install a photocell on the rig to create a pulse signal every time the test-shaft rotates, to be used as trigger signal when acquiring data for next experiment.

(iii) Modify the radial loading mechanism.

(iv) Modify support structure for the test bearing,

(v) Manufacture a new test-shaft made from high strength material (EN19T Steel) and ground finish with tolerance of ± 0.005mm.

All the measurement parameters and the set-up for future experimental work were noted and tested. The cylindrical roller bearing will be used in the next stage of the study because the dynamic behaviour of this type of bearing is easier to explain, therefore the theoretical analysis work can be done with better accuracy and with higher confidence.

COMPARISON STUDY: TIME DOMAIN ANALYSIS

4.1 Continuation of Previous Work

The initial task to be carried out in this study was to modify and to improve the test-rig as suggested in the previous chapter. The next task was to determine and to specify all the settings required to carry out the experimental works. The overall layout of the test-rig complete with the ancillary equipment are shown in the photograph labeled as Plate 4.1 below.

Plate 4.1 Photograph of the test rig.

The sound intensity transducers and measuring system were calibrated and checked regularly to ensure that they were working correctly. The type of bearing used for the initial experimental work was the cylindrical roller bearing NSK NF209K. The dimensions of the test-bearing used were d_{re} = 10mm, d_p = 65.0mm and number of rolling elements, n = 14 as shown in Figure 4.1, the test-bearings used for the experiment were cleaned using 1.1.1 Trichloroethane and Universal Oil was used as lubricant for all the bearings. The minimum load required for the rolling element bearing was 2% of the dynamic load rating to ensure ideal behavior of the roller as stated in the SKF general catalogue (1989). Therefore, during the study the radial load was maintained at 1.5KN. Defects were created by scratching a line across an outer race, an inner race and a rolling element using an etching pen. The width of the defects ranged from 1.40mm to 2.40mm and the depth ranged from 0.44mm to 1.50mm. Typical defects are shown in Plate 4.2(a) to (c) which represent line defects on the rolling element, outer race and inner race of the test-bearing respectively.

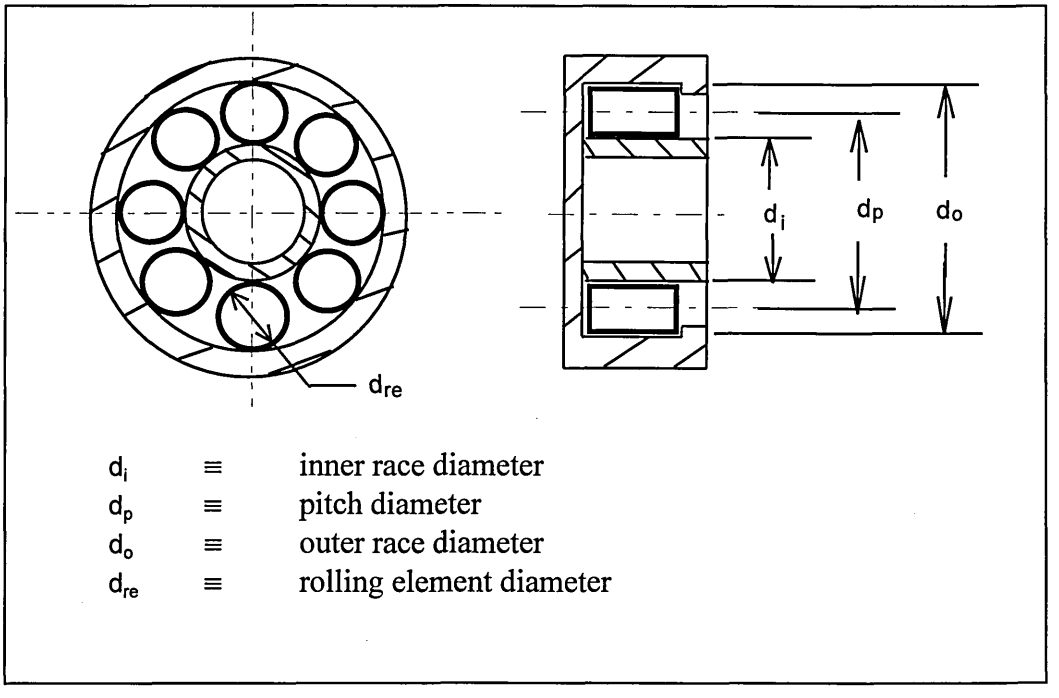

Figure 4.1 Schematic diagram of a cylindrical roller bearing

(a) Rolling element defect

(b) Outer race defect

(c) Inner race defect

Plate 4.2 Photographs of the bearing defect manufactured using etching pen.

4.2 Set up for the Measuring and Analysing Equipment

The maximum voltage at the input channels must be set for the Bruel and Kjaer 2032 dual channel analyser before sound or vibration measurements can be carried out. For sound measurement, equation (2.1) was used to derive the formula required to calculate the estimated maximum voltage settings, given the overall dB value of the sound signals.

$$p_{rms} = p_{ref} \times 10^{(L_p/20)} \tag{4.1}$$

$$v_{rms} = p_{rms} \times (microphone\ \ sensitivity). \tag{4.2}$$

For sinusoidal signals, the maximum voltage $V_{\max} = \sqrt{2} \times v_{rms}$. Some values of this variable are presented in Table 4.1, the value for microphone sensitivity is set to $41.5mV/Pa$ which was determined during calibration of the two microphones.

Table 4.1 A guideline for setting the maximum voltage for the Bruel and Kjaer 2032 analyser.

Lp (dB)	p_{rms} (Pa)	v_{rms} (mV)	V_{max} (mV) (sinusoidal)
80	0.200	8.3	11.7
85	0.335	13.9	19.7
88	0.502	20.8	29.4
90	0.632	26.2	37.1
92	0.796	33.0	46.7
95	1.125	46.7	66.0
98	1.589	65.9	93.2
100	2.000	83.0	117.4
105	3.557	147.6	208.7
110	6.325	262.5	371.2
115	11.247	466.8	660.2
120	20.000	830.0	1173.8

Most sound level measurements carried out fell between 80dB to 100dB. Therefore, the maximum input voltage for the Bruel and Kjaer 2032 analyser was set between $15mV$ up to $120mV$. However, the value of maximum voltage setting will affect the amplitude resolution of the sampled sound signals. The format used by the analyser to represent the amplitude of measured signals is real single precision with 2's complement notation, and each amplitude value is stored using a 16-bit word in a format as indicated in Figure 4.2.

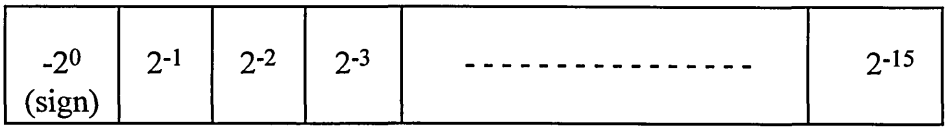

Figure 4.2 Real single precision data format.

The formula for calculating the amplitude resolution can be written as

$$Resolution = \frac{V_{max} - (-V_{min})}{2^{15}}. \qquad (4.3)$$

Therefore, if the maximum voltage was set to $15mV$ the amplitude resolution of the displayed signals was $916\text{x}10^{-9}V$ ($22.1\mu Pa$), and the amplitude resolution for maximum voltage setting at $120mV$ was $7.32\text{x}10^{-6}V$ ($176\mu Pa$).

The other parameters set up as shown in Table 4.2 were used for measuring vibration and sound signals for the research work. These parameters were chosen based on the results obtained during the pilot study, which gave optimum results for the different shaft speeds so that the signals being measured contain samples of true signals to represent the characteristics of the test-bearing. Trigger signals obtained from the slotted-disk mechanism attached to the shaft were used to start each measurement to ensure that the signals measured always begin from the same position relative to the shaft revolution.

Table 4.2 Measurement set up for the Bruel and Kjaer 2032 analyser.

Speed of Shaft (rpm)	Control Knob Position	Frequency Range (KHz)	No. of Shaft Revolution per Sampling Period	Length of Microphone spacer (mm)
500	20	1.6	4.16	50
1000	27	3.2	4.16	12
1500	34	6.4	3.12	12
2000	41	6.4	4.16	12
2500	48	6.4	5.20	12
3000	55	12.8	3.12	6
3500	61	12.8	4.16	6
4000	67	12.8	5.20	6
4500	75	12.8	6.24	6
5000	82	12.8	7.28	6

The practical range of frequency that can be covered from using the sound intensity measurement technique was dependent on the length of microphone spacer that was used to separate the two microphones as indicated in Table 4.3 below.

Table 4.3 Practical frequency range for sound intensity measurement

Length of Microphone Spacer (mm)	Frequency Range (Hz)
6.0	128 to 12800
8.0	100 to 10000
12.0	64 to 6400
50.0	16 to 1600

All signals captured and displayed using the Bruel and Kjaer 2032 analyser were then imported to a desktop computer. Data was imported using an IEEE card for post-processing using time domain, frequency domain, and wavelet analysis methods. A list of the macros and command files used for importing the data, for post-processing and for displaying the processed data using Dadisp(TM) software is presented in Appendix B.

4.3 Identification of Bearing Defects Using Statistical Method

The performance of utilising different types of signal, namely, sound intensity, sound pressure, air-particle acceleration and vibration signals to detect the presence of line defect in a rolling element, an outer race and an inner race of a bearing component was evaluated at this stage. The type of defects used for the experiment were already shown in Plate 4.2.

4.3.1 Statistical Moments and Beta Distribution Function Parameters

The well established statistical central moments such as the crest factor, and kurtosis were utilised to indicate the presence of a defect on the rolling element, inner race and outer race of the test bearing. In addition, other statistical parameters derived from the beta distribution function were also used. A comparative study from results obtained using the different types of signal and from results obtained using different types of statistical analysis was performed at this stage.

The statistical analysis method was used first because of its simplicity and fast computation time. A computer program was developed using C language to perform the calculations, a listing of the program is shown in Appendix C. A theoretical derivation of all the statistical parameters used in this study are presented in Chapter 2.

Typical statistical parameter values obtained from deterministic signals are shown in Table 4.4 and Figure 4.3. All of the statistical parameters including kurtosis, crest factor, and variables derived from beta distribution function a and b for the deterministic signals were less than 2. For random signals with normal distribution, the kurtosis value was 3 and the values of beta function variables a and b were both close to 6.

Table 4.4 Summary of the statistical analysis of deterministic and random signals.

Type of Signals	Kurtosis	Crest Factor	'*a*'	'*b*'
Sine wave	1.5	1.4	0.5	0.5
Triangle wave	1.8	1.7	1.0	1.0
Square wave	1.0	1.0	0	0
Random Signals, Normal distribution	3.1	1.8	6.3	5.9
Random Signals, Flat distribution	1.8	1.7	1.0	1.0
Sine + Normal	1.8	1.8	1.9	1.9
Sine + Flat	1.8	2.0	1.4	1.4

The statistical variables utilised for the study were kurtosis, crest factor, and beta distribution function parameters a and b. The third central moment namely skew was not included in the study because the odd central moment of the statistical distribution only indicates whether the distribution is skewed to the right or to the left of the median value, and this value does not reflect the condition of the test bearing.

Samples of the different shape of Beta distribution function derived from different values of parameters a and b are shown in Figure 4.4. As the values of a and b become large the peak of the distribution become sharp and thin, and as the values of a and b becomes small, the shape of the distribution becomes wide and spread. When the values of a and b are both equal to 1.0, the shape of the distribution becomes a flat horizontal line. When the value of a is greater than b the shape of the distribution is skewed to the right and when the value of b is greater than a the shape of the distribution was skewed to the left. These are the common shapes that are encountered when using the beta distribution function parameters.

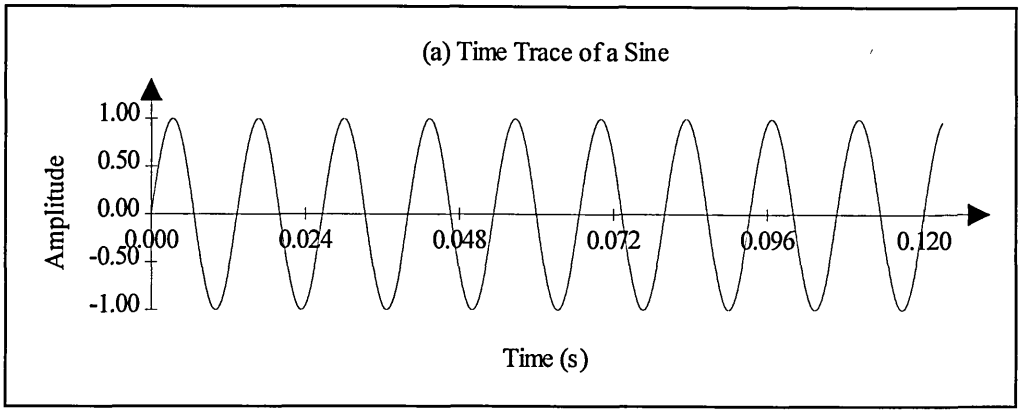

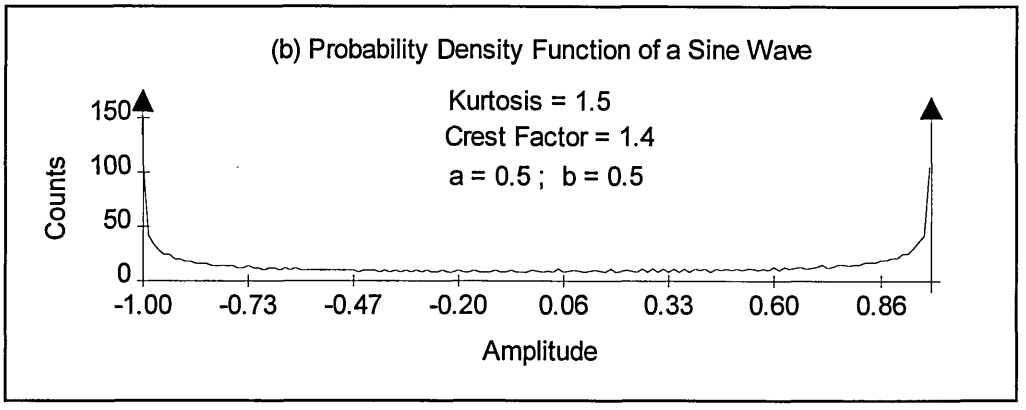

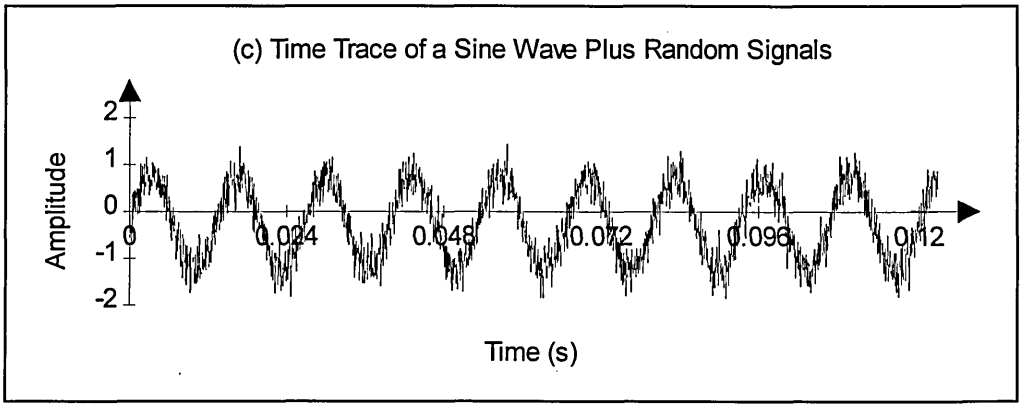

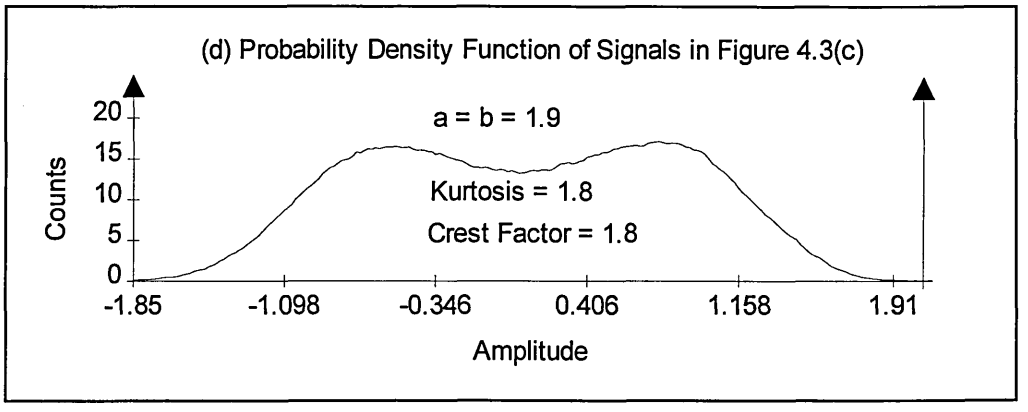

Figure 4.3 Plots of the time traces and probability density functions of deterministic and random signals.

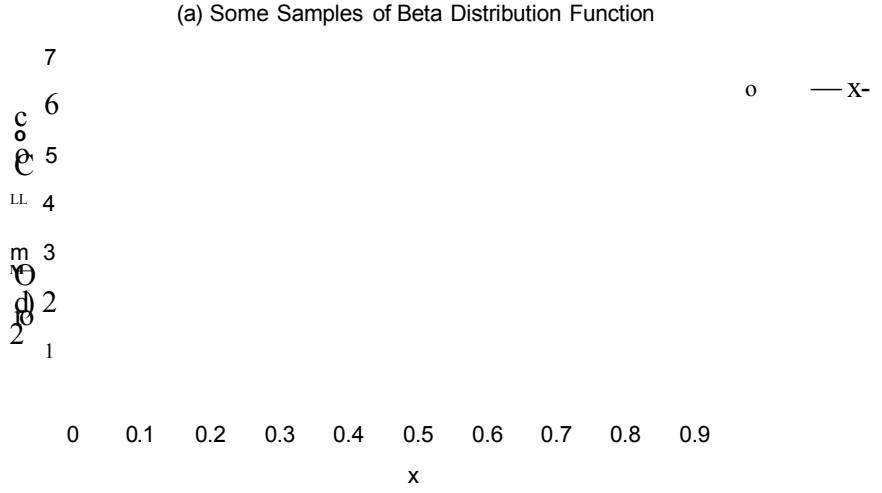

Figure 4.4 Several shapes of Beta distribution function for different values of 'a' and 'b \

Kurtosis and crest factor were used to describe the spread of the probability distribution function. However, crest factor was less sensitive to the presence of an extreme maxima in a signal compared to kurtosis. This can be seen by observing Equations (2.29) and (2.30) where a maximum value affect crest factor by a factor of one, and kurtosis is affected by a factor to the power of four. On the other hand, both of the beta function parameters *a* and *b* are less affected by the presence of an extreme maxima in a signal compared to kurtosis as shown in Equations (2.34) and (2.35).

Defective rolling element bearing components as shown in Plate 4.2 were used to study the performance of utilising the air particle acceleration signal to identify the type of defect present in the test bearing. Results from the analysis of sound pressure and vibration signals are also included for comparison.

As a start the time series of vibration, sound pressure and air particle acceleration signals from the bearing without induced defect are presented in Figure 4.5 and the time series of the same signals from the bearing with an outer race induced defect are shown in Figure 4.6. In both cases, the speed of the shaft was maintained at 2000rpm. These readings were taken under typical laboratory condition where the effect of background sound level was considered to be minimal. It is obvious from Figure 4.5 that the vibration signals from the normal test bearing do indicate some random peaks due to imperfections in the bearing elements. The time series of sound pressure for the same bearing shows the effect of amplitude modulation between two components of a high and a low frequency signals. Whereas, the time series of air-particle acceleration signals show uniform oscillations with smaller amplitude modulation by the low frequency components compared to the previous two signals. Vibration signals from Figure 4.6 indicate uniform peaks with equal interval which is the characteristic of an outer race line defect in the test bearing. The peaks from the sound pressure signals are not as sharp as the peaks shown in the vibration signals and the low frequency modulation is still indicated from the sound pressure signals. The peaks in the air-particle acceleration signals are about the same feature as the peaks from sound pressure signals but the low frequency modulation has been eliminated, this shows that the low frequency modulation presence in the sound pressure signals was not emitted by the test bearing. This modulation could be due to other moving components in the test rig such as the belt-drive unit or the motor. The quality of air-particle acceleration to indicate an impulsive signals is better than the quality of sound pressure and slightly inferior to the quality of vibration signals. This shows that the vector property of the air-particle acceleration signals give better signal-to-noise ratio compared to the signals obtained from the measurement of sound pressure.

The effect of background noise on the measurement of sound pressure signals is highlighted in Figure 4.7(a). This signal was taken in the presence of transient

background noise emitted by slamming the door in the laboratory. All statistical variables calculated from this signal do not indicate the presence of an impulsive defect signal coming from the test bearing. However, in Figure 4.7(b) the air-particle acceleration signals clearly discard the effect of background noise, and the statistical variables calculated from this signal are able to indicate the presence of defect in the test-bearing.

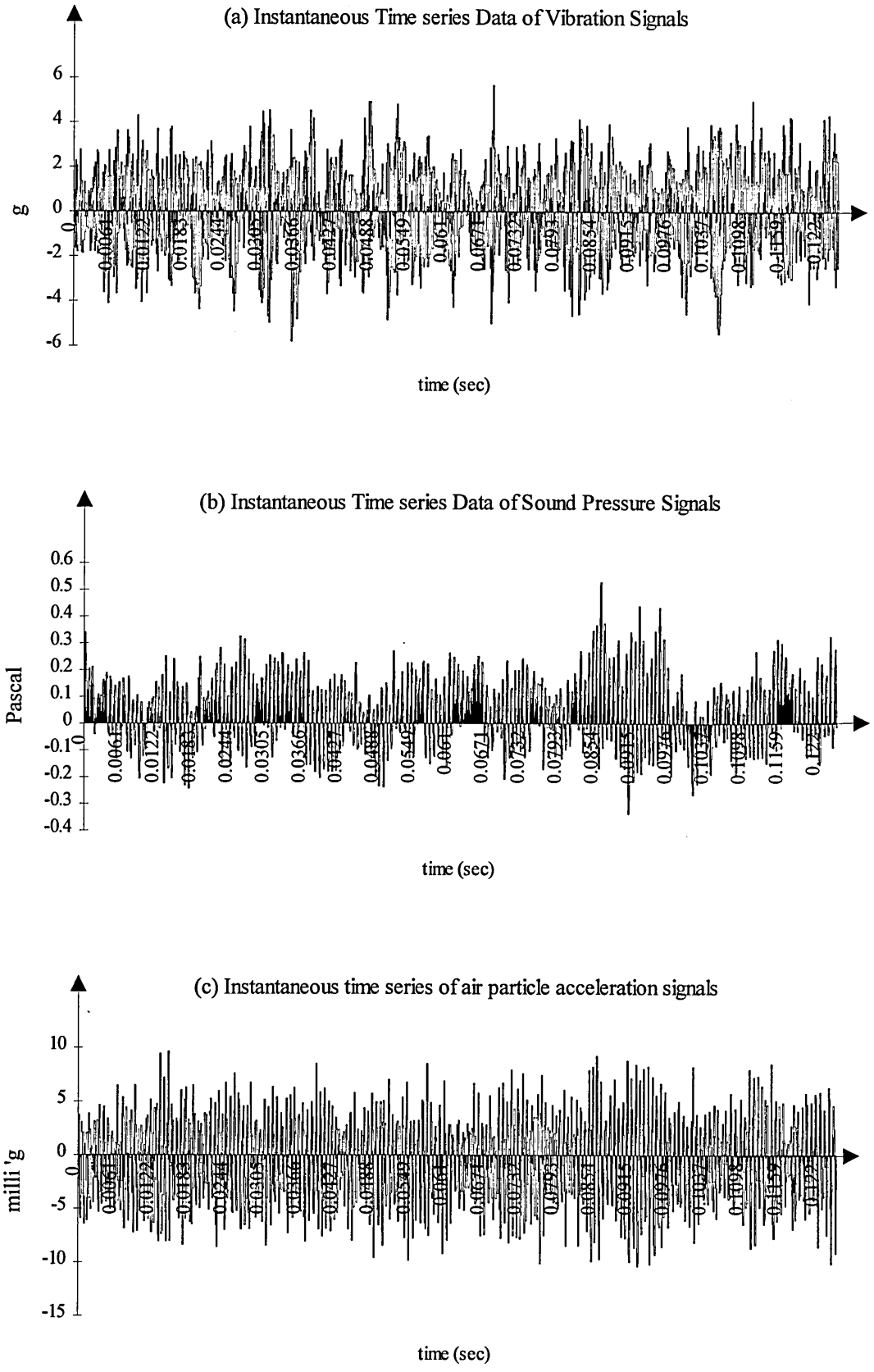

Figure 4.5 Instantaneous time series of different types of signal from normal bearing running at 2000rpm.

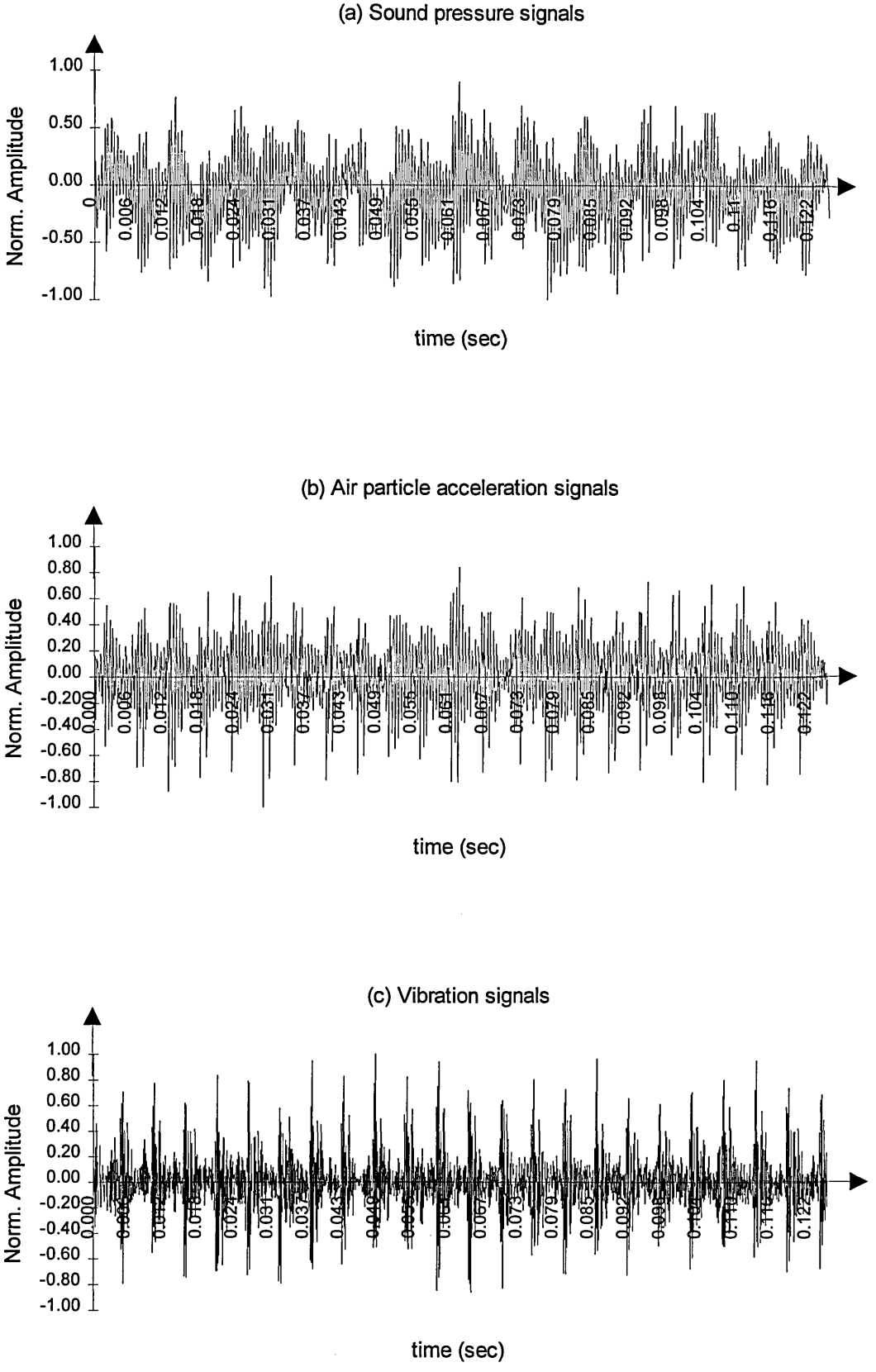

Figure 4.6 Instantaneous time traces of different types of signal from bearing with outer race defect running at 2000rpm.

(a) Sound pressure signals from bearing with rolling element defect

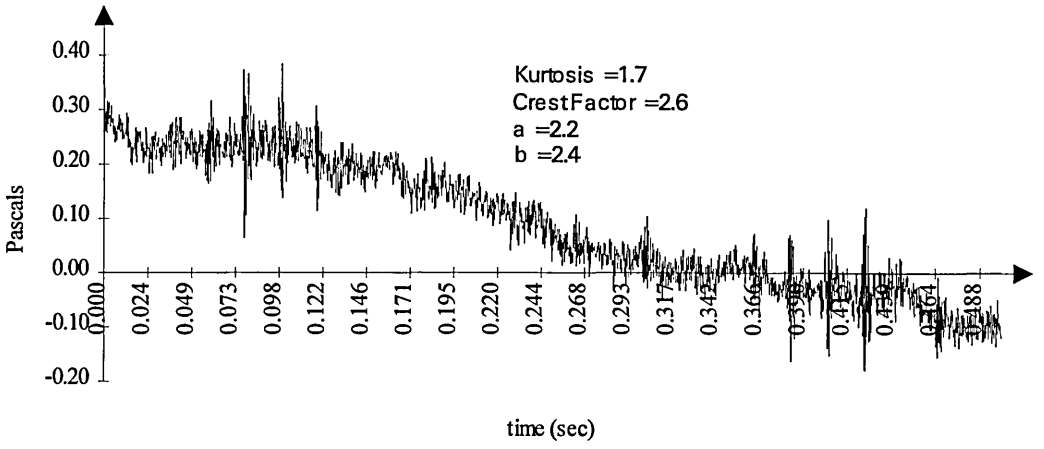

(b) Air particle acceleration signals from bearing with rolling element defect

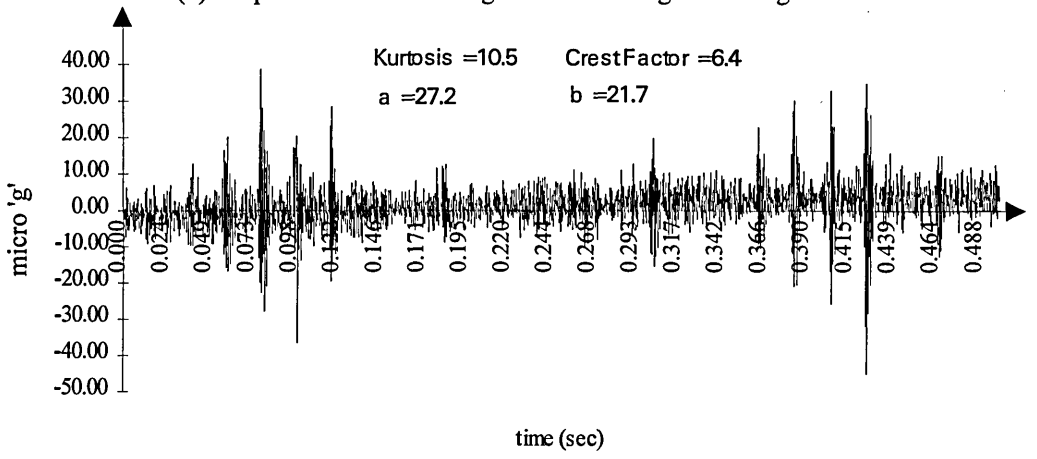

Figure 4.7 Time traces of sound pressure and air particle acceleration signals from bearing running at 500rpm.

The advantages of using air-particle acceleration signals compared to using sound pressure signals were also indicated even when the background noise level was considered to be minimal. Figure 4.8 shows time traces of sound pressure signals from rolling element bearing with several different conditions. The induced defects used for this test were created using an etching pen and these defects are already shown in Plate 4.2. Statistical variables calculated from the time traces in Figure 4.8, shows that using sound pressure signal it is difficult detect and identify the presence of defect on the outer race, and on the inner race of the test-bearing. However, the presence of the rolling element defect can be detected qualitatively and quantitatively, by observing the overall impulses shape and by calculating the statistical variables respectively as shown in Figure 4.8(c). The amplitude in this Figure was normalised to the maximum value in order to maintain a uniform scaling on the graph.

Figure 4.9 shows the air particle acceleration signals from the same experimental conditions as in Figure 4.8. These results show that air-particle acceleration signals can indicate the presence of a defect in the test-bearing better than from using sound pressure signals. The overall background noise level for this experiment ranged from 54.0 to 58.0dB, and the overall noise level from the test-bearing ranged from 70.0dB to 78.0dB linear scale. Therefore, the effect of background noise in this case was considered to be minimal. The presence of background noise, even at a low level can affect the measurement of sound pressure signal. The result can give a false indication on the condition of bearing being monitored if only the statistical variables were used. In both cases the results from using air-particle acceleration signal are superior at picking up the impulsive nature from a defective bearing. Therefore, the results obtained from measurement of air-particle acceleration signals are more reliable compared to the results from measurement of sound pressure signals.

Results from the measurement of vibration signals are shown in Figure 4.10 for comparison purposes. As expected the indication of impulsive signals from a defective bearing was much clearer from the vibration signals. One interesting feature is observed from these signals, the impulses are evenly spaced in the case of outer race and inner race defects. Whereas, for the case of rolling element defect, the time of occurrence of the impulsive signals are unpredictable. This is due to the complex mechanism that

caused these impulsive signals in a defective rolling element bearing. These signals are dependent on the relative rotation of the defective rolling element with respect to the outer race and inner race of the bearing component. Moreover, since the test bearing was only loaded at the top, the rolling element was tightly squeezed when it passed through the top of the shaft. On the other hand, at the bottom of the shaft the clearance between the rolling element and the races were relatively loose. Any micro stick-slip that occurs during each revolution of the rolling element around the shaft caused a shift in the position of the rolling element defect with respect to the inner and outer races of the bearing. Therefore, the timing when the defect was in contact with either the inner or the outer race was randomised. As a result, the train of impulses which was the product of this process, occurred randomly in the time trace of the measured signals.

The amplitudes in Figures 4.7, 4.8 and 4.9 are normalised with respect to the largest amplitudes that were measured from each type of signal. For instance, all of the largest amplitudes occur from the operation of the bearing with a rolling element defect. Therefore, all the graphs for rolling element defect are normalised from zero to one. The rest of the graphs are normalised with respect to this largest value. A summary of the statistical variables calculated from this study is shown in Table 4.5. This table shows the relative performance of air-particle acceleration signals to indicate the presence of defect in a rolling element bearing, compared to the performance of sound pressure and vibration signals.

It is interesting to see that the scaling of the normalised amplitude in all the graphs in Figure 4.9 are almost the same as their counterpart in Figure 4.10. This shows that the sensitivity of air-particle acceleration and vibration signals to detect defect signals are almost identical. However, the absolute values of the amplitude obtained from each type of signal are very far apart. For example, the vibration signals are measured in units of 'g' ($1g = 9.81 m/s^2$) and the air-particle acceleration signals are measured in units of micro 'g' ($1 \times 10^{-6}\, g$).

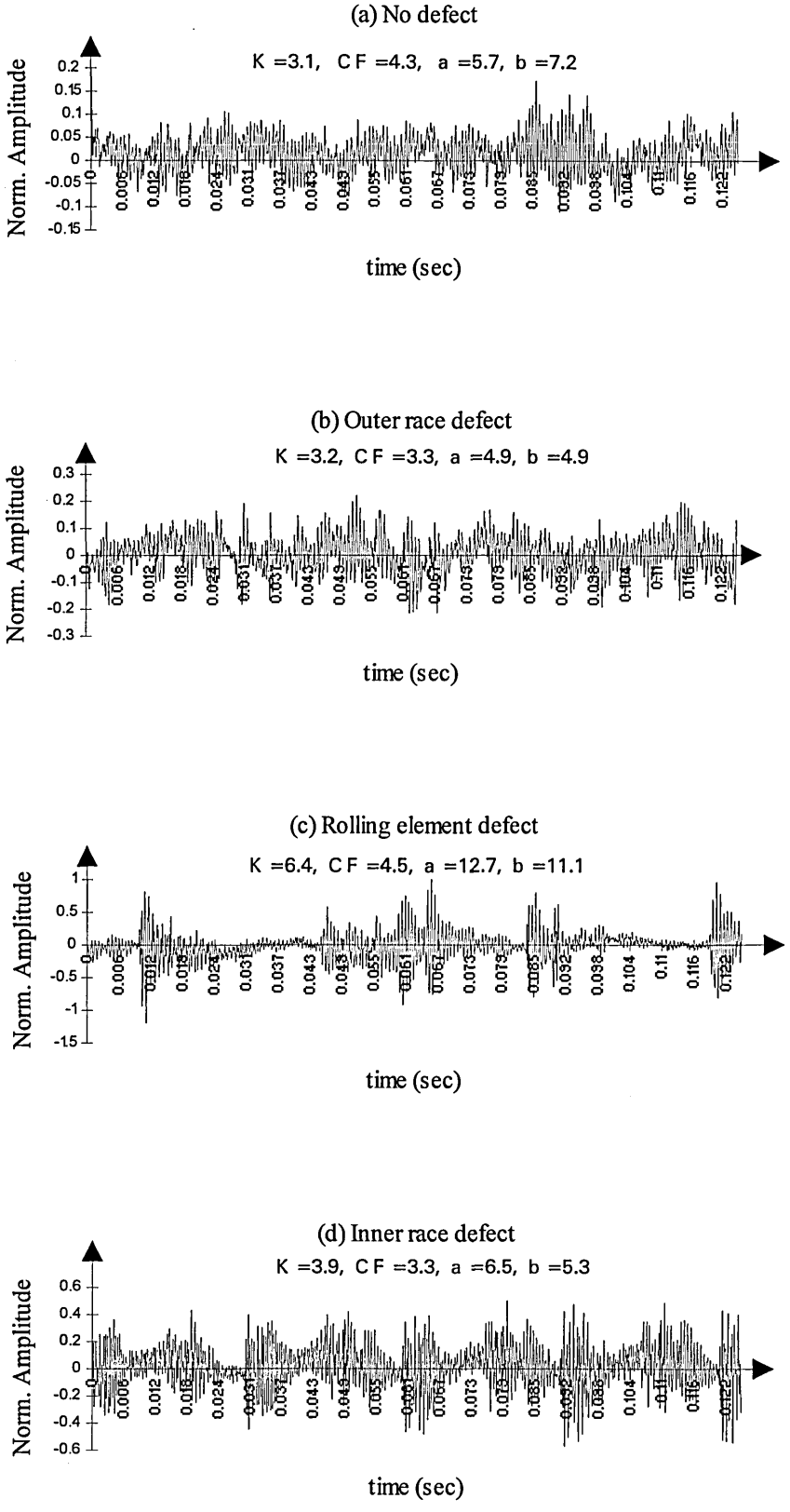

Figure 4.8 Sound pressure signals from bearing running at 2000rpm

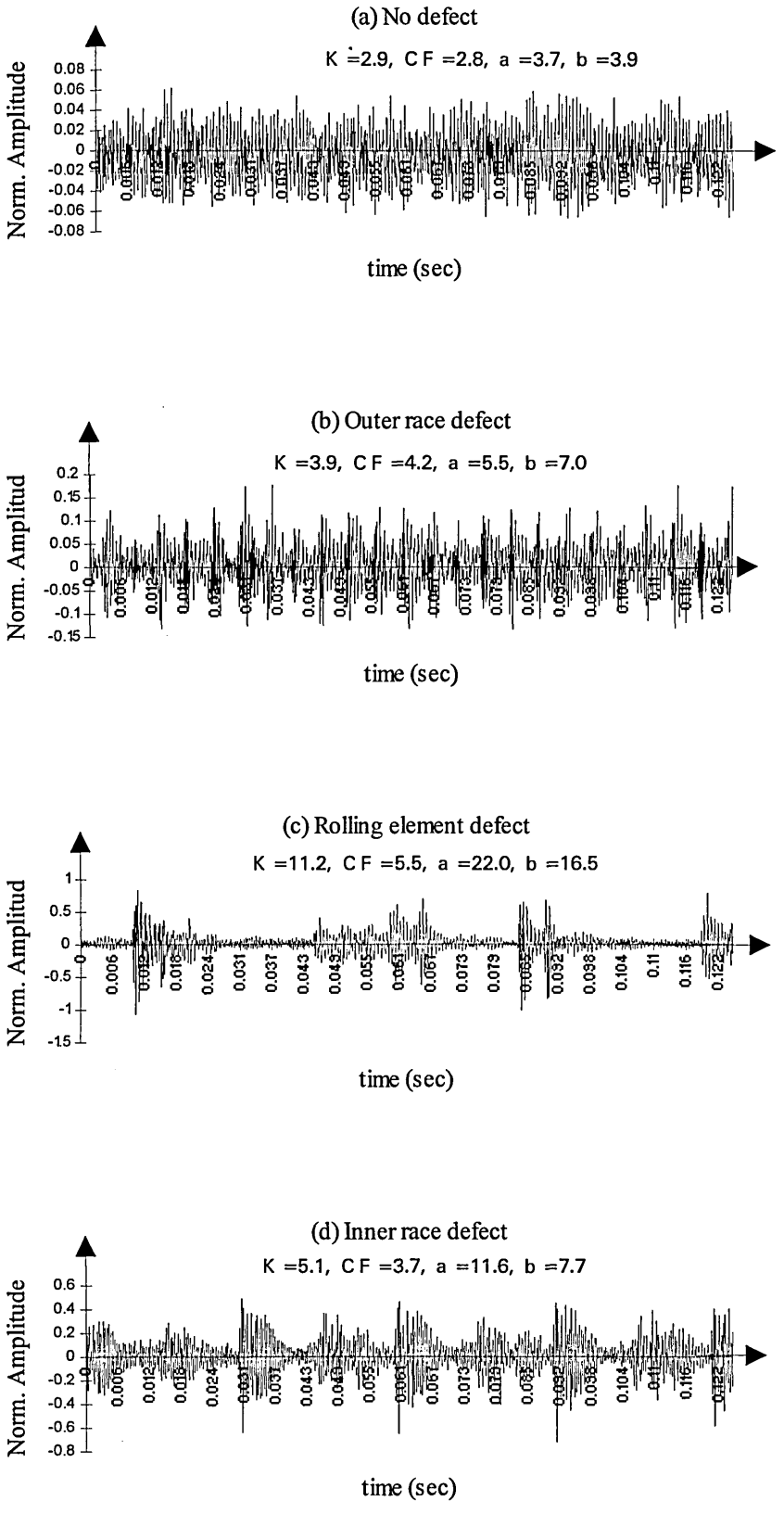

Figure 4.9 Air particle acceleration from bearing running at 2000rpm

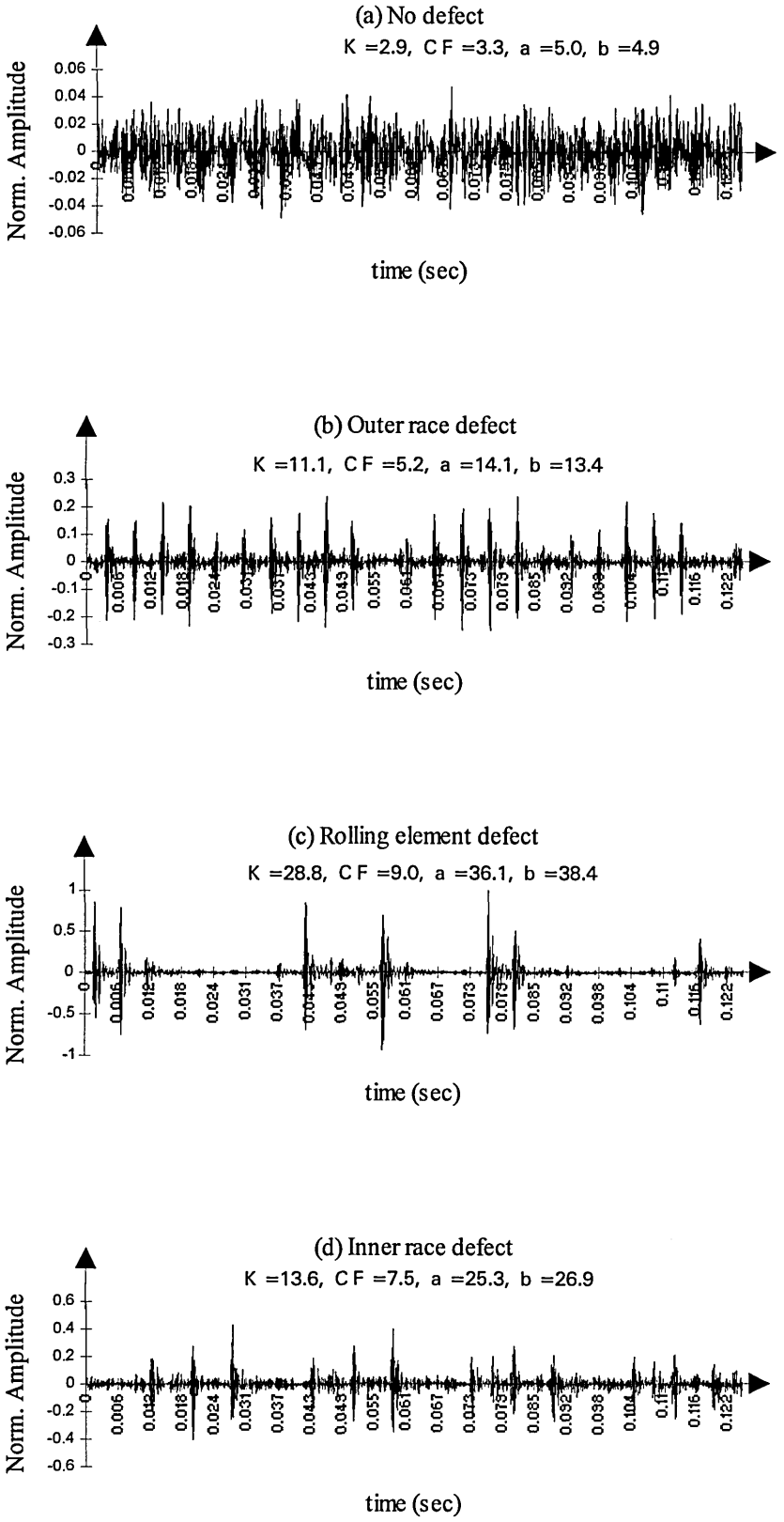

Figure 4.10 Vibration signals from bearing running at 2000rpm.

Table 4.5 A Summary of the statistical variables from the time-domain analysis study. Speed of shaft = 2000rpm.

	No Defect	Outer Race Defect	Rolling Element Defect	Inner Race Defect
Sound Pressure	+Kurt. = 3.1 C. F. = 4.3 a = 5.7 b = 7.2	Kurt. = 3.2 C. F. = 3.3 a = 4.9 b = 4.9	Kurt. = 6.4 C. F. = 4.5 a = 12.7 b = 11.1	Kurt. = 3.9 C. F. = 3.3 a = 6.5 b = 5.3
Air-particle Acceleration	Kurt. = 2.9 C. F. = 2.8 a = 3.7 b = 3.9	Kurt. = 3.9 C. F. = 4.2 a = 5.5 b = 7.0	Kurt. = 11.2 C. F. = 5.5 a = 22.0 b = 16.5	Kurt. = 5.1 C. F. = 3.7 a = 11.6 b = 7.7
Vibration	Kurt. = 2.9 C. F. = 3.3 a = 5.0 b = 4.9	Kurt. = 11.1 C. F. = 5.2 a = 14.1 b = 13.4	Kurt. = 28.8 C. F. = 9.0 a = 36.1 b = 38.4	Kurt. = 13.6 C. F. = 7.5 a = 25.3 b = 26.9

+Kurt. ≡ Kurtosis
C. F. ≡ Crest Factor

4.3.2 Classification of Defect Using Statistical Method

At this stage, an attempt was made to classify the type of defect present in the test bearing based on the calculated values of kurtosis, crest factor and beta distribution function parameters a and b. A comparison study was also performed to evaluate the effectiveness of using the different types of signal to indicate the presence of a defect in the rolling element bearing. Another type of defect was included, whereby the test bearing was operated with one missing rolling element. Some of the results from this study are presented as a scatter plot of kurtosis versus crest factor and beta function parameter a versus b as shown in Figures 4.11 and 4.12.

Results from the study show that all of the signals used in the experiment failed to differentiate between the condition of a normal bearing and the condition of a missing roller. This is the case, even from the results obtained using vibration signals. From

Figure 4.11, the plot of kurtosis versus crest factor from air-particle acceleration and vibration signals are able to group the different types of defect used into different areas on the graph. However, this can only be used as a guide in identifying the type of defect used in the experiment. Other analysis methods must be implemented to determine the type of defect presence in the test bearing. The magnitude of beta function parameters a and b are consistently larger than the magnitude of kurtosis and crest factor as indicated in Figure 4.12. However, there is no significant advantages obtained from using beta function parameters a and b compared to using kurtosis and crest factor from the experiment. Both of the statistical methods could indicate the presence of abnormality in the test bearing but the type of abnormality is difficult to determine.

4.3.3 Effect of Shaft Speed

In an ideal situation, the results from using a statistical method should be independent of the speed of shaft. However, from the experimental results obtained in the study, the statistical variables are affected by speed of the shaft as shown in Figure 4.13. The features in this figure represent the overall characteristics of the results from using the statistical method. Each data in the figure is taken from an average of ten readings from bearing with the rolling element defect.

The pattern of the plots are similar in all the three types of signal measured when the shaft speed is between 500rpm to 1500rpm. It is interesting to see that each signal behaved differently than the others when the shaft speed is higher than 1500rpm. From the sound pressure signals, the magnitude of the statistical variables become smaller as the speed increases. In the case of air particle acceleration, the values of the statistical variables decrease when the speed is higher than 1000rpm. Most of the variables reach a minimum value when the shaft speed is equal to 2000rpm, and after that they start to increase again slightly as the speed is set higher than 2000rpm. Finally, the statistical variables calculated from vibration signals oscillate about their mean level when the shaft speed is set higher than 1000rpm.

The main reason why the statistical variables are lower at the speed range of 1500rpm and 2500rpm is that at this speed range, the longitudinal natural vibration of the test-bearing support mechanism is encountered. As a result, the bearing housing vibrated more rigorously at this speed, and the overall vibration and sound signals produced are corrupting the signals produced by the defective component. The difference between the peaks and standard deviations of the measured signals tend to become smaller at this speed range. Since all of the statistical variables used are dependent on this variable they also tend to become smaller. Therefore, the relatively poor performance of the statistical method are mostly due to the natural frequency of the test-rig structure. This is confirmed by the frequency spectra obtained from another set of impact tests shown in Figure 4.14. The spectra show critical frequency peaks at 26Hz, 35Hz, and 49Hz which are very close to the operating frequency of the shaft speed at 1500rpm (25Hz), 2000rpm (33.3Hz), and 3000rpm (50Hz) respectively.

Other examples which reveal the effect of exciting the natural frequencies of the support structure are shown in Figures 4.15 and 4.16. The earlier figure presents the time traces of sound pressure, air particle acceleration, and vibration signals from bearing with outer race line defect. The speed of the shaft at this instance was set to 1000rpm. The latter figure presents similar types of signals with the same bearing condition but the shaft speed at this stage is set to 2000rpm. It is clear that the peaks in Figure 4.15 are sharper and cleaner than the peaks in Figure 4.16, and the natural vibration of the support structure for the test bearing has corrupted the signals in the latter figure resulting in poor performance of the statistical method.

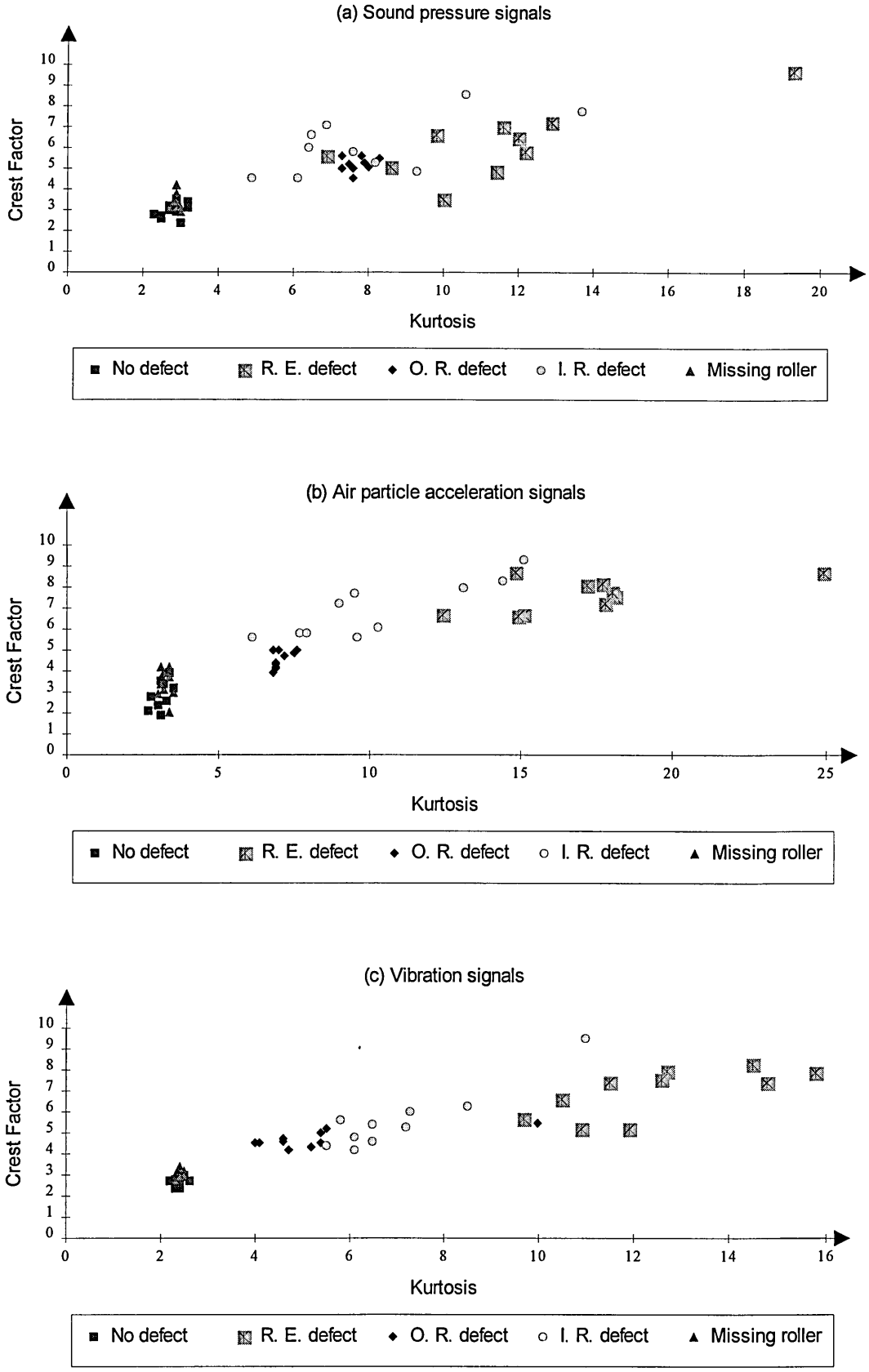

Figure 4.11 Plot of kurtosis versus crest factor from a test-bearing running at 500rpm

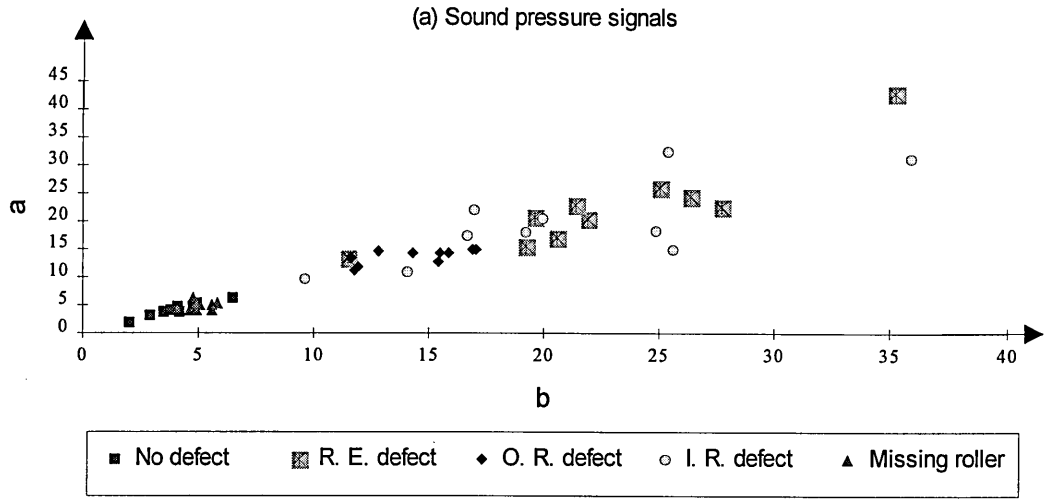

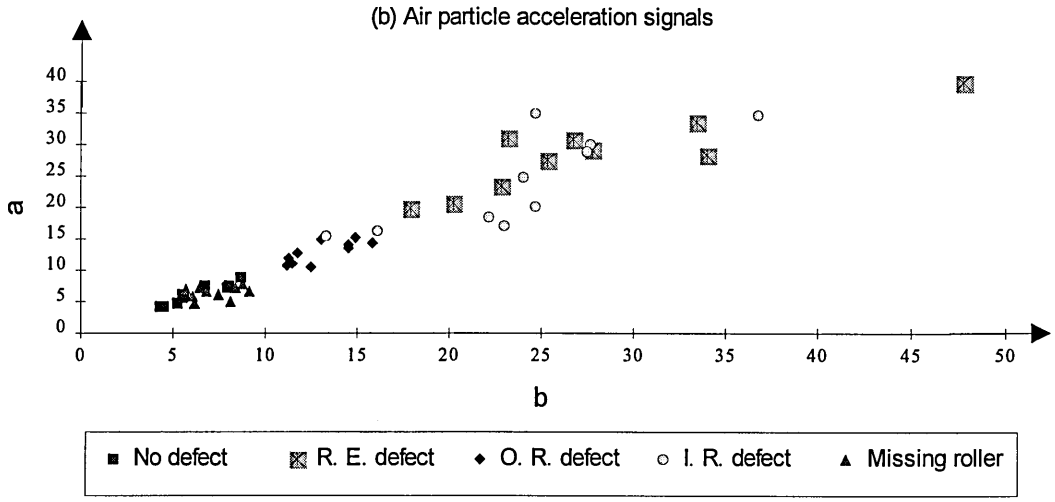

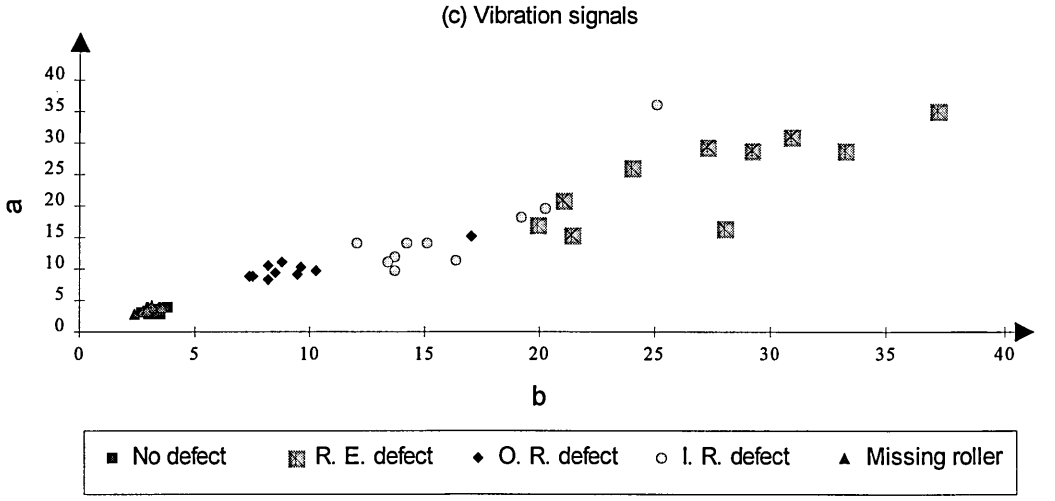

Figure 4.12 Plot of beta function parameters a vs b from a test-bearing running at 500rpm

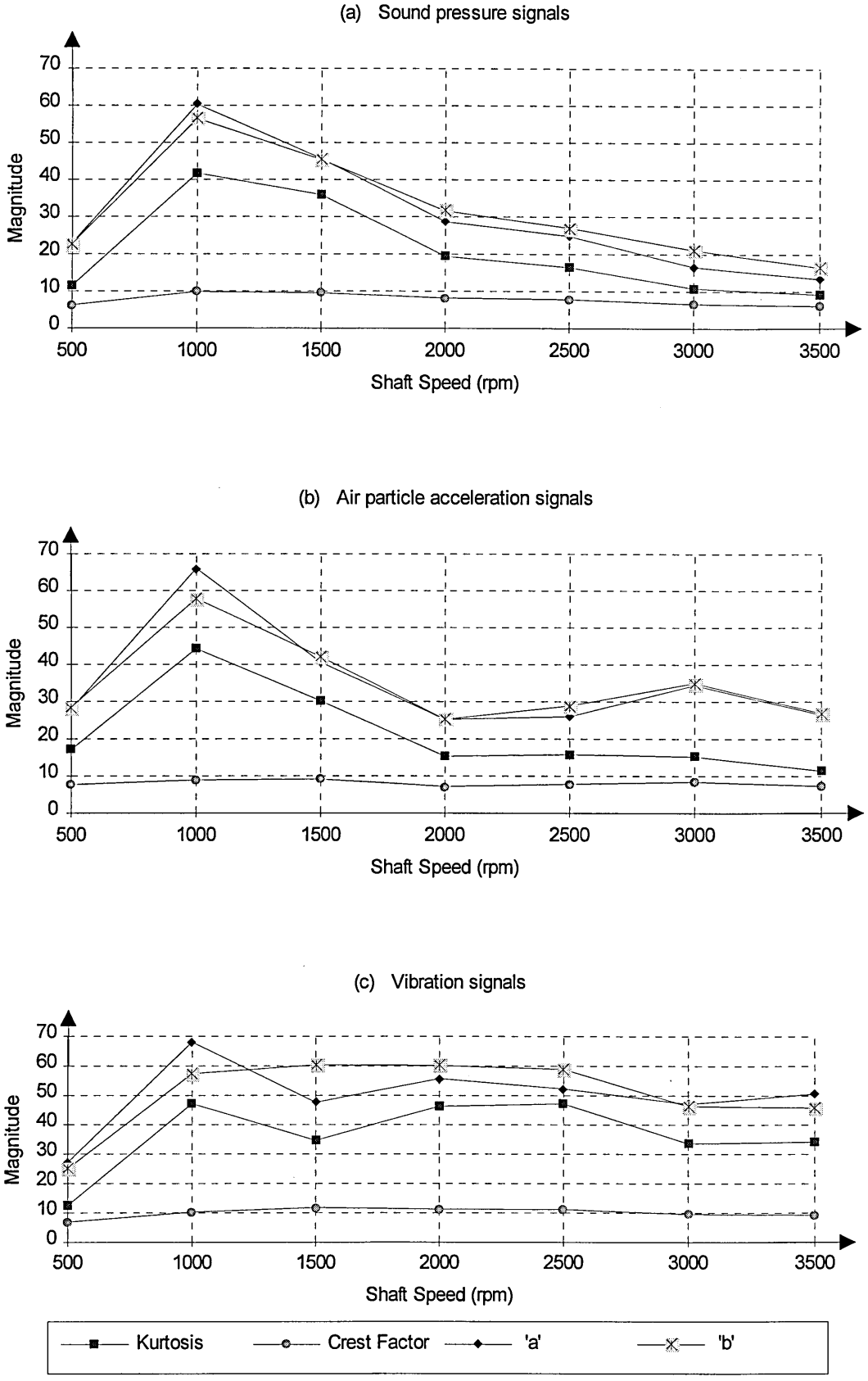

Figure 4.13 Plot of statistical variables versus shaft speed from bearing with rolling element defect.

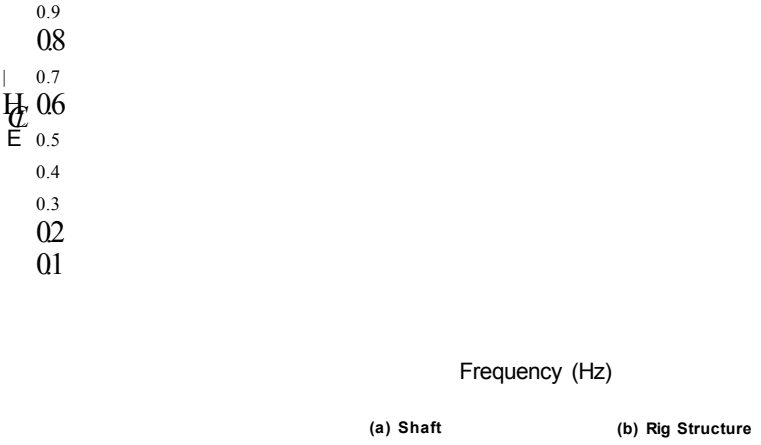

Figure 4.14 Vibration spectra from longitudinal impacts on the shaft and rig structure.

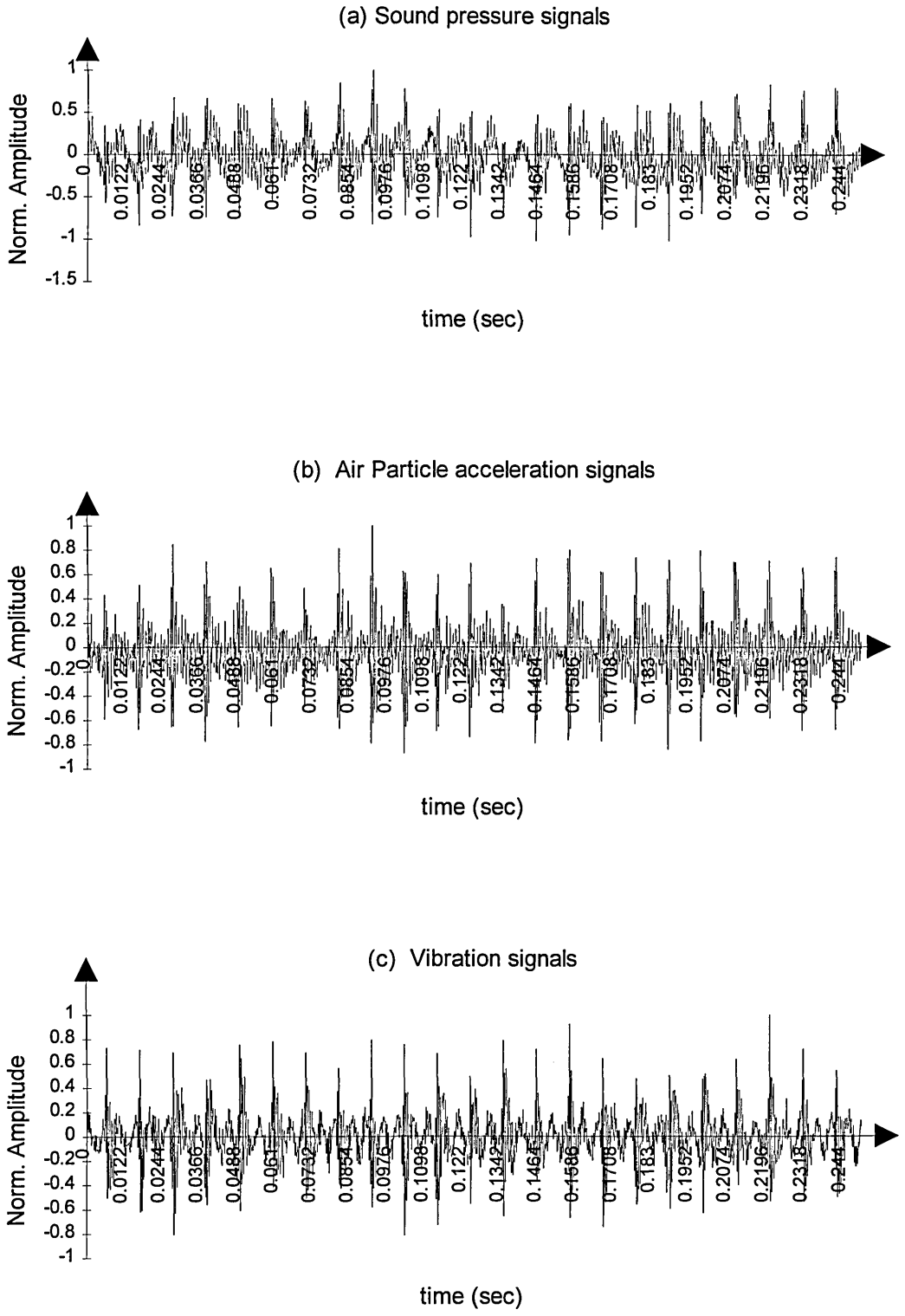

Figure 4.15 Time traces of different types of signals from bearing with outer race defect running at 1000rpm.

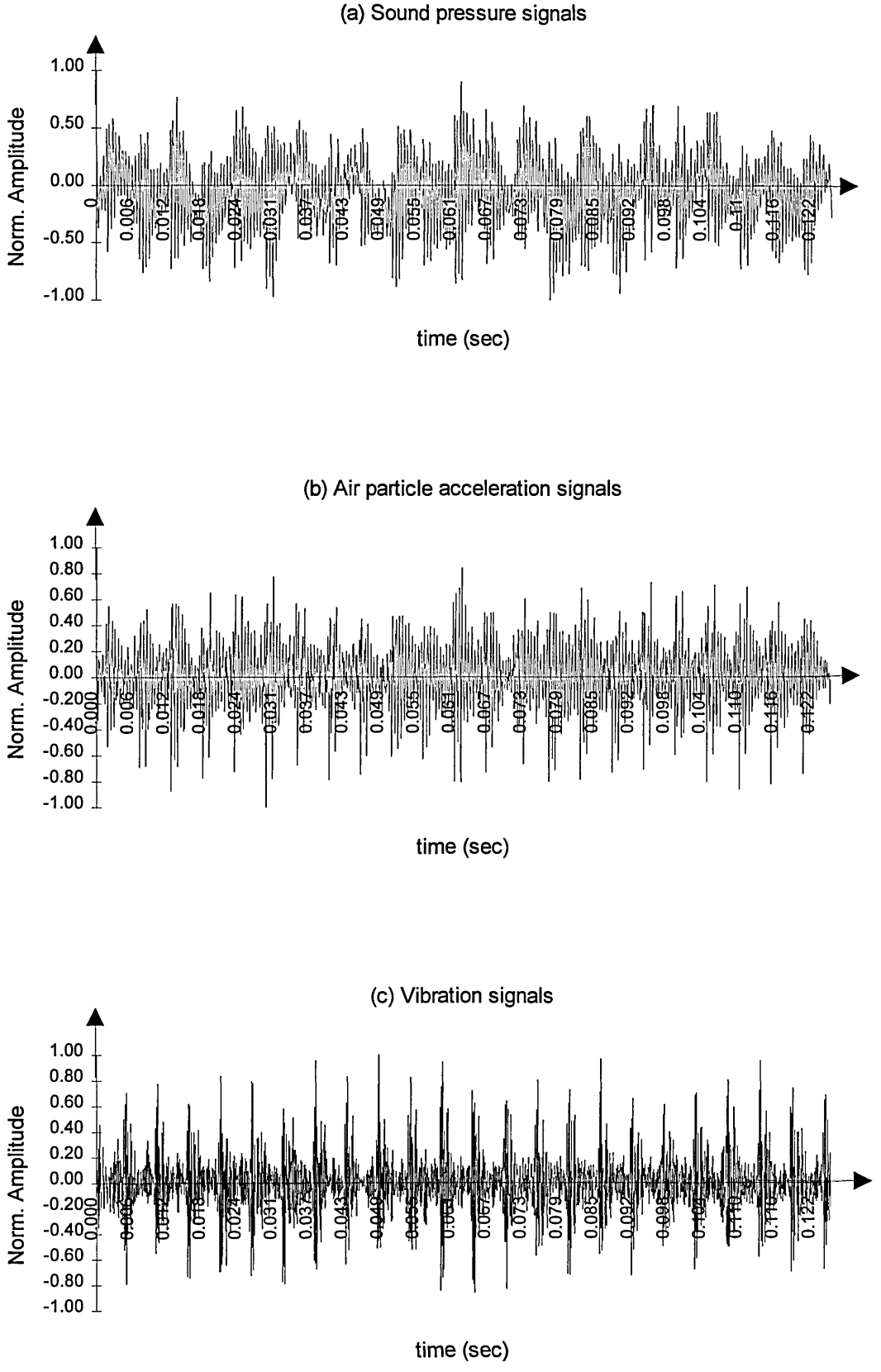

Figure 4.16 Time traces of different types of signals from bearing with outer race defect running at 2000rpm.

4.4 Development of Correlated Time Averaging Method

It is extremely difficult to perform synchronous time averaging on the signals measured from the bearing with a defective rolling element. This is due to the random phase of the impulses that are measured from such a bearing as shown in Figures 4.8(c), 4.9(c), and 4.10(c). As a result, the position of impulses in one time trace will be different than in the other traces, and when many averages from these traces are added together all the impulses that are characteristics of a defective bearing will disappear. These impulses are disappearing together with the random noise because of their randomness in phase. A new method called correlated time averaging is developed in this study to overcome this problem. One of the advantages from using this method is that a higher signal-to-noise ratio can be achieved even if the signals are measured without a trigger mechanism.

The main objective of the correlated time averaging method is to capture the family of impulses that occur due to the presence of a defect in a bearing component. In a rotating machine component such as bearings or gears, a defective component in operation will generate a family (or a series) of impulses. In each rotation, this family of impulses will repeat itself but the time of occurrence might be random depending on the type of defect present.

The first step in this method is to capture the family of impulses from a time trace. This is performed using a time window that slides along the time trace and capturing a family of impulses inside this window by positioning the window in the middle of a peak. Once the desired signal is captured it is saved for the next step and this procedure is repeated until a maximum number of captured signals is obtained for the next step of the averaging process. The procedure in these steps is shown in graphical form in Figure 4.17. The width of the capturing window is adjusted to optimise the total number of data points captured, so that enough data is obtained to represent the different types of defect that can occur. In this study, the total number of data points for the sliding window is set to 256. This represents 0.52 to 0.91 rotations of the bearing shaft depending on its speed. For the type of defects studied, this setting is enough to capture

the impulses and the different characteristics of each type of defects being studied can be identified.

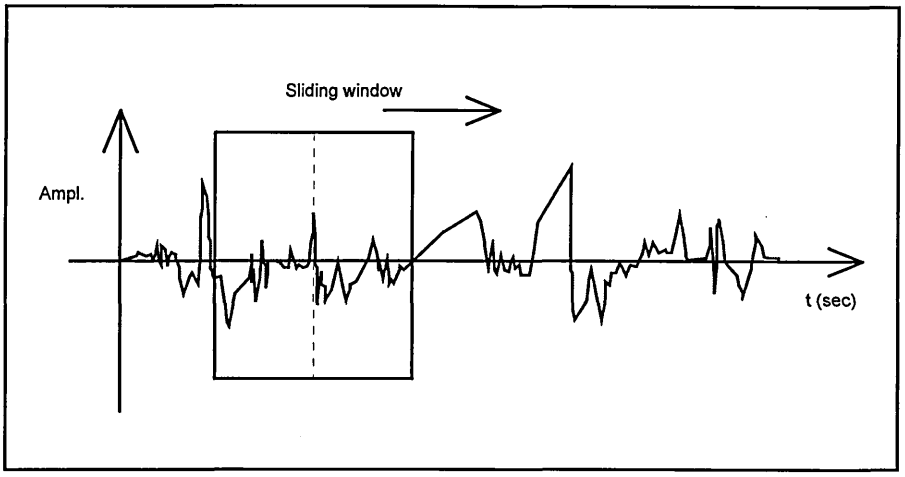

Figure 4.17 Procedure for capturing a family of impulses from a time trace.

In the second step, a pair of the captured signals is selected and a cross correlation routine is performed. Then, these two signals are aligned so that the maximum coefficient of the cross correlation function is set to zero time. Next, the two captured signals are added and averaged to obtained an averaged time trace signal. Then, another pair of the captured signal is selected and this routine is repeated until there is no more signal left to be processed. Figure 4.18 below shows a schematic diagram of this procedure to obtain correlated time averaged signal from eight samples of time trace.

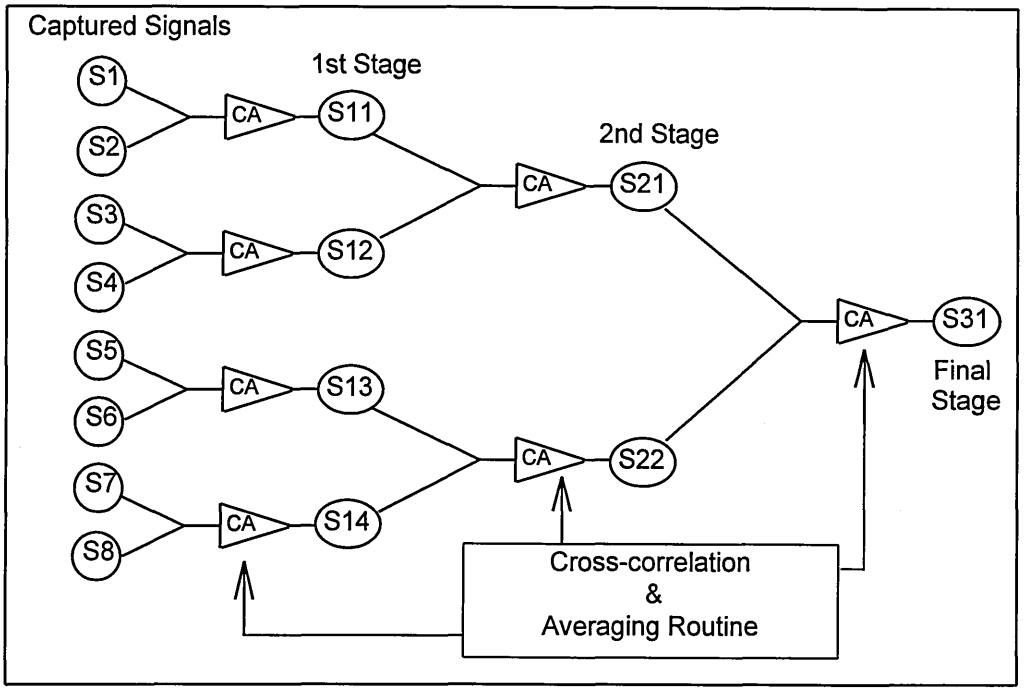

Figure 4.18 Schematic diagram on the correlated time averaging process from eight captured time traces.

Figure 4.19 shows some examples on the effectiveness of the correlated time averaging procedure to obtain a high signal-to-noise ratio from a defective rolling element bearing. As the number of averaging process is increased, the quality of the signal becomes better as shown in the figure. Comparison results between time-averaged signals obtained from a bearing with rolling element defect and time-averaged signals from a normal bearing are presented in Figure 4.20. As expected these signals represent amplitude modulation signals, whereby the higher frequency acts as a carrier frequency and the low modulation frequency contains the information that is characteristic of the bearing being tested.

The amount of noise reduced during the averaging process is dependent on the total number of averages used. Figure 4.21 shows a time trace of the noise reduced from thirty-two averaged signals. This signal is obtained by subtracting signal in Figure 4.19(d) from the signal in Figure 4.19(a). The percentage of noise reduced is calculated using the following formula:

$$\% \ of \ noise \ reduction \ = \ \frac{\sum x_{inst}^2 - \sum x_{avged}^2}{\sum x_{inst}^2} \times 100 \qquad (4.4)$$

where x_{inst} is the instantaneous data, and x_{avged} is the time-averaged data. The percentage of noise reduction from Figure 4.21 is calculated to be:

$$\% \ of \ noise \ reduction \ = \ ((15284.17 - 4561.296) / 15284.17) * 100$$

$$= \ 70.2 \ \%$$

This result shows that a large amount of noise is eliminated from the correlated time averaging process. Therefore, the presence of abnormality in bearing component is easily detected using this method as proven in this case study.

4.5 Summary

This chapter presents a comparison study on the detection of defects in a rolling element bearing using time domain analysis methods. The type of defects being studied are mainly outer race line defect, inner race line defect and rolling element line defect. These defects are created using an etching pen and pictures of these defects are shown in Plate 4.2. Statistical moments such as crest factor and kurtosis are utilised in this study. In addition, the applications of beta distribution function parameters a and b are also performed. A comparison study on the effectiveness of using sound pressure, vibration and air particle acceleration signals to detect the presence of defect in rolling element bearing is carried out. Finally, the correlated time averaging method is successfully developed and applied to minimise the amount of noise in the measured signals.

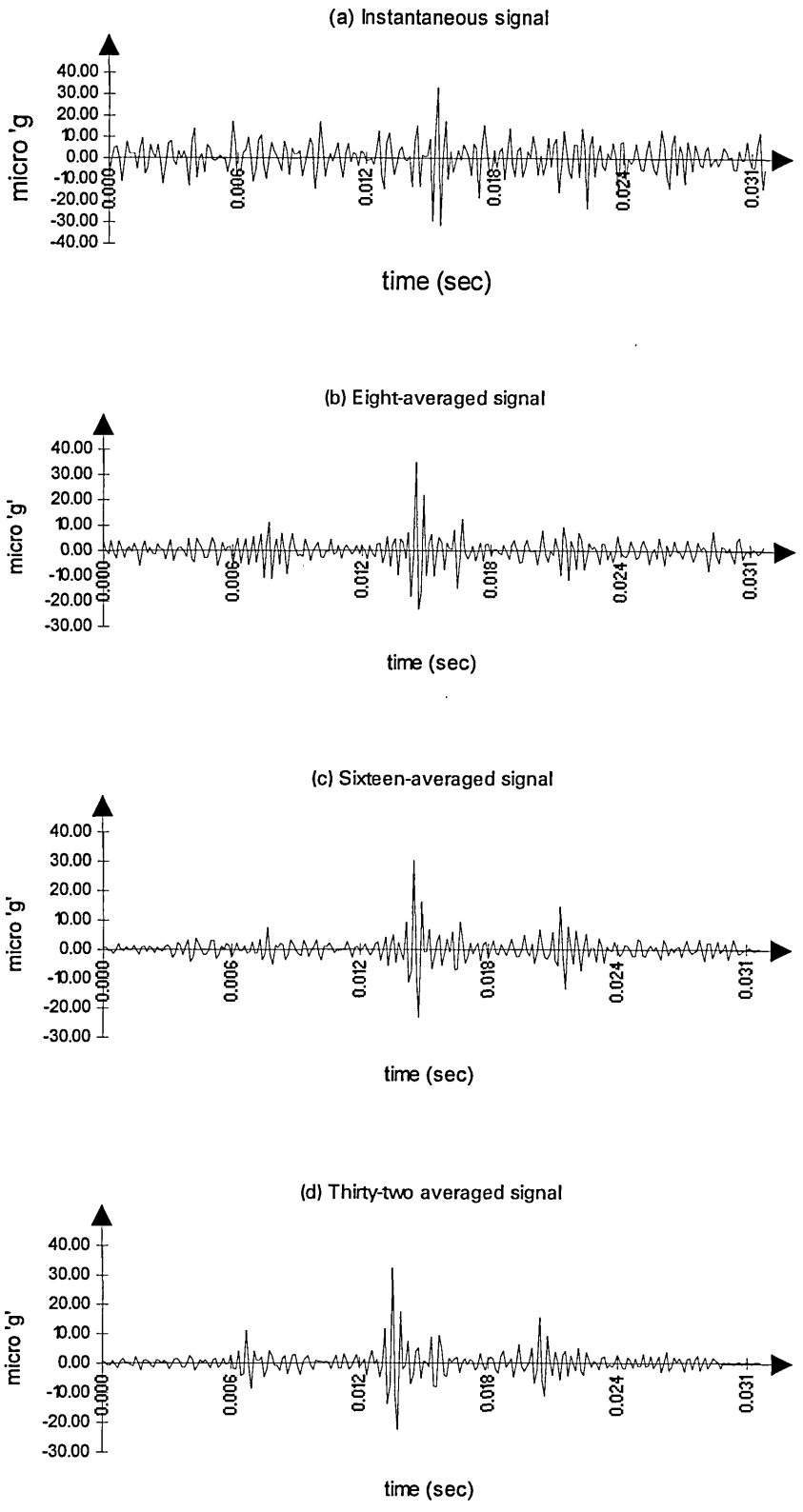

Figure 4.19 Correlated time averaging process of air particle acceleration signals from bearing with rolling element defect. Speed of shaft = 1500rpm.

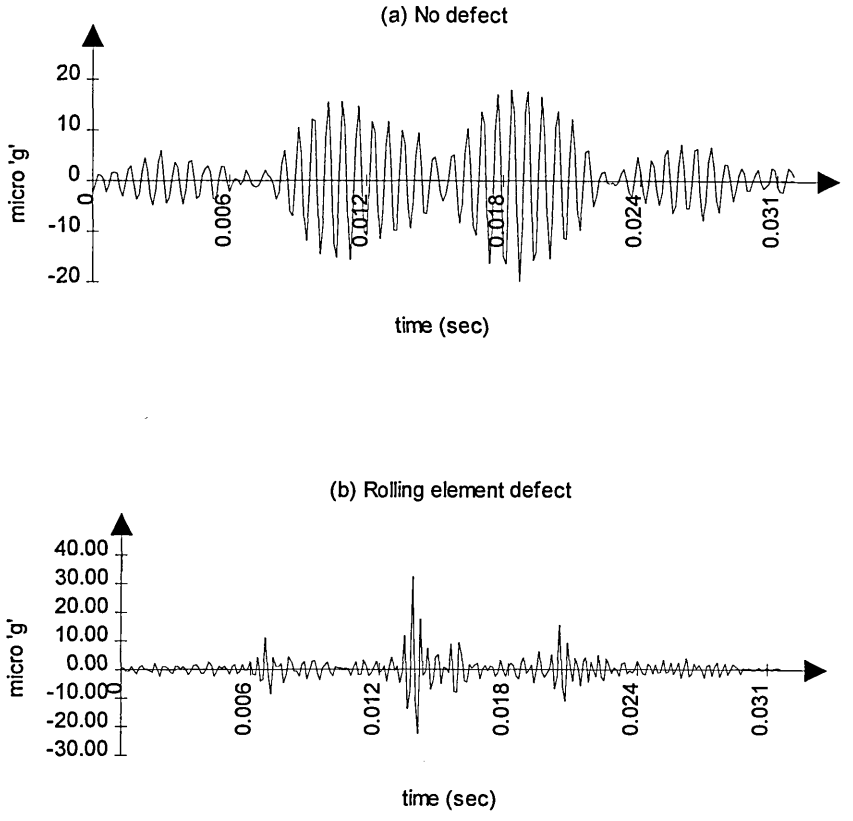

Figure 4.20 Thirty-two correlated time-averaged signals from bearing running at 1500rpm.

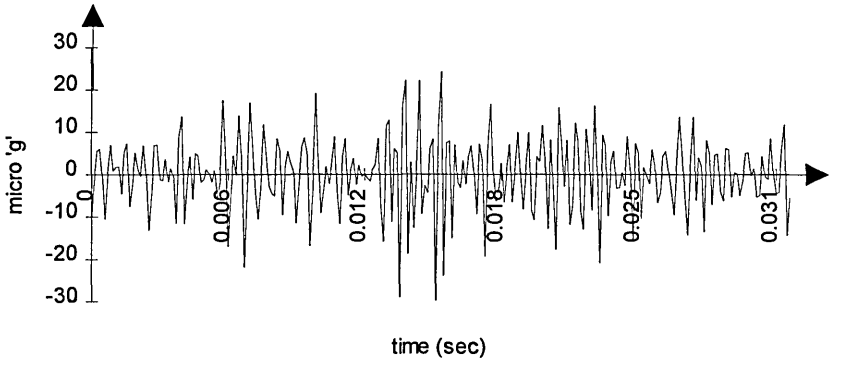

Figure 4.21 Plot of noise reduced from the thirty-two averaged signal.

CHAPTER 5

COMPARISON STUDY: FREQUENCY DOMAIN AND SIMULTANEOUS TIME-FREQUENCY DOMAIN ANALYSIS METHODS

5.1 Introduction

The format of this chapter is similar to Chapter 4, whereby a comparison study is carried out to evaluate the effectiveness of using vibration, sound pressure, sound intensity and air-particle acceleration signals. However, at this stage frequency domain analysis methods are used including spectral analysis, cepstral analysis, zoomed-spectral and cepstral analyses, and wavelet analysis methods. Spectral analysis is one of the most widely used techniques in machine condition monitoring. It can offer some advantages such as the mixture of complex sinusoidal components in a signal are easier to be recognised in the frequency domain. In addition, huge data reduction can be achieved using spectral analysis methods. The zooming facility in spectral analysis method enables us to increase frequency resolution with the same number of spectral lines.

The newly developed wavelet analysis method is included in the study. In contrast to Fourier transform, wavelet transform is very efficient in identifying and representing the presence of short duration transient components in a signal. In general, the wavelet analysis method is used to map a time-domain function onto a representation that is localised in both time- and frequency-domains. The types of defect studied at this stage are the same as in the previous chapter unless otherwise mentioned specifically to be different.

5.2 Spectral and Cepstral Analysis Methods

For a stationary random signal, power spectral density is commonly used to represent this signal in the frequency domain. The power spectral density function can be derived from autocorrelation function of a signal as already discussed in Chapter 2.

Alternatively, the power spectrum which is also the spectrum of squared amplitudes of a real valued function can be implemented in order to obtain a signature of the measured signals. The transformation of a real valued function from time-domain into frequency-domain and the derivation of power spectral are shown in Figure 5.1. It is clear from this diagram that it is not possible to recover the original signal from the power spectrum since only the magnitude of the signals are retained, and the phase information are lost in the process. For a real valued function, which is usually the case in vibration and sound pressure measurement, each component at frequency f_n must be matched by a component at $-f_n$ which has equal amplitude but opposite phase. Therefore, the resultant signal will always be real because the imaginary components at each frequency will always be equal to zero. The Bruel and Kjaer 2032 dual-channel analyser used in this study computes the imaginary parts of a real-valued time signal $x(t)$ using the Hilbert transform $H[]$ as shown below. In essence, it corresponds to a -90° phase shift of the original signal.

$$H[x(t)] = \tilde{x}(t) = \frac{1}{\pi}\int_{-\infty}^{\infty} x(u)\frac{1}{t-u}du. \qquad (5.1)$$

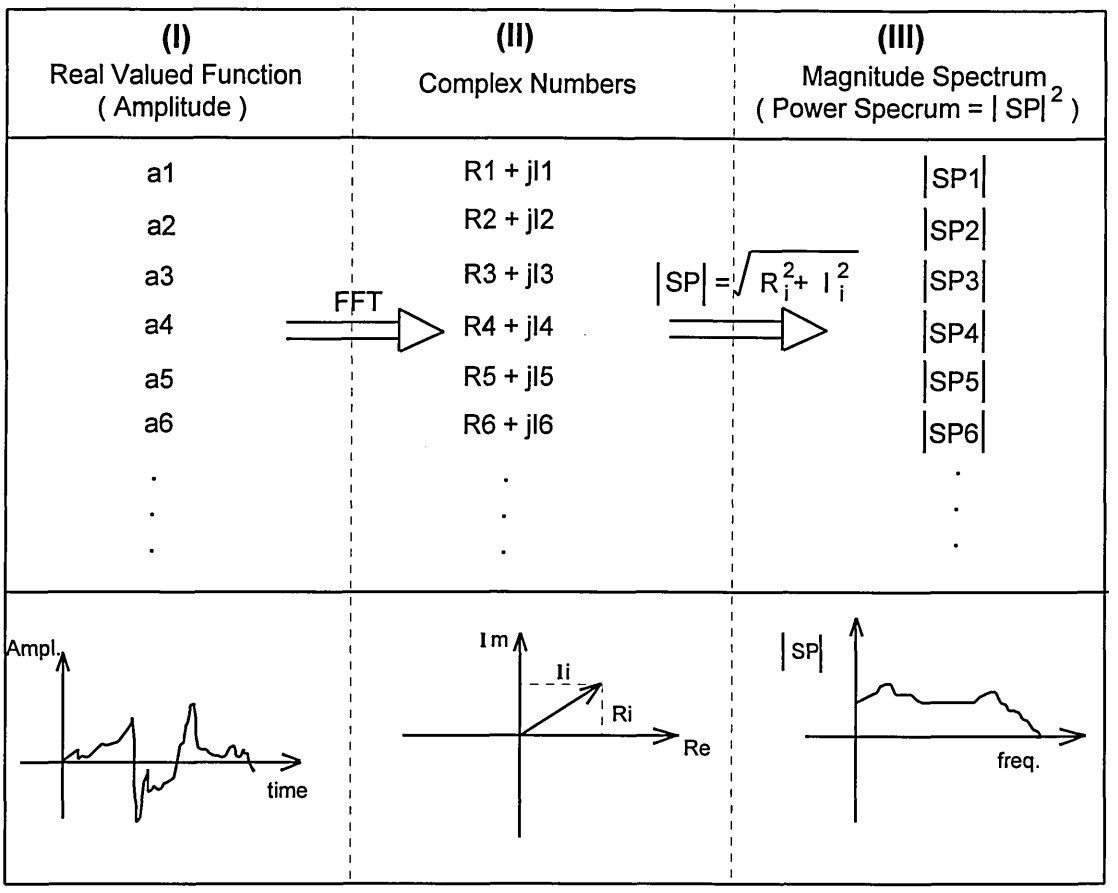

Figure 5.1 Transformation of time-domain signals into power spectral in frequency-domain.

The total number of data points N, measured using the Bruel and Kjaer 2032 analyser is set equal to 2048. To avoid aliasing using Nyquist criterion the total number of frequency lines used for display is set to 800 (which is equal to 2048/2.56). The two-sided frequency spectrum $S_X(k)$ is defined as:

$$S_X(k) = \Im\left[W(m)\cdot x(m)\right] \tag{5.2}$$

where $W(m)$ is the weighting function; $\Im[\,]$ is a symbol for Fourier transform process; $0 \le m \le N-1$; $0 \le k \le N-1$; and $N = 2048$. The displayed function is derived from a one-sided frequency spectrum $G_X(k)$, where $0 \le k \le 800$:

$$G_X(k) = \begin{cases} S_X(k) \text{ for } k = 0 \\ 2S_X(k) \text{ for } 1 \le k \le N/2 - 1 \\ 0 \text{ for } N/2 \le N-1 \end{cases} \tag{5.3}$$

This can be displayed in the form of real and imaginary parts, or magnitude and phase components, and the magnitude can be scaled as rms, power, power spectral density, or energy spectral density.

A simple mathematical derivation of cepstral analysis method is already shown in Chapter 2. However, for convenience, another version of the mathematical formula to describe the concept of cepstrum analysis method is also shown below. If the power spectrum of a measured signal is written as:

$$PS(f) = \left| G_X(f) \right|^2 \tag{5.4}$$

Then the power cepstrum can be written as:

$$C_X(\tau) = \left| \Im \left\{ \log \left[PS(f) \right] \right\} \right|^2 \tag{5.5}$$

The cepstrum analysis method is commonly used to show the complex features of a signal containing mixture of different families of harmonics and sidebands.

Frequency averaging process for sound pressure, sound intensity, and vibration signals are performed directly by the analyser. However, for the air-particle acceleration signals a further post-processing procedure needed to be carried out based on the principle shown below.

Air-particle acceleration signals: $\boldsymbol{ap}(t) = p_2(t) - p_1(t)$, (5.6)

Fourier transformed of equation (5.6): $\boldsymbol{AP}(f) = \boldsymbol{P}_2(f) - \boldsymbol{P}_1(f)$ (5.7)

Frequency averaging of the complex air-particle acceleration signal is performed as follow:

$$\frac{1}{N}\Sigma \Delta P(f) = \frac{1}{N}\Sigma P_2(f) - \frac{1}{N}\Sigma P_1(f)$$

$$= \frac{1}{N}\Sigma \{ P_2(f) - P_1(f)\} \qquad (5.8)$$

Since all of the variables are vector quantities, the summations of the real and imaginary components are carried out separately, and the magnitude of the resultant vector is calculated from the real and imaginary components.

5.2.1 Detection of Defect

5.2.1.1 Calculation of bearing defect frequencies

Basically, the formulae for calculating defect frequencies on the outer race, inner race, and rolling element can be summarised as follow:

$$f_{or} = \frac{nN}{120}\left(1 - \frac{r}{R}\cos\beta\right) \qquad (5.9)$$

$$f_{ir} = \frac{nN}{120}\left(1 + \frac{r}{R}\cos\beta\right) \qquad (5.10)$$

$$f_{re} = \frac{NR}{60\, r\, Cos\,\beta}\left[1 - \left(\frac{r}{R}Cos\,\beta\right)^2\right] \qquad (5.11)$$

where

for	=	outer ring defect frequency
fir	=	inner ring defect frequency
fre	=	rolling element defect frequency
N	=	shaft rotational speed (revolution per minute)
r	=	radius of roller (5mm)

R = pitch circle radius for the roller (32.5mm)

n = number of rolling element (14)

β = contact angle.

5.2.1.2 Signals from other moving components of the rig

The other moving components in the test rig were identified to be the motor, the drive-shaft and the toothed-belt connecting the motor and the drive-shaft. The mean diameter of the motor-sprocket is 290mm and it has 72 teeth on its circumference. On the other hand, the mean diameter of the shaft-sprocket is 70mm, and it has 18 teeth on its circumference. Calculation of the pulse frequencies generated by the shaft-sprocket and the motor-sprocket due to the passage of the toothed-belt were carried out using the following equations:

$$f_{ps} = \frac{n_{ts}\, N}{60} \tag{5.12}$$

$$f_{pm} = \frac{n_{tm}\, N_m}{60} = \frac{n_{tm}\, N}{60}\frac{D_s}{D_m} \tag{5.13}$$

where

fps = pulse frequency due to the shaft-sprocket

fpm = pulse frequency due to the motor-sprocket

n_{tm} = number of teeth on the motor-sprocket (72)

n_{ts} = number of teeth on the shaft sprocket (18)

N_m = rotational speed of motor-sprocket

D_m = mean diameter of motor-sprocket (290mm)

D_s = mean diameter of shaft-sprocket (70mm).

Equations (5.7) to (5.11) are used to calculate the frequencies to be monitored from the test rig and the results are presented in Table 5.1.

Table 5.1 Calculated defect-frequencies from bearing and other moving components of the test-rig.

Speed of shaft (rpm)	Outer race defect freq. (Hz)	Inner race defect freq. (Hz)	Rolling element defect freq. (Hz)	Pulse freq. of motor-sprocket (Hz)	Pulse freq. of shaft-sprocket (Hz)
500	49.3	67.3	52.9	144.8	150
1000	98.7	134.6	105.8	289.6	300
1500	148.1	201.9	158.7	434.5	450
2000	197.4	269.2	211.5	579.3	600
2500	246.8	336.5	264.4	724.1	750
3000	296.1	403.8	317.3	869.0	900
4000	394.9	538.5	423.1	1158.6	1200
5000	493.6	673.0	528.9	1448.3	1500

5.2.2 Analysis of Results

For the initial part of the study, three types of signal are used: sound pressure, sound intensity, and vibration signals. The main purpose of this study is to compare the effectiveness of using different measurement techniques to indicate the presence of a defect in a rolling element bearing. In addition, studies on the advantages and limitations of the spectral and cepstral analyses method are also performed. Magnitude spectra of the measured signals from bearing with no defect, a missing roller, and a line defect on one of the rolling element are shown in Figure 5.2. Spectra of sound pressure and sound intensity signals are displayed in dB scale with reference to p_{ref} = 20 μPa and I_{ref} = 10^{-12} watts/m^2 respectively. On the other hand, the spectra of vibration signals are displayed in a normalised linear scale in order to fit all the spectra into one graph. All spectra are obtained by averaging one hundred instantaneous spectra to minimise the effect of random noise.

Results from Figure 5.2 indicate that under typical laboratory condition with low background noise, the spectra of sound pressure and sound intensity signals are almost identical. The results also indicate that different types of defect will excite different a

frequency region depending on the transfer function of the physical system being measured. In the case of a defective bearing, modulation of the frequency spectra above 1.6KHz are clearly indicated from all the signals measured. However, the type of defect presence is difficult to diagnose if only the frequency spectrum is monitored. Other method such as cepstrum analysis must be carried out in order to determine the type of defect presence in the test-bearing.

Figure 5.3 shows results obtained from implementing cepstral analysis method using the same signals as in Figure 5.2. However, only sound intensity and vibration signals are used because for this case, results from the sound pressure signal would be similar to the result from using sound intensity signal. The peaks in Figure 5.3 clearly indicate the modulation of the frequency spectra representing the repetitive impulsive signals from the rolling element defect. The calculated defect frequency in this case is 317.3Hz, whereas the frequency peaks indicated from the figure are 316Hz and 320Hz. But the frequency resolution of the spectra is 8Hz. These results show that cepstral analysis method can accurately indicate the type of defect present in the test-bearing.

The effect of high background noise on sound pressure and sound intensity measurement is shown in Figure 5.4. The background noise is generated using a white noise generator connected to a speaker, and the instantaneous spectrum is presented in Figure 5.4(a). The averaged frequency spectra for sound pressure and sound intensity signals are also included in the same graph for comparison. This figure shows that the overall level of sound pressure spectrum is higher than the overall level of sound intensity spectrum. However, from Figure 5.3(b) and (c) the magnitude of the peak due to the presence of rolling element defect is higher in sound intensity cepstrum compared to sound pressure cepstrum. This shows that the defect signal is better detected using the sound intensity technique when the background noise level is high.

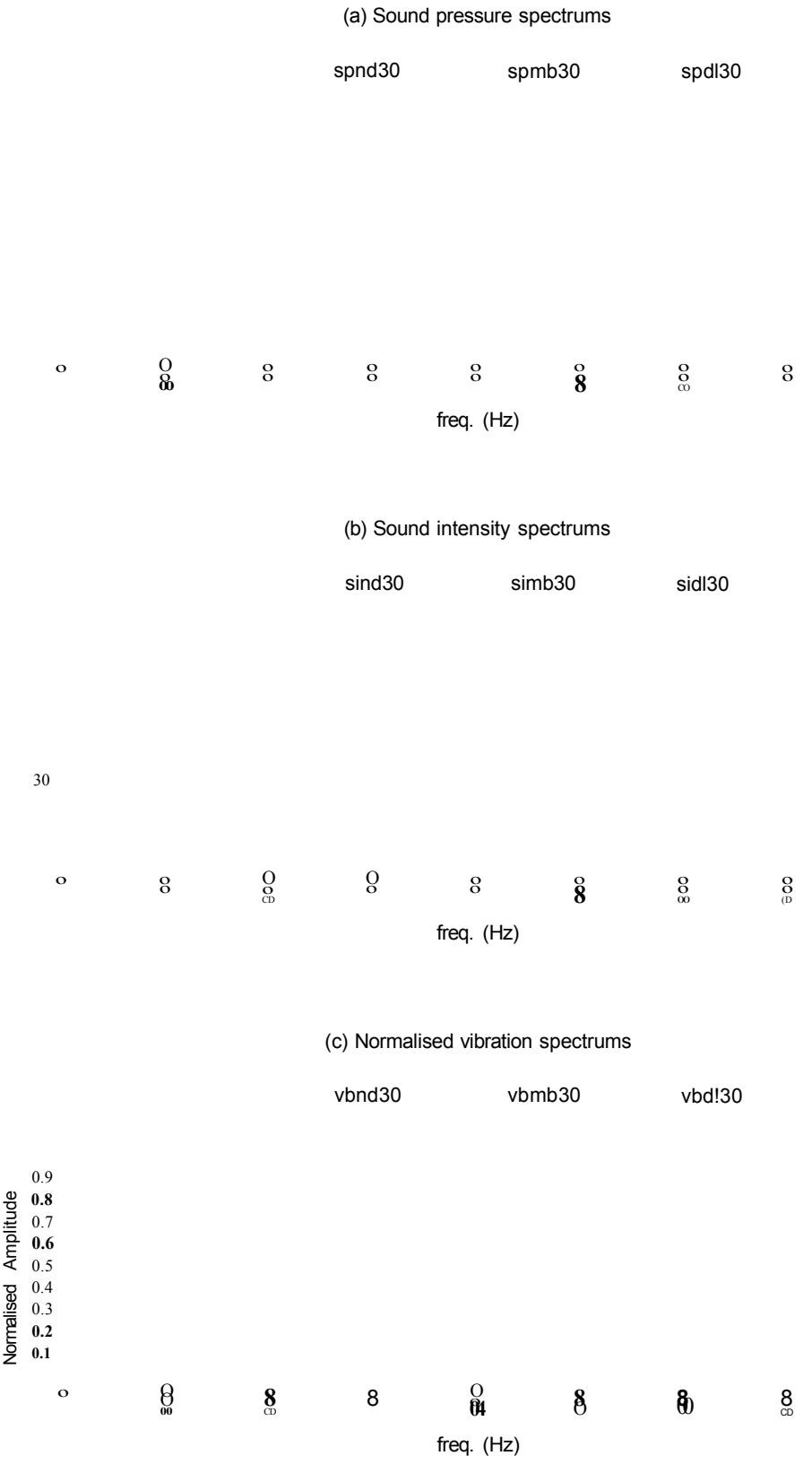

Figure 5.2 Frequency spectra of sound pressure, sound intensity, and vibration signals. Speed of shaft = 3000rpm.

(a) Cepstrums of sound intensity signals

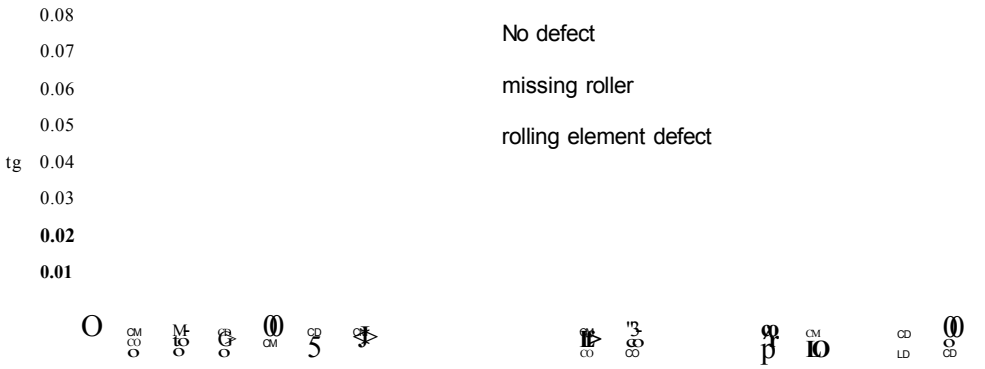

(b) Cepstrums of vibration signals

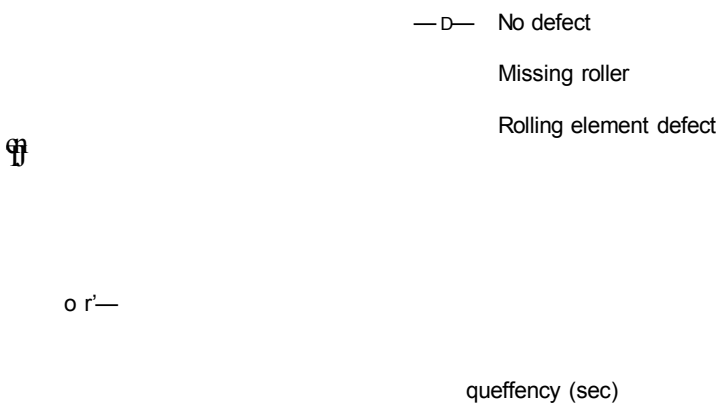

Figure 5.3 Cepstra of sound intensity and vibration signals.
Speed of shaft = 3000rpm.

(a) Spectrums of sound pressure and sound intensity signals

(b) Cepstrum of sound pressure signals

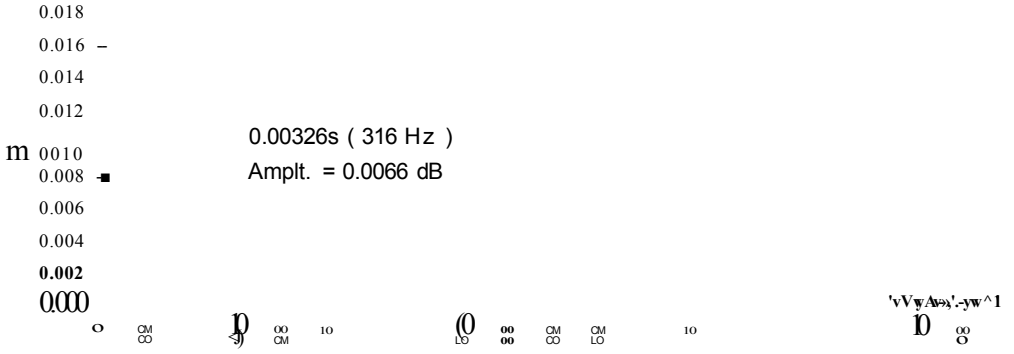

(c) Cepstrum of sound intensity signals

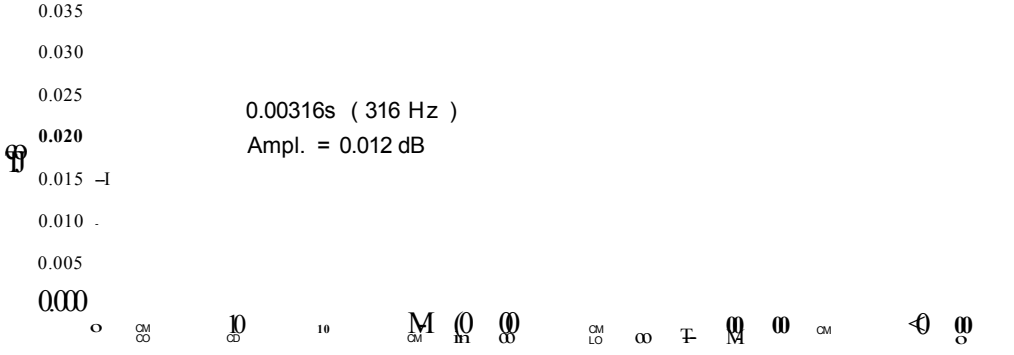

Figure 5.4 Spectra and cepstra of sound pressure and sound intensity signals in the presence of background noise.

5.3 Zoomed Spectral and Cepstral Analysis

5.3.1 Zoom Fourier Transform

Zoom analysis in the analyser was performed using frequency shift and low pass filter operations. If $x(t)$ is a periodic function such that

$$x(t) = x(t+nT) \tag{5.14}$$

where n is an integer number and T is the time taken for the function to cover one complete cycle . The Fourier transform equation is written as

$$X(f_k) = \frac{1}{T}\int_{-T/2}^{T/2} x(t)\, e^{-j2\pi f_k t}\, dt \tag{5.15}$$

where f_k is the k_{th} harmonic frequency component of f_1.

The multiplication of the input function $x(t)$ by a rotating unit vector $e^{-j2\pi f_k t}$ effectively shifted the frequency origin to frequency f_k. The component at frequency f_k was stopped in the position it occupied at time zero, and virtually becomes a new dc component. The positive and negative sampling frequencies $\pm f_S$ were like wise moved by an amount f_k as illustrated in Figure 5.5. The modified complex signal was then filtered to remove all frequency components outside the range of expanded region. Finally, the resampled sequence of the filtered complex function was transformed using FFT algorithm to give the "zoomed" spectrum.

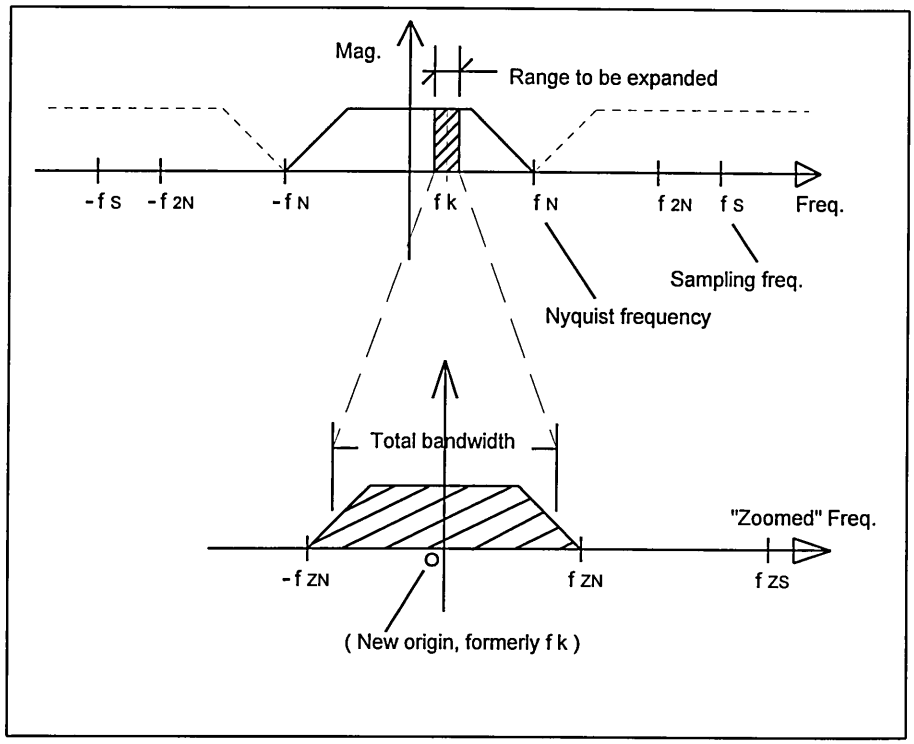

Figure 5.5 Schematic diagram of the "Zoomed" algorithm.

When the defect signals were not very clear, especially in low speed bearing operation, cepstrum analysis of a broadband frequency spectrum sometimes fail to indicate the presence of defect in the bearing component. However, by zooming into the high amplitude region of the frequency spectrum, the defect signal was detected much easier and shown in the plot of the zoomed cepstrum. Figure 5.6 presents the results from a case study whereby a test bearing with a defective outer race was operated with the shaft speed of 430rpm. The calculated defect frequency for this case was 42.4Hz. It is shown from the zoomed sound intensity cepstrum that a small peak is indicated which represent a defective frequency component at 43.7 Hz. This frequency peak is very close to the calculated defect frequency of the test-bearing. On the other hand, there is no peak indicated near the calculated defect frequency value from the broadband cepstrum analysis shown in Figure 5.6(c). Similarly, the same results were obtained from the zoomed cepstrum analysis of vibration signal as shown in Figure 5.7. However, as expected the results obtained from vibration signals were more clearer compared to the sound intensity results. The results from all the different types of defect used in Figure 5.8 show that only the component of the defect frequency is shown

from the zoomed cepstrums analysis method. Where, the complex frequency modulation from the transfer function of the physical system has been isolated from the defect signal. The calculated defect frequencies for the study is shown in Table 5.2, and the shaft-speed for this case was maintained at 820rpm.

Table 5.2 Calculated defect frequencies when the speed of shaft is set to 820rpm.

Defect Type	Calculated Defect Frequency (Hz)
Outer race defect	80.9
Rolling element defect	86.7
Inner race defect	110.4

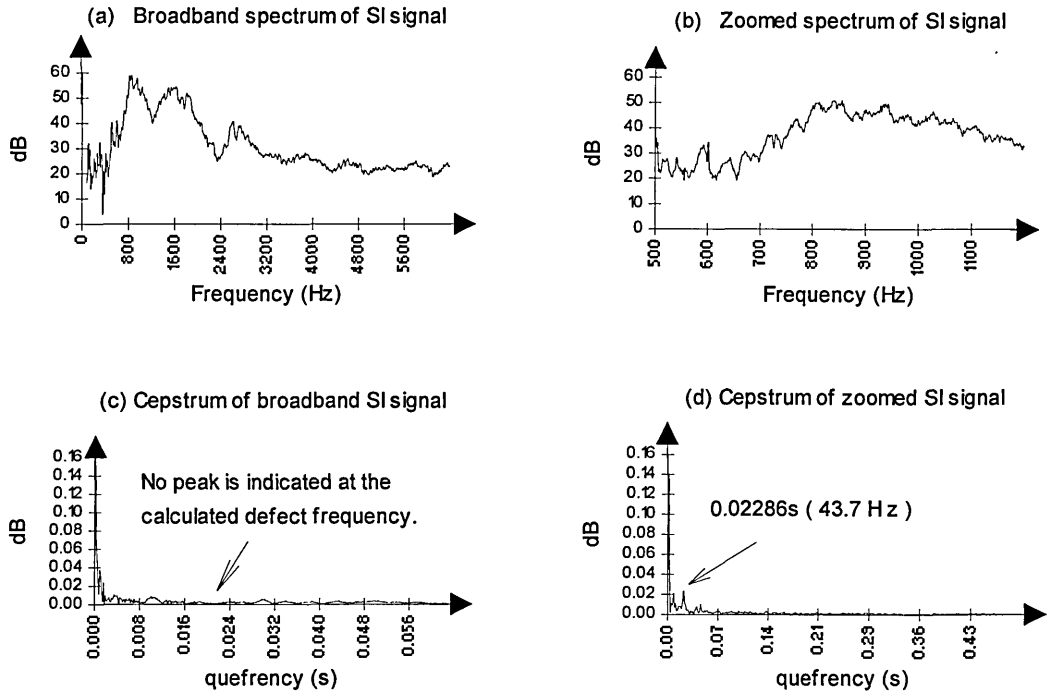

Figure 5.6 Broadband and Zoom cepstral analysis of sound intensity signal. Speed of shaft = 430rpm. Outer race defect.

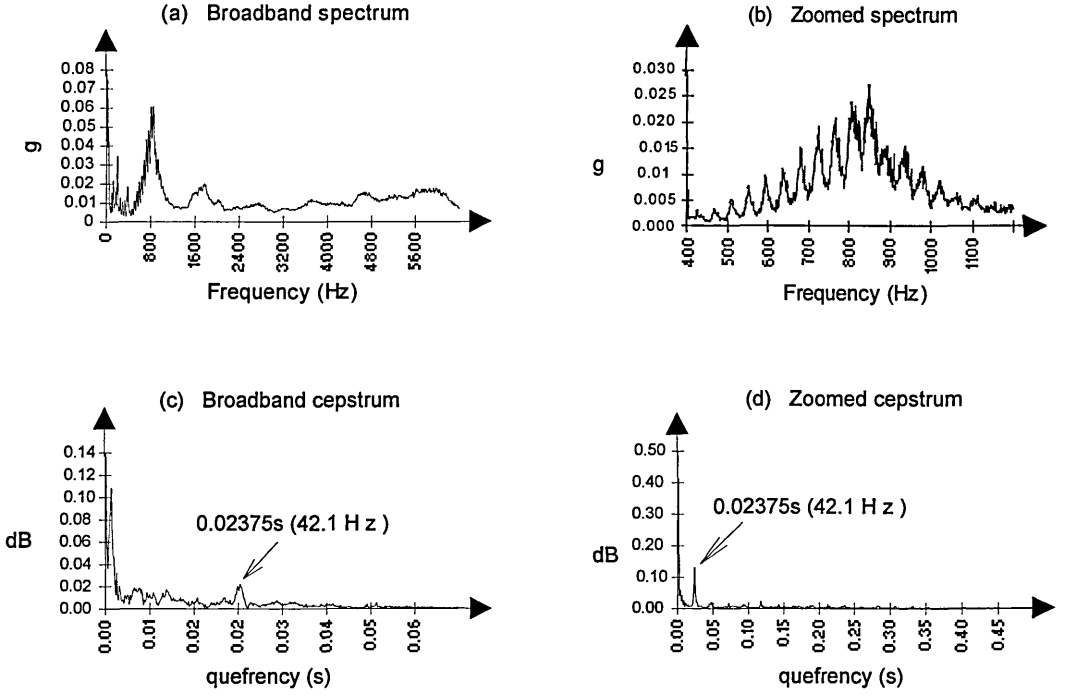

Figure 5.7 Broadband and zoomed cepstral analysis of vibration signal. Speed of shaft = 430rpm. Outer race defect.

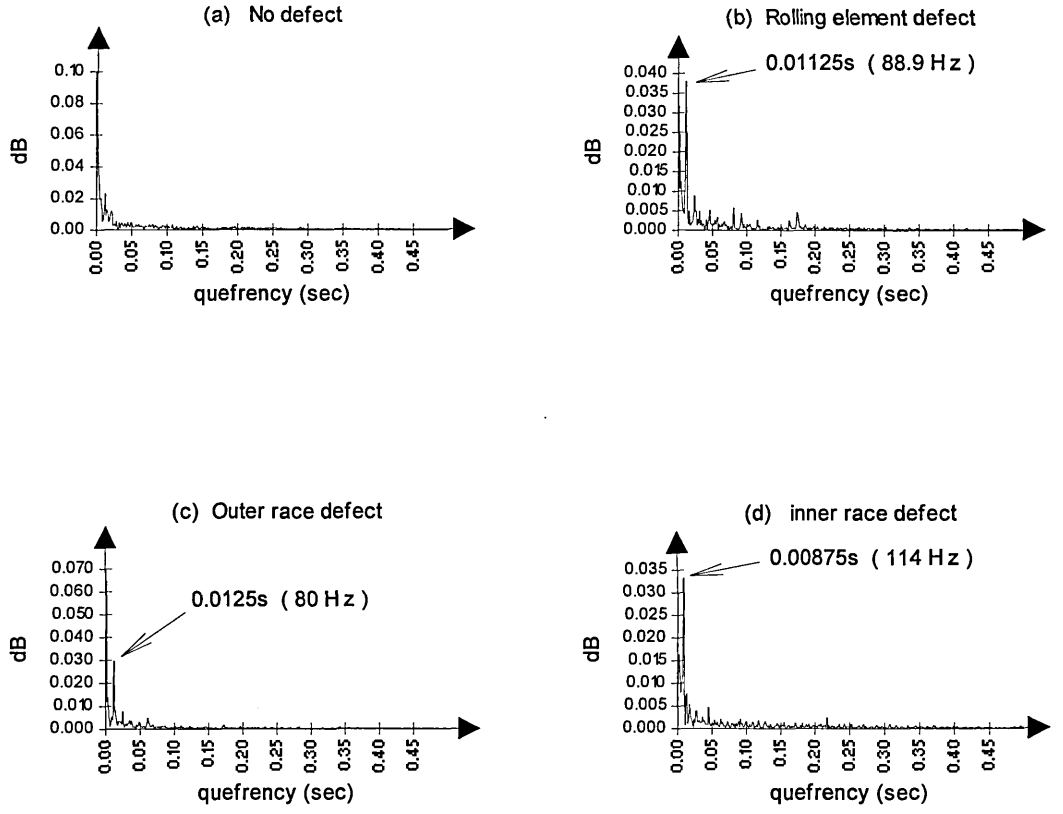

Figure 5.8 Zoomed cepstrum from different types of defect using sound intensity signals. Speed of shaft = 820rpm.

5.4 Simultaneous Time-Frequency Analysis Method

The theory of dilation wavelets that will be used in this study has already been presented in Chapter 2. This section discusses the general concept of the simultaneous time-frequency analysis method and presents the results of applying this method in monitoring the rolling element bearing condition. Basically, wavelet transform method is used to decompose an arbitrary function into its basic unit and the coefficients of the wavelet transform are obtained by dilation and translation of the mother wavelet. A wavelet transform can indicate local transient-oscillation of a signal at a particular point which is typical in a defective machine component. This is not possible using the Fourier transform method because it assumes that the coefficient of a particular frequency component exists for the whole lifetime of the signal. An analogy on the concept of dilation, compression and translation of a mother wavelet transform is presented in Figure 5.9. Three types of wavelet transform analysis product will be studied in this section: best level, best basis, and wavelet basis. In addition, the local cosine transform (LCT) method will also be implemented to generate acoustic signatures of the bearing component. The local cosine transform method is an extension of the short time Fourier transform (STFT) method, whereby the input signal is cut into several segments and Fourier cosine transform is performed on each segment. The length and the number of segment used is dependent on the level of the LCT as presented in Chapter 2.

At this stage, the simultaneous time-frequency analysis method is used to capture the signature of signals measured from a rolling element bearing. The different signatures obtained from the measured signals will be used to identify and to classify the type of defect present in a bearing component. Next, diagnostic works are carried out from the simultaneous time-frequency patterns of the signal, in order to identify the type of defect present in the bearing component. In addition, the wavelet transform method is also applied to minimise the random noise in a signal. All signal analysis work performed in this section are carried out using WPLW$^{(TM)}$ software package. This software package was developed by Coifman and Wickerhauser (1993) and distributed by Digital Diagnostic Corporation, Yale University, USA. Two-dimensional time frames will be used to represent the pattern of a signal and this representation is known

as the phase plane diagram. Effectively, the wavelet packet transform method is utilised for the following purposes: to capture the time-frequency signature of a signal, to perform multi-scale analysis on a signal, to filter out noisy components in a signal, and to select important features that represent a signal (Coifman and Wickerhauser 1993).

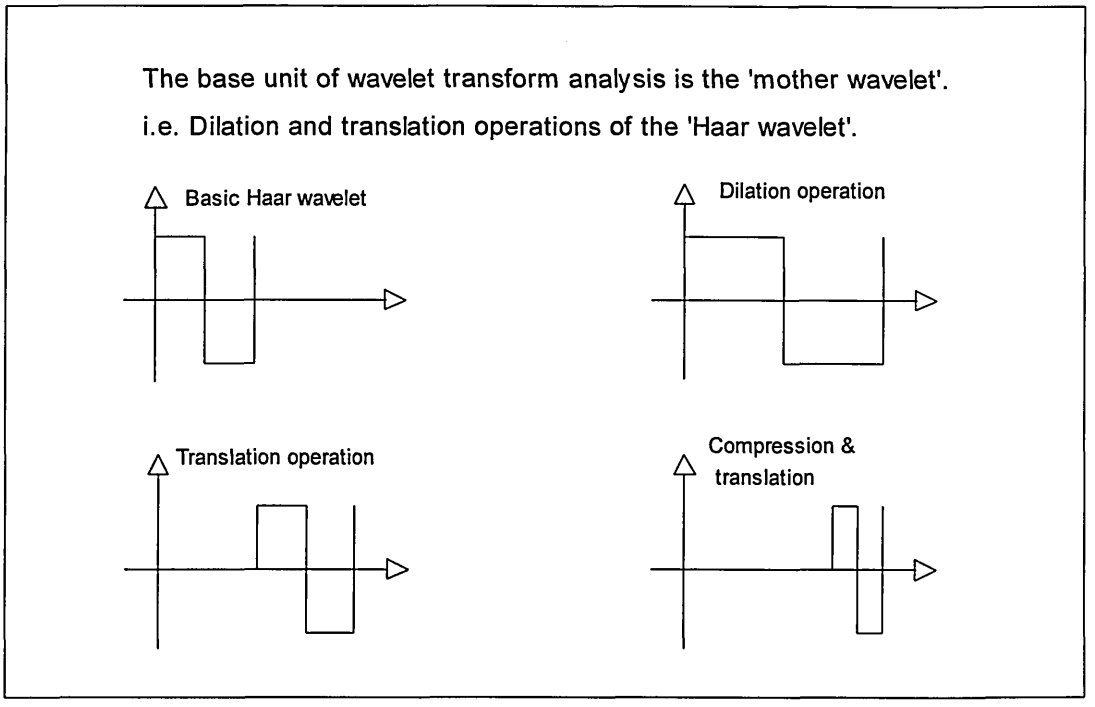

Figure 5.9 The concept of wavelet basic-unit operations to represent a signal.

5.4.1 Performance of Simultaneous Time-Frequency Analysis Method

The effectiveness of wavelet transform method to localise and to identify local frequency components in a signal depends on the type of mother wavelet used and on the nature of the input signals. The number of coefficients used to represent the mother wavelet will also affect the performance of a wavelet transform. The larger the number of coefficients the smoother the mother wavelet becomes. The diagrams in Figure 5.10 below represent a wavelet known as the Daubechies wavelets, the numbers that follow the letter 'D' in the diagram indicate the number of coefficients used to develop the mother wavelet.

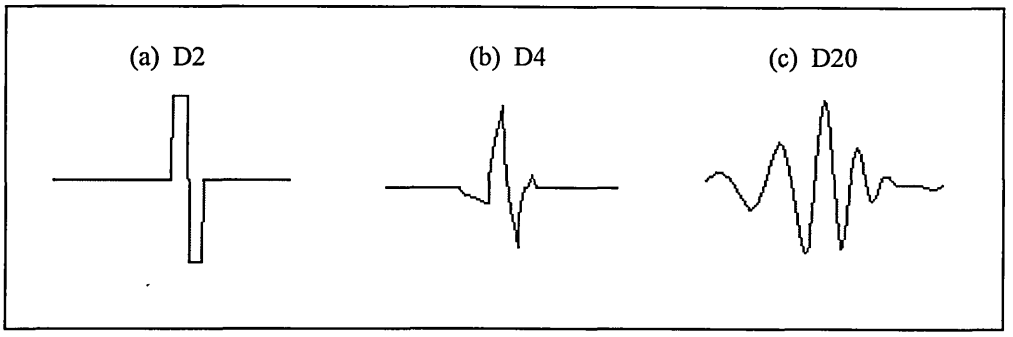

Figure 5.10 Diagrams of Daubechies wavelets developed using several different coefficient numbers.

A simple signal has been created to carry out an initial study on the performance of wavelet packet transform and local cosine transform in analysing a signal. This is a combination of two transient-sinusoidal signals joint back-to-back as shown in Figure 5.11. A high frequency component of the signal (1KHz) begins with high amplitude and then decays exponentially and finally disappear in the middle of the sampling period. At this instance, a second frequency component (500Hz) starts to emerge and gradually increased in amplitude until it reaches a maximum value near the end of the sampling period. In Figure 5.11(b), the frequency spectrum of the signal indicates two clear peaks at 500Hz and 1KHz representing the two frequency components of the input signal. However, it is impossible to see time-behaviour of the input signal from the spectrum diagram.

In the following section, the wavelet transform and wavelet packet transform methods will be utilised to study the behaviour of the above signal in time- and frequency-domain simultaneously. Four types of mother wavelets are used for the initial study as indicated in Figure 5.12. These mother wavelets were chosen from a list of wavelets available in the WPLW$^{(TM)}$ software. A Phase plane diagram which represented a time-frequency plot of a signal was used to compare the performance of each of the mother wavelet. The results from the initial study are shown in Figure 5.13. The dark patches in the phase plane diagram represent areas of high values of the wavelet coefficients Results from the applications of Beylkin wavelet (B18) and Daubechies wavelet (D12)

clearly show the two-temporal frequency components in the input signal but the time-position of the 500Hz component has been shifted and wrapped around into the left-hand side of the phase plane diagram. This is due to the inherent properties of the orthogonal wavelet bases function which do not have a linear phase response. However, the results from using Coifman wavelet (C12) shows minimum phase shift compared to the results of using other wavelets. The gradual decrease of the high frequency component (1KHz) and the gradual increase of the low frequency component are also clearly indicated by the difference in the intensities of the phase plane diagram. If the time-position (phase information) of the input signal need to be preserved the local cosine transform (LCT) method can be utilised as shown in Figure 5.13(d).

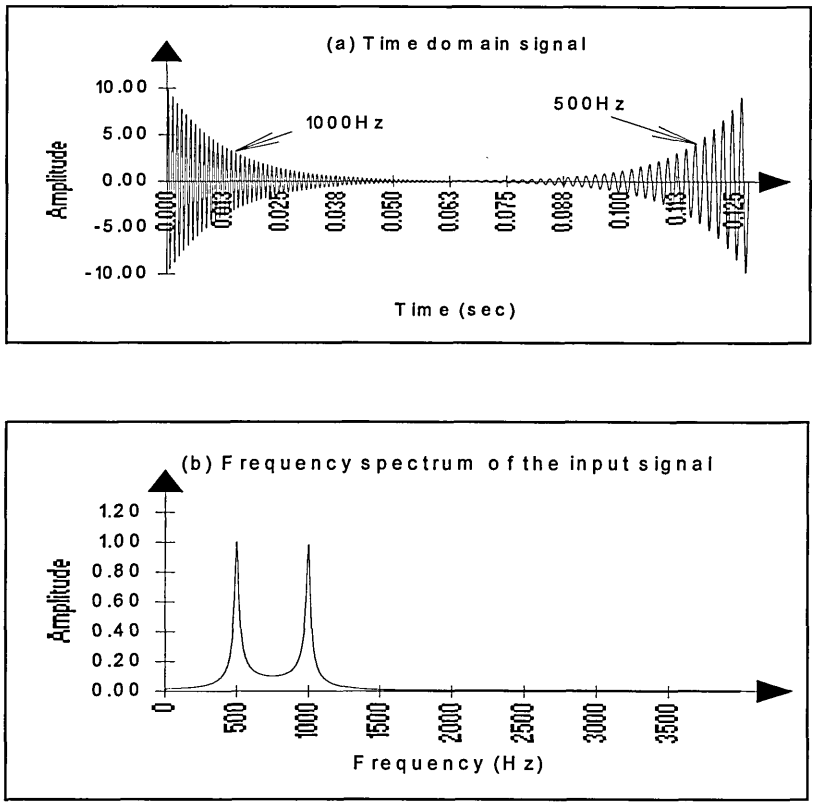

Figure 5.11 Input signal used for the initial study of simultaneous time-frequency domain analysis.

(a) Beylkin wavelet [B18]

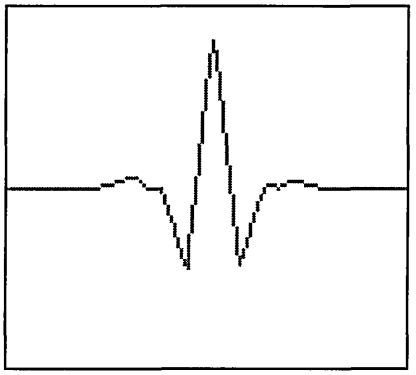

(b) Coifman wavelet [C12]

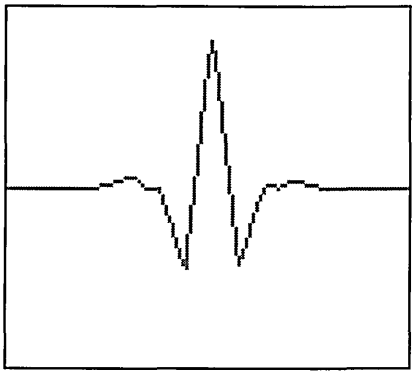

(c) Daubechies wavelet [D12]

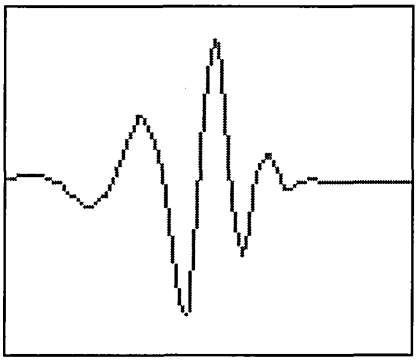

(d) Local cosine [LCT]

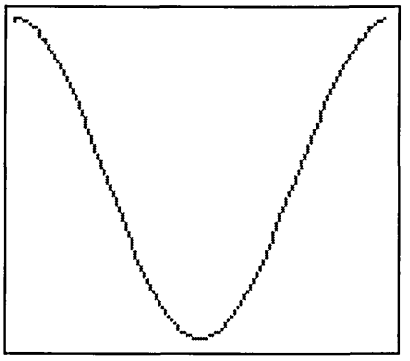

Figure 5.12 Different types of mother wavelets used for the initial study of simultaneous time-frequency domain analysis.

(a) Result from B18 wavelet

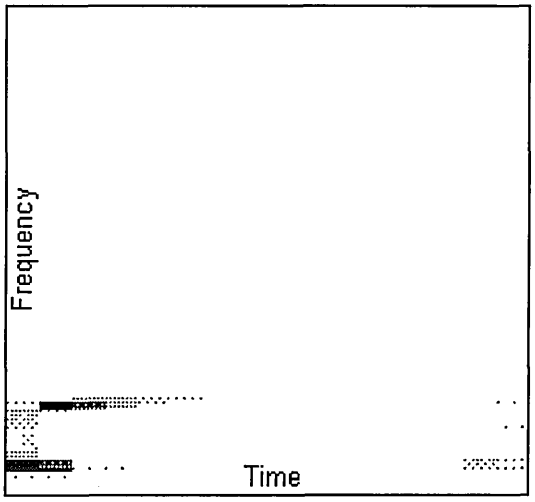

(b) Result from C12 wavelet

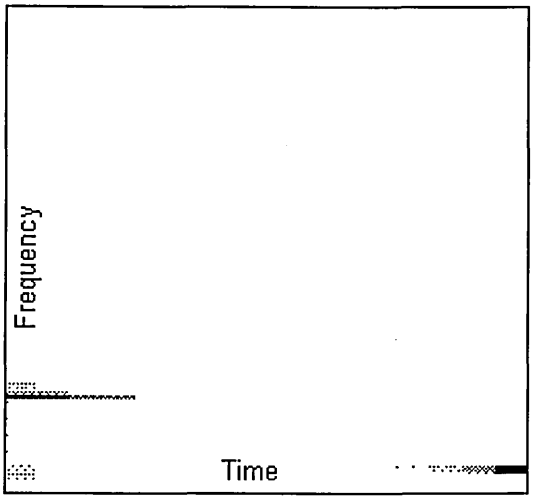

(c) Result from D12 wavelet

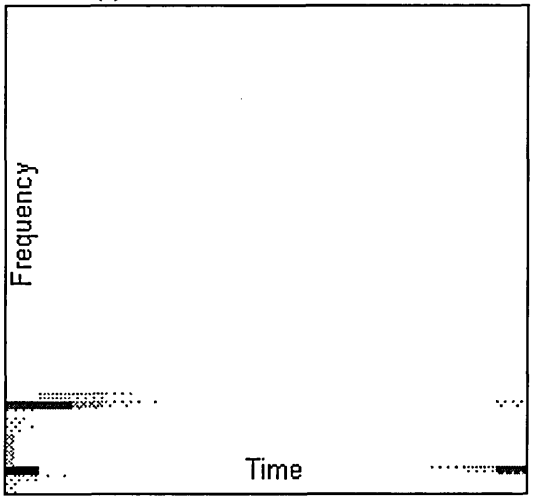

(d) Result from LCT

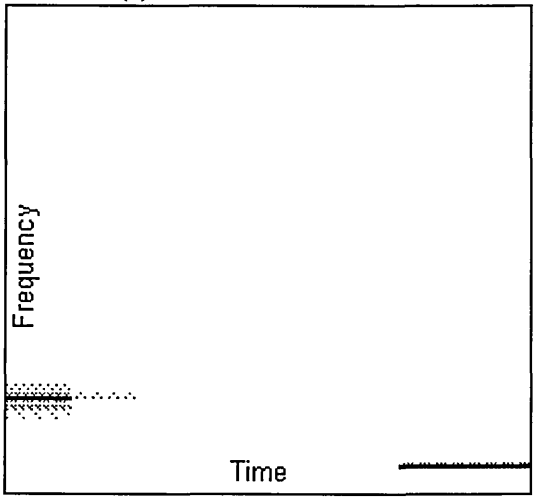

Figure 5.13 Phase plane diagrams from the best basis representation of wavelet packet transform.

5.5 Analysis of Bearing Signals Using Wavelet Transform Method

In this section, results from the applications of wavelet transform and wavelet packet transform to analyse signals from cylindrical rolling element bearing are presented. The analysis of signal at this stage can be classified into the following categories:

(i) to capture the time-frequency signature of a signal using the phase plane diagrams obtained from best basis, best level, and wavelet basis,

(ii) to perform denoising operations on a signal using multilayer analysis in the wavelet packet transform method, denoising is the name given to the process of eliminating random noise using the wavelet packet transform method.

(iii) to perform multi-scale analysis on a signal from the result of a wavelet transform,

(iv) to select important features that represent a signal, and

(v) to compress a signal.

Phase plane diagrams from the wavelet packet transform of air-particle acceleration signals are shown in Figure 5.14. These diagrams were obtained from the best basis of wavelet packet transform. From this stage onward Coifman wavelet (C12) was chosen to perform wavelet analysis because it has been shown from previous results that it can minimise phase shift in the phase plane diagram when compared to other wavelets. The signals are measured from the operation of a cylindrical rolling element bearing with different conditions, such as normal condition, rolling element line defect, outer race line defect, and inner race line defect. The speed of the test-shaft for this study was maintained at 2000rpm. The patterns of air-particle acceleration signals from different bearing condition display different characteristics as shown in Figure 5.14. The frequency content and time-behaviour of the signals were different for different bearing conditions. These patterns were used as signatures that represent the condition of the bearing in operation. In general, the signal from the bearing with no defect was rich with broadband frequency content that occur uniformly along the time domain. Whereas, the signal from a defective bearing contain a repetitive short duration of pulses that can be identified from vertical lines in a phase plane diagram. These repetitive

vertical lines in the phase plane diagram represent the impulsive nature of a defective bearing signal.

Several different patterns of the phase plane diagrams can be constructed from the same signal, depending on the type of basis used to construct it. Figure 5.15 presents the phase plane diagrams from a bearing with a rolling element line defect. These diagrams are obtained from the best level, best basis, and wavelet basis of a wavelet packet transform results. All of the coefficients chosen from the best level basis are taken only from one fixed level. Therefore, the time-frequency frames in the phase plane diagram have a uniform rectangular shape as shown in Figure 5.15(a). These uniform square frames also show that the uncertainties of time-position and frequency-component of the signal obtained from this display are constant.

Although the general shape of the phase plane diagram from best basis are almost the same as the best level basis, the shape of time-frequency frames as shown in Figure 5.15(b) are not uniform. All of the coefficients used to construct this diagram are selected from the high-valued coefficients available from all the different levels of the wavelet packet transform. Because different levels will have different time-frequency resolution, the shape of time-frequency frames in the phase plane diagram will also be different. This is the most effective way to represent an input signal since all the high-valued coefficients from any level can be selected and displayed in the phase plane diagram.

The third phase plane diagram shown in Figure 5.15(c) is constructed from the wavelet basis. The main feature of a wavelet basis is the multiscale octave segmentation of the input signal. The high-frequency components are contained in Level 1 as shown in the figure. The frequency range in this level is set from $\frac{1}{2}F_{max}$ to F_{max} of the input signal. Where F_{max} is the maximum frequency that can be extracted from the input signal. The next lower frequency components are contained in Level 2, and the frequency range in this level is half of the frequency range in Level 1. These relationships are continued into the next level and so on until the maximum level is reached. As the number of levels increases, the shape of the time-frequency frames become shorter and wider

which indicate that the frequency resolution is smaller and the time-resolution is bigger. Therefore, in this diagram the best frequency resolution is obtained from the highest level and the worst frequency resolution is obtained from the lowest level, and vice-versa. The wavelet basis is best used to represent and to detect transient components in a signal.

The next application of wavelet packet transform method implemented in this study was the de-noising algorithm or also known as the coherent structure extraction of an input signal. In Figure 5.16, the process of the de-noising algorithm was carried out on sound pressure signal obtained from a bearing operated in the presence of high background noise. The diagram in part (a) was the original input signal and the second diagram in part (b) was obtained by transforming the input signal using C12 wavelet and reconstructed from the best basis display. Only the coefficients with high values were selected for the reconstruction, and these selected coefficients represent twenty percent of the total energy in the input signal. This was the first coherent component of the input signal. The remainder of the signal not selected in the process called the residual component, was transferred into the next layer and transformed again using the same mother wavelet. Next, high-valued coefficients which represent twenty percent of the residual component were selected from the best basis display and reconstructed to obtain the second coherent component. The next remainder of the signal which was the second residual component was transferred again into the next layer and the same process was repeated to obtain the third coherent component of the input signal. This component is presented in part (c) of the figure. Finally, the input signal was obtained from the summation of all the coherent components and a residual component of the last layer as shown in equation 5.16.

$$s = coh(0) + coh(1) + coh(2) + \ . \ . \ . \ + coh(n) + res(n) \qquad (5.16)$$

Where s is the input signal $coh(0)$, $coh(1)$ up to $coh(n)$ are the coherent components from all the different layers, and $res(n)$ is the residual component from the last layer.

As the number of layer increases in Figure 5.16(b) and (c), the background noise component indicated by the presence of random broadband signal become more

apparent. Whereas the repetitive impulsive signals due to bearing component defect were easier to be detected from the first coherent component in part (a) of the figure. Different types of mother wavelet can be chosen to transform the coherent component at each layer. This is useful when different features of the input signal need to be identified from each layer of the wavelet transform process.

Another important feature of the wavelet transform method is the ability to look at a signal using different time-frequency scales simultaneously. Figure 5.17 shows how the defect signal from a bearing component is easily detectable from multiscale analysis of the wavelet transform method. The wavelet basis of the air-particle acceleration signal from bearing with an outer race line defect is used for the analysis. The speed of the test-shaft for this case was set to 2000rpm. Reconstruction of the signal based on all the coefficients selected from Level 1 shows the impulsive high frequency components as shown in Figure 5.17(b). The time period of impulses are clearly shown from this diagram. The low frequency oscillation of the defect signal is clearly shown in the reconstructed signal based on the coefficients in Level 6 as shown in Figure 5.17(d). These signals can be used to diagnose the condition of a bearing component. The frequency spectrum of the reconstructed signal from Level 6 is shown in Figure 5.18. In this diagram, a very strong peak is indicated at 200Hz which indicate the presence of outer race defect in the test-bearing. The calculated defect frequency is 197.4Hz and the frequency resolution of the spectrum diagram is 8Hz. This study showed that the condition of the bearing component can be diagnosed easily using multiscale analysis of a wavelet transform.

Finally, one of the most significant features of a wavelet transform method is the ability to compress a signal. Only a few of the wavelet coefficients are required to represent a signal without losing the important information contained in the signal. Figure 5.19(a) shows a sample of air-particle acceleration signal measured from bearing with inner race line defect. A total of 2048 data points were used to record the amplitude in time domain. In Figure 5.19(b) a reconstruction of the same signal was obtained from the top 102 wavelet coefficients selected from the best basis. The compression ratio accomplished from this process is 1:20, and the reconstructed signal carry seventy-six percent of the total energy contained in the original signal. From the two diagrams, it is

evident that the reconstructed signal looks very similar to the original signal. Whereas only $1/20$th of the total coefficients were used for its representation. This method can be used to minimise the number of features needed to represent a signal for further analysis and to minimise the space required to store a signal.

5.6 Summary

Frequency domain and simultaneous time-frequency domain analyses methods have been implemented to diagnose the condition of a cylindrical rolling element bearing. Sound pressure and air-particle acceleration signals are measured and analysed. Although the frequency spectrum of a bearing signal changes in the presence of a defect, the type of defect detected is difficult to determine. Cepstrum and zoomed cepstrum analyses method were used successfully to detect the frequency content of a defective signal. Next, the types of defect present are determined by comparing the frequency content of the measured signals with the calculated defect frequencies that are expected from the test-bearing.

Wavelet transform and wavelet packet transform methods are used to analyse and represent the measured signals in simultaneous time-frequency domain. Signatures of a bearing signals are obtained from the phase plane diagram of wavelet packet transform. Classification of the bearing signals are performed from the phase plane diagrams. Further analysis and diagnosis work are performed using the multi-layered and multi-scale algorithms that are available in wavelet transform and wavelet packet transform methods. It was shown that the exact frequency component from a defective bearing signal can be determined using these algorithms. Finally, the wavelet transform method is used to compress a signal whereby only a small number of wavelet coefficients are needed to reconstruct the signal. This feature is very important if small space is available to store the signal and if only a few coefficients are required to represent the signal.

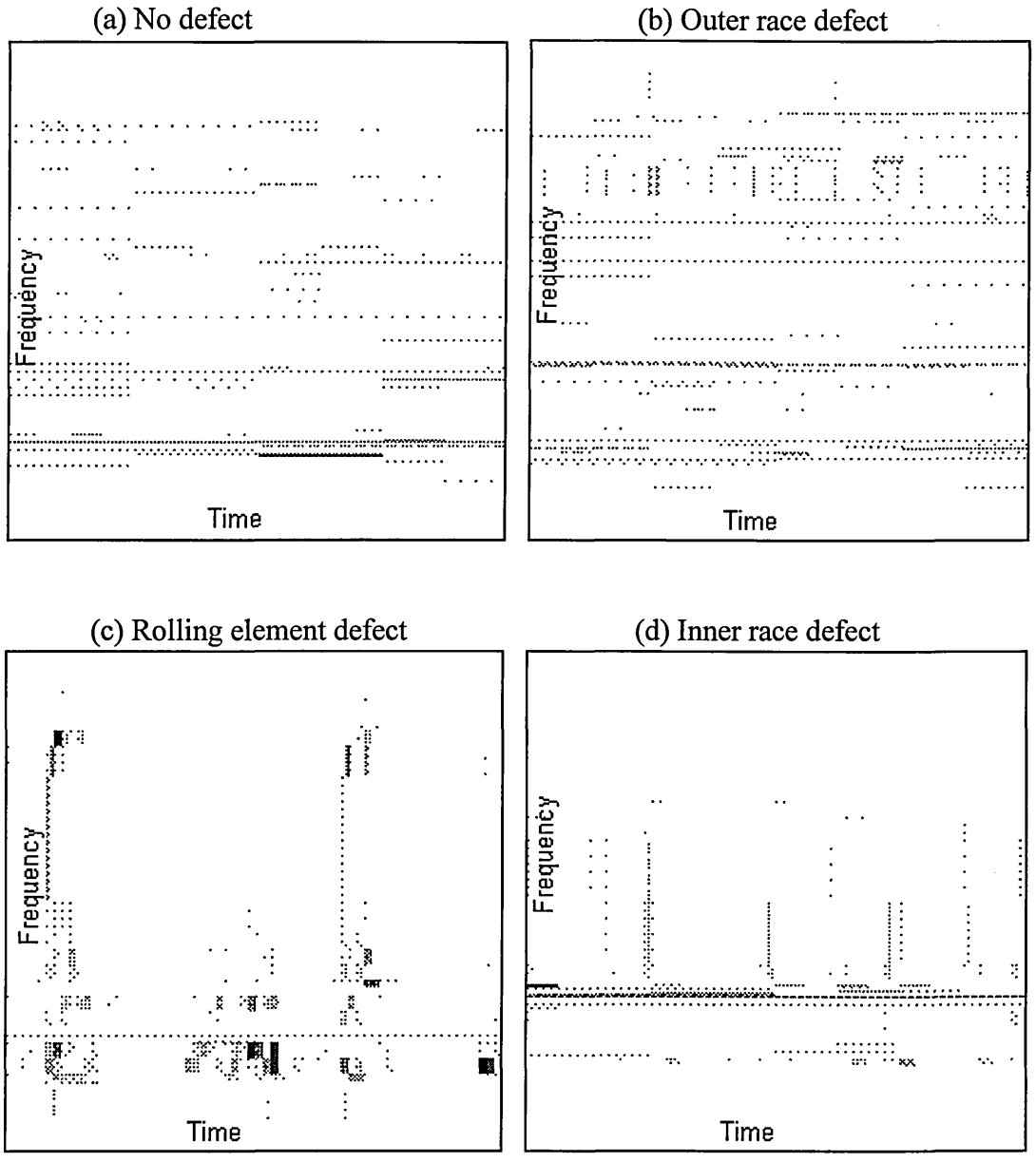

Figure 5.14 Phase plane diagram of air-particle acceleration signal measured from cylindrical rolling element bearing.

(a) Best level from rolling element defect

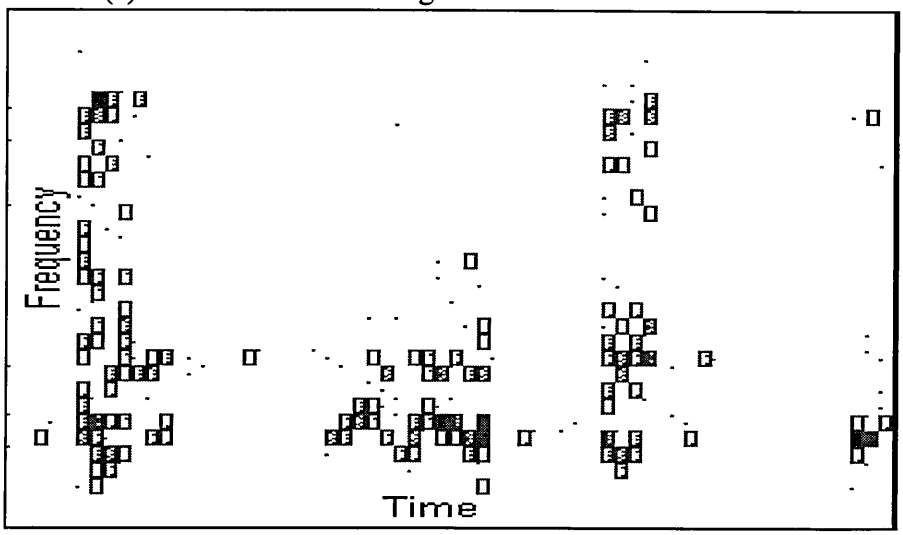

(b) Best basis from rolling element defect

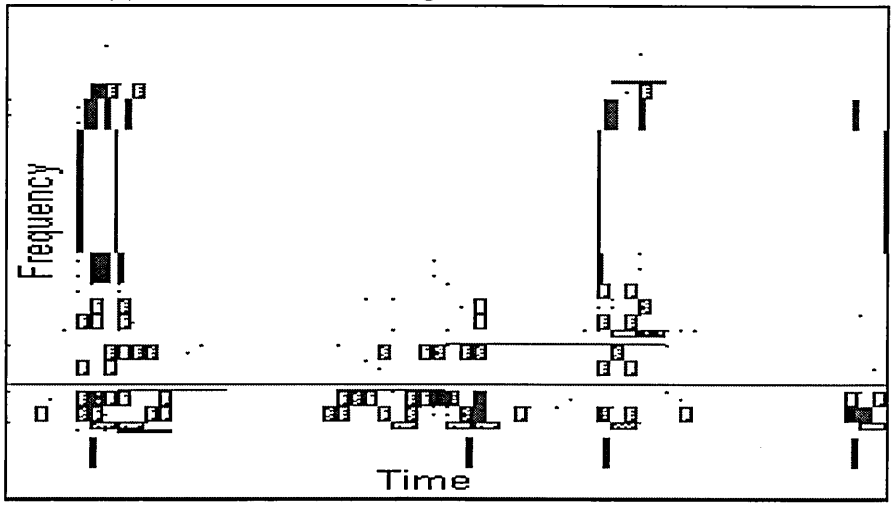

(c) Wavelet basis from rolling element defect

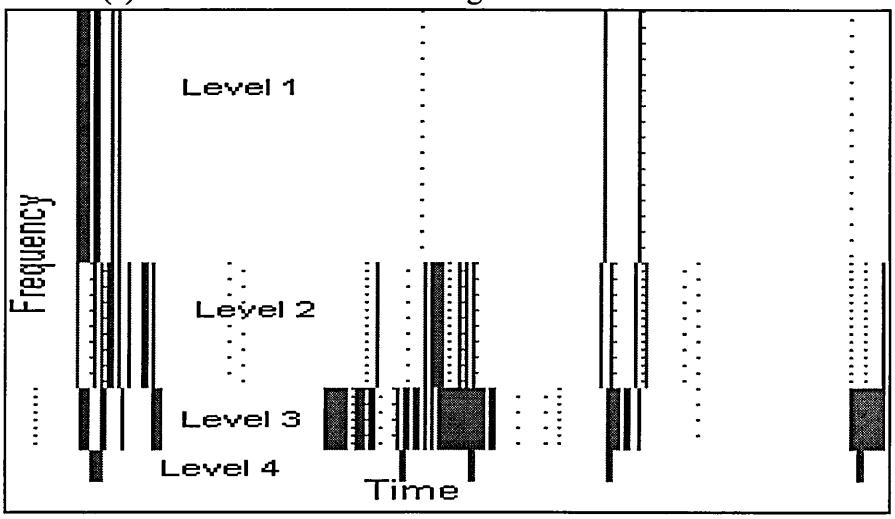

Figure 5.15 Phase plane diagram from different representations of wavelet transform method using air-particle acceleration signal.

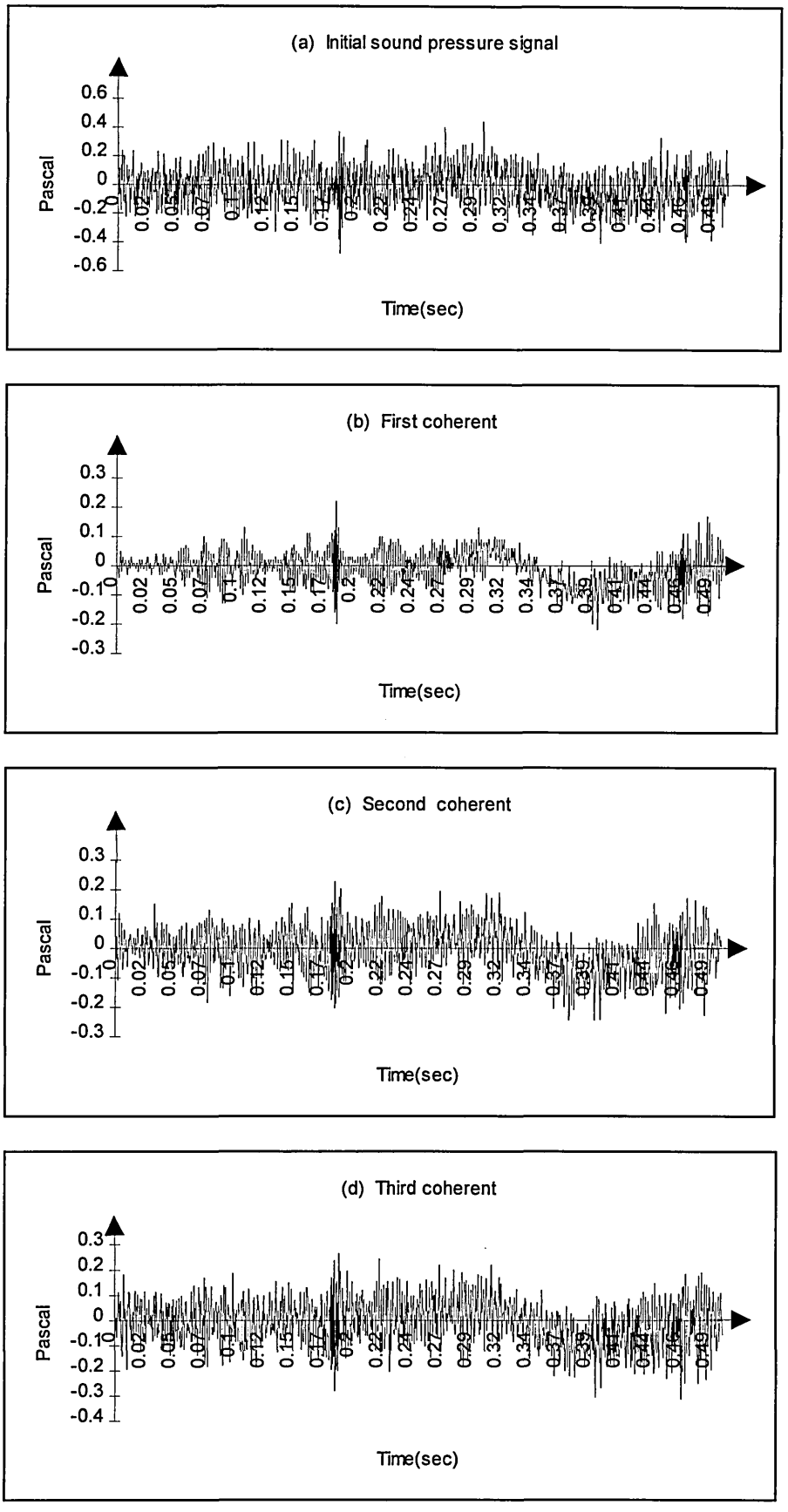

Figure 5.16 Denoising of a sound signal using wavelet packet transform.

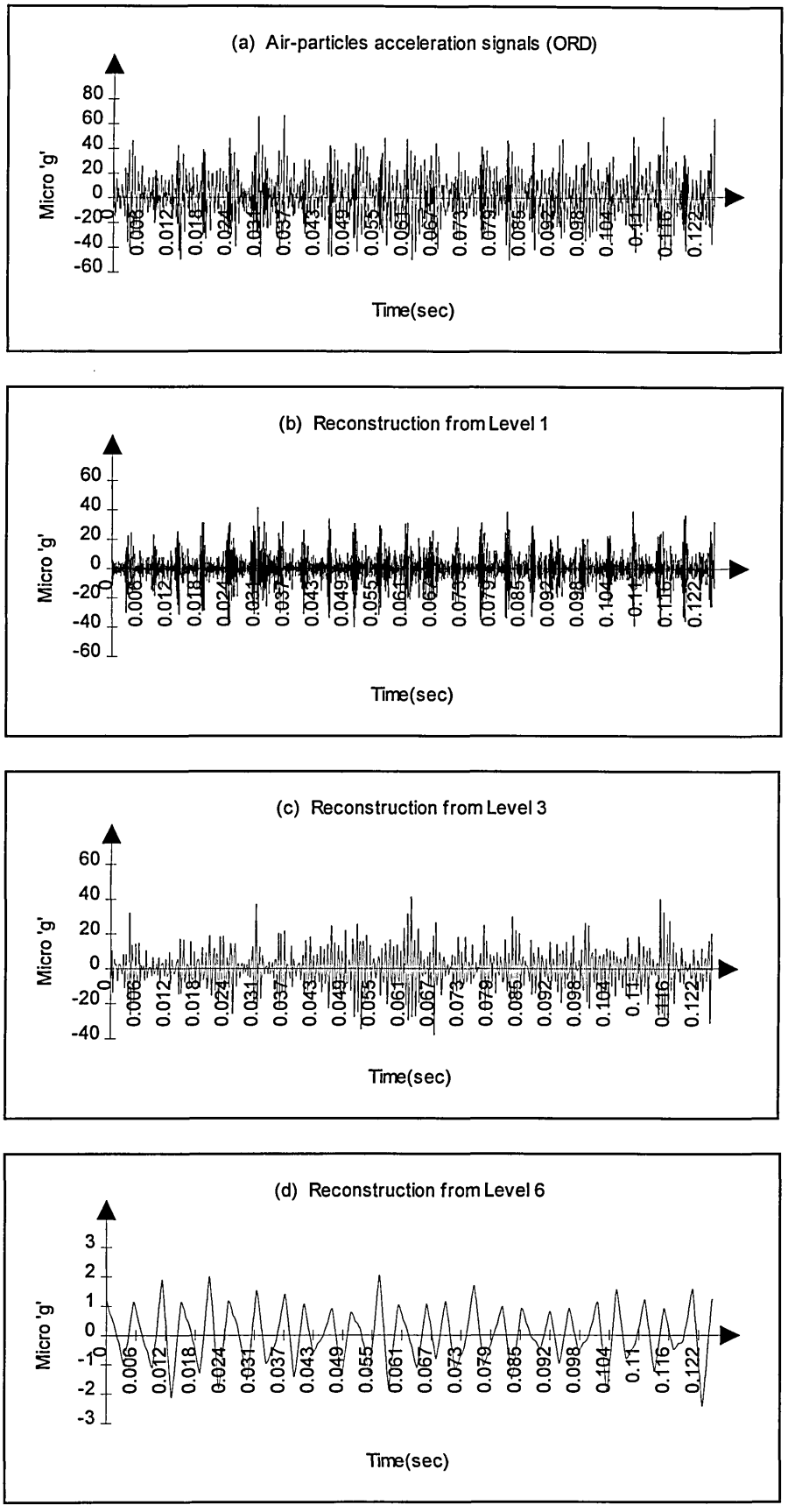

Figure 5.17 Multiscale analysis of air-particle acceleration signal from different level of wavelet transform method.

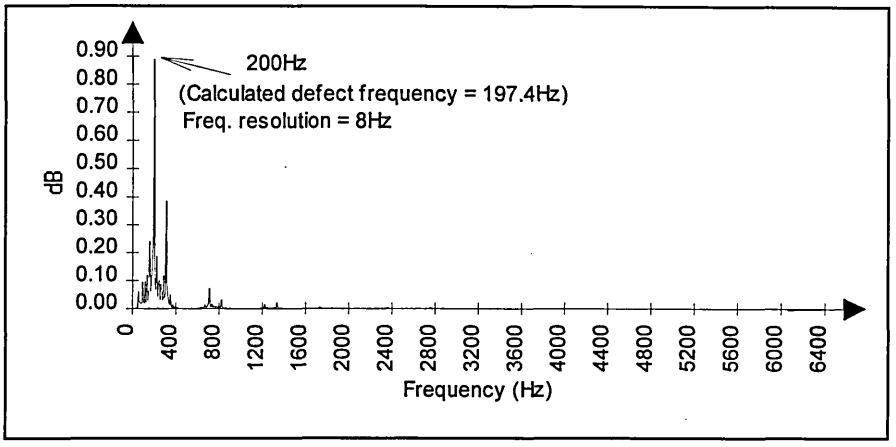

Figure 5.18 Frequency spectrum of the reconstructed wavelet transform from level 6.

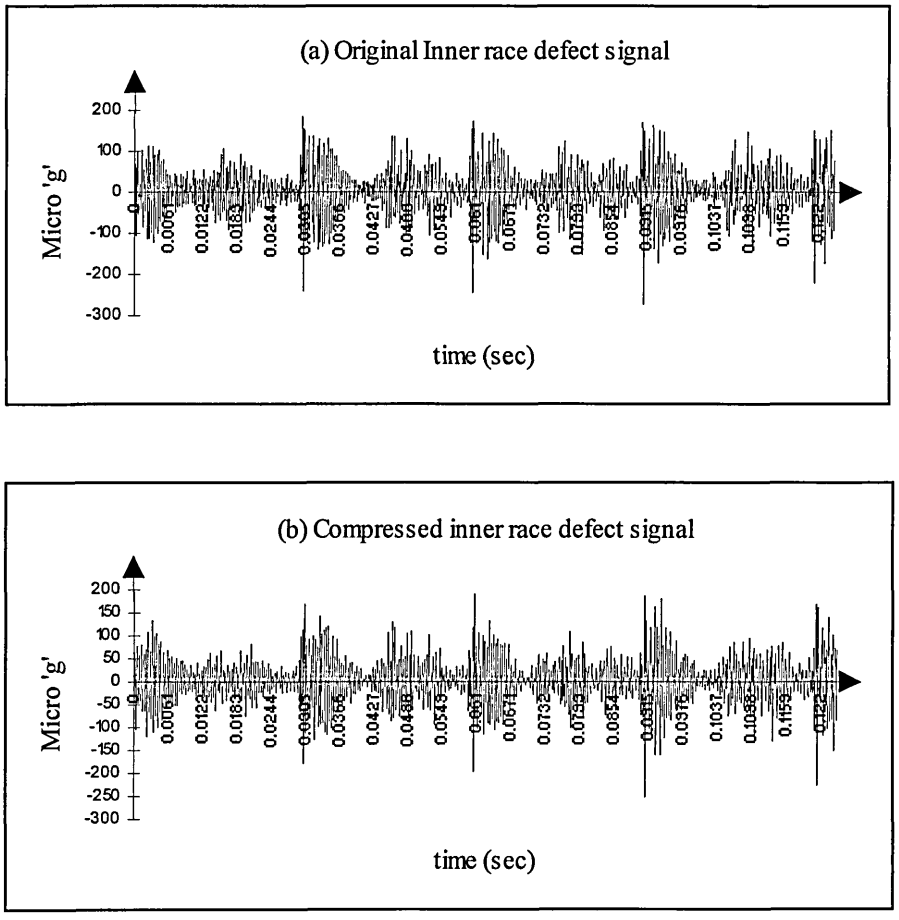

Figure 5.19 Compression of a bearing signal using wavelet packet transform. (Compression ratio 1:20).

CHAPTER 6

NEW METHOD FOR MONITORING BEARING CONDITION USING AIR-PARTICLE ACCELERATION SIGNALS

6.1 Introduction

The operation of a machine component, such as a rolling element bearing, will result in the emission of sound energy into its surroundings. The sound energy produced by a good condition bearing is mostly due to manufacturing inaccuracies in the bearing components. In this simple example, the bearing in operation becomes the sound source which radiates sound power and the effect is the variation of sound pressure in the surrounding area. The sound pressure signal measured using a microphone is dependent on the distance between the sound source and the measuring position. It also depends on the acoustic environment, also called the sound field when the sound waves are present. Because sound pressure is a scalar quantity, its measurement can easily be affected by the presence of other sound sources near the measurement position. This makes it difficult to measure sound pressure due to a machine component in a noisy environment.

With the development of the sound intensity measurement technique, the sound power of a source can be measured in situ even in a noisy environment. Sound intensity is a measure of sound energy flow per unit area at a specific position and direction. Because it is a vector quantity, the presence of a steady external background noise will not have any damaging impact on sound intensity measurement. The vector property of sound intensity measurement is also useful in locating and identifying the source of a noisy component in a complex environment. However, the requirements on the measuring probe and the analysing system are very strict. Because this technique utilises the phase difference between signals from the two microphones to compute the velocity component of the air-particle, any inherent phase mismatch in the microphone pair and analysing instrument will cause errors in the measurement.

The difference between sound pressure and sound intensity measurement is best visualised from the analogy of ripples produced on the surface of a pond if a rock is thrown into it. The behaviour of surface waves in the water is shown in Figure 6.1. The oval shape solid lines in the diagram show maximum displacements of the water level and the dashed lines indicate minimum displacements. These are analogous to the maximum and minimum sound pressure areas in a sound field. Furthermore, the magnitude and direction of wave energy propagation shown by the arrows in the diagram, is measurable using the sound intensity technique in the case of an acoustic disturbance.

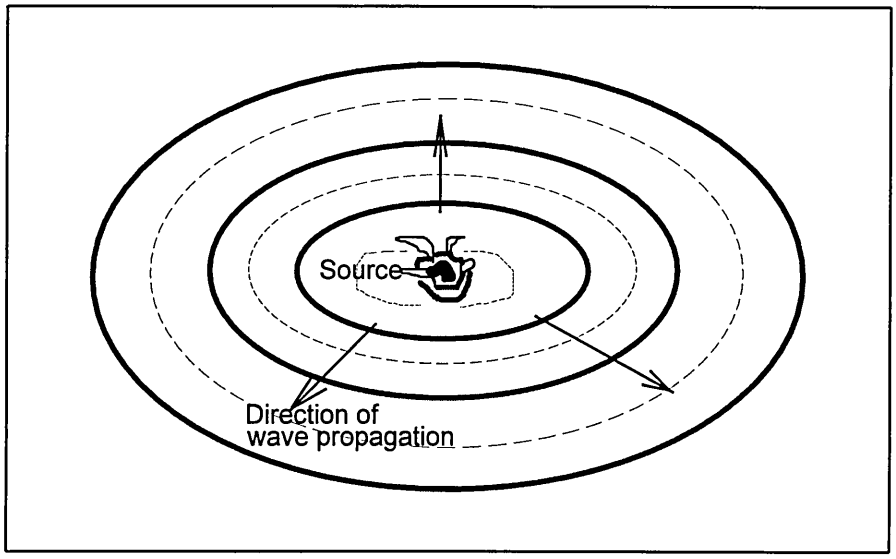

Figure 6.1 Propagation of surface waves in a pond.

A new and novel method is proposed in this study to measure the effect of an acoustic disturbance caused by a sound source. The new parameter introduced in this study is capable of tapping the advantages of using a vector quantity similar to the measurement of sound intensity signal but without its strict requirements on the probe and analysing system. The new parameter proposed in this study is the air-particle acceleration signal which is derived from a two-microphone method similar to sound intensity measurement technique. However, the two microphones do not have to be phase-matched. The only requirement imposed on the microphone pair and the analysing system is that the amplitude response from each channel has to be identical. This

requirement is easily fulfilled by performing amplitude calibration on the two microphones and the analysing system. The easiest way to measure air-particle acceleration signal is using two sound level meters separated by a fixed distance. It is also cheaper to buy the hardware for measuring air-particle acceleration compared to sound intensity measurement system. The formula to compute air-particle acceleration signal using the two-microphone method is presented again in this section for convenience.

$$\boldsymbol{ap}(t) = \left(\frac{p_1(t) - p_2(t)}{\rho_o \Delta r} \right) \qquad (6.1)$$

where

$\boldsymbol{ap}(t)$	is the vector quantity of air-particle acceleration
$p_1(t)$	is sound pressure signal from the first microphone
$p_2(t)$	is sound pressure signal from the second microphone
ρ_o	is the density of air in the acoustic field, and
Δr	is the distance between the two microphones.

This equation shows that knowing the pressure gradient between the two microphones and the air density, the air-particle acceleration signal can be calculated. This parameter does not measure the absolute strength of the sound source rather it is an indication of how much the acoustic field is being disturbed by the sound source. This is sufficient if the signal is to be used to monitor the condition of the sound source.

6.2 Characteristics of the Measuring System

In this study all measurements of the air-particle acceleration signals are carried out using the same instruments that are used to measure the sound intensity signals. Basically, it consists of a pair of condenser microphone arranged face-to-face separated by a solid spacer, and a dual channel signal analyser. Further post processing and display are carried out using a desktop computer.

Because the pressure gradient was calculated using a finite difference approximation from the two microphone positions, it causes a restriction on the upper frequency limit on the measurement of air-particle acceleration signal. Therefore, the smaller the length of spacer used, the higher the frequency range of measurement will be. This is similar to the restriction imposed on the measurement of sound intensity signal. Normally, the frequency range that can be covered using a pair of half-inch microphones with a 12mm spacer is between 64Hz to 6.4KHz. However, a recent study (Jacobsen et al 1996) has proven that the combination of half inch microphones with 12mm spacer is capable of giving an accurate measurement at frequency one octave higher than the limit imposed by the finite difference error. Therefore, the combination of half-inch microphones with 12mm spacer can be used to measure sound intensity and air-particle acceleration up to frequency of 10KHz accurately.

6.3 The Origin of Mechanical Sound

The origin of sound in industry is always associated with the vibration of machine components. However, this is not the only source of sound that is being studied in engineering applications. In this section some of the dominant causes of sound generation in industry are presented.

The first and most common type is sound generated by vibrations of machine component in the audible frequency range which is between 20Hz to 20KHz. This is the common source of sound from vibration of panels and plates on a machine component such as the panels that are used to cover gearboxes or other machine components.

The second type of sound is due to a sudden deceleration or sudden acceleration of rigid bodies. For example, if a small steel sphere is dropped onto a solid floor a sharp "tick" sound is emitted even though the steel sphere is vibrating above the audible frequency range. The sudden deceleration when the sphere hits the floor and the sudden acceleration when it starts to bounce back causes an impulsive motion of the air around

the sphere. The sound produced from this process is often called the acceleration noise and mostly occurs when there are rapid metal to metal contact in machinery.

The next type of sound is normally encountered in an exhaust pipe. The sound signal is produced by an oscillating piston which causes sound waves to travel along a pipe. A body of air at the open end of the exhaust pipe oscillates similar to the sound waves caused by the piston and transmits sound to the surroundings.

Finally, the sound signal caused by turbulent eddies in jet flow is also frequently encountered in industry. This type of sound is sometimes called aerodynamic sound. No vibration of rigid bodies are involved to produce the sound. A common example is the sound produced by gas turbines that are used to propel modern aircrafts.

6.3.1 Noise From Rolling Element Bearing

Sound produced by a bearing is mostly due to irregularities and imperfections on the rolling elements and raceways of the bearing component. About fifty percent of bearing noise is caused by incorrect installation. This is particularly true in the case of roller-contact bearings (Diehl 1973). Sound emitted by a defective bearing is mostly impulsive in nature due to a repetitive metal-to-metal contact of the defective component. This sound signal is also accompanied by sound due to ringing and the resonance effect of the bearing housing. The air-particle acceleration signal is an ideal parameter that can be used to detect abnormality in a rolling element bearing component due to the impulsive nature of such a signal.

6.3.2 Utilising of Air-Particle Acceleration Signals

Predictive maintenance using sound and air-particle acceleration signals can serve two purposes, namely, to reduce the noise level produced by machines and to increase productivity. A properly planned acoustical maintenance program can be coordinated with the predictive maintenance program in industry. Each activity will enhance the

other and an optimised effort is achieved. The equipment needed for these activities are also almost identical. The fitness of a machine in operation and the noise level it produces is determined from a single measurement step. In fact, the method of sound measurement proposed in this study can be used for several purposes such as noise hazard study, hearing conservation, engineering noise control and predictive maintenance programs.

Initially, a baseline study on a new machine under normal operating condition must be carried out. These readings are used as reference levels, whereby the trend of the sound pressure and air-particle acceleration signals is compared to the reference level. An overall dB level can be used for this type of measurement. The equations as presented in Chapter 2 are shown again here for convenience.

$$L_p = 20\,log_{10}\left(\frac{p_{rms}}{p_{ref}}\right)\ dB \qquad (6.2)$$

where p_{rms} is the root mean square value of the sound pressure signals, and p_{ref} is the reference sound pressure at 20 μPa.

$$L_{ap} = 10\,log_{10}\left(\frac{ap_{rms}}{ap_{ref}}\right)\ dB \qquad (6.3)$$

where ap_{rms} is the root mean square value of the air-particle acceleration signals, and ap_{ref} is the reference value at 9.81×10^{-6} m/s^2 (1 micro 'g'). Similarly, an overall dB level of vibration signals is calculated from the equation:

$$L_{vb} = 10\,log_{10}\left(\frac{vb_{rms}}{vb_{ref}}\right)\ dB \qquad (6.4)$$

where vb_{ref} used for this study is 0.01g (10 milli 'g').

If an abnormal high acoustic signal is detected from a machine component, a detailed analysis can be carried out to diagnose the fault present in the machine component. In this study, several different types of analysis method are used for the diagnosis including statistical, spectral, cepstral, and wavelet transform methods. Some samples of diagnosis work to determine the type of defect presence in a cylindrical rolling element bearing were already presented in the previous chapters.

6.4 Validation Study

A new set of bearings were used for the validation study. The type of bearing used is an *RHP* cylindrical roller bearing Type *NF209ETNCNSK* with diameter of rolling element, d_{re} = 10.97mm, pitch diameter, d_p = 65.47mm and number of rolling element, n = 16. The cage for the rolling element was made from plastic material and the operation of this type of bearing was quieter than the previous type of test-bearing used in this study.

Two types of experimental study were carried out at this stage. First, the sensitivity of using the air-particle acceleration signal to detect a defective bearing component was compared to the performance of using sound pressure and vibration signals. For this experiment, a uniform line defect was created on the rolling elements using Spactron Electro Discharge Machine (EDM). Several different sizes of line defect were manufactured as shown in Plate 6.1 and the nominal size of these defects are presented in Table 6.1. The smallest size of line defect shown in the table was made using a TEER ST200, Scratch Test Machine. Measurements of the defect size were carried out using a Laser Form Talysurf 120L Machine manufactured by Taylor Hobson Company.

Table 6.1 Different sizes of rolling element line defect used in this study.

Rolling Element Line Defect no.	Nominal Width (mm)	Nominal Depth (mm)
Sample no.1	0.500	0.430
Sample no.2	0.250	0.275
Sample no.3	0.190	0.041
Sample no.4	0.090	0.003

(a) Defect sample no.1, nominal width = 0.50mm

(b) Defect sample no.2, nominal width = 0.25mm

(c) Defect sample no.3, nominal width = 0.19mm

(d) Defect sample no.4, nominal width = 0.09mm

Plate 6.1 Different sizes of rolling element defect tested in the study

The second study was concerned with the effectiveness of using air-particle acceleration signal in the presence of high background noise. The performance using air-particle acceleration signals was compared to the results from using sound pressure signals. For this study the background noise was produced by connecting a white noise generator Type 419C, manufactured by Dawe Instrument Limited, to a Q-Max Wedge Monitor, CSPWM152 loud speaker. The set-up for this experiment is shown in Figure 6.2 below. The sound pressure microphones were located 230mm above the test-bearing during all of the experiment activities.

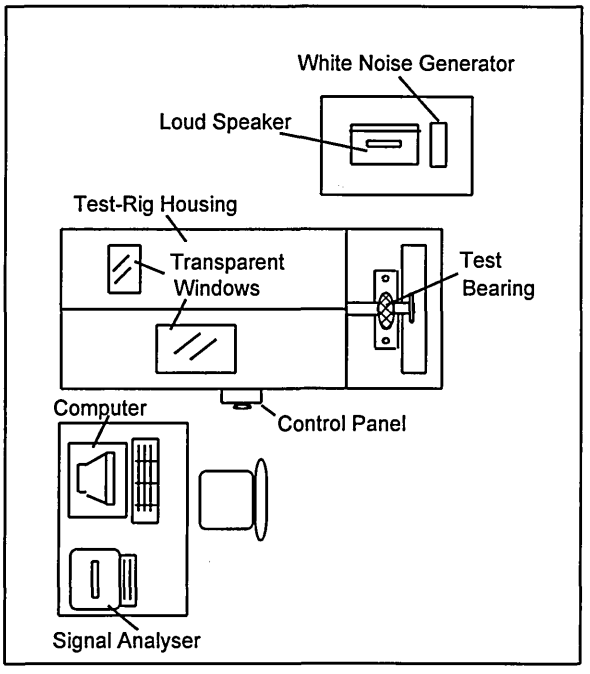

Figure 6.2 Top view of the experimental set-up.

6.4.1 Detailed Study of Defect Detectability

A study to establish the effectiveness of using air-particle acceleration signals compared to sound pressure and vibration signals was performed the results of which are presented in this section. Four different sizes of line defect as shown in Plate 6.1 were introduced on rolling elements of a cylindrical roller bearing. The study was carried out at three different speeds of the shaft, namely: 500, 1500 and 3000rpm. These speeds represent a low speed, a medium speed and a high speed of the shaft respectively. For each case,

eight samples of data were measured, analysed and recorded. The type of variables used for the study were the overall dB levels calculated from the rms value of a signal and Kurtosis value calculated from statistical method established in the previous chapters.

The results obtained from defect sample no.1 (0.5mm nominal width) and sample no.2 (0.25mm nominal width) showed clear indications of the presence of defect in the test-bearing. This was consistent with all the different types of signal used in the study. Therefore, they are not shown here because they do not show the relative performance of using different types of signal to indicate the presence of defect in a bearing component.

Table 6.2 shows result obtained from the measurement of signals from a test-bearing with no defect. The values in brackets show the range of the calculated parameters obtained from eight samples of data for each case. The values shown above the brackets are the statistical mean values of the calculated parameters from all eight samples. Notice that the overall dB value increases as the shaft speed increases, whereas the Kurtosis value remain almost the same at all speed. This scenario is consistent with all the different types of signal used in the study. Therefore, the Kurtosis value from a bearing with no defect at any shaft-speed should be very close to three.

Results from the experimental work carried out using the test-bearing with defect sample no.3 (0.19mm nominal width) are shown in Table 6.3. Although the overall dB value increases as the shaft-speed is increased, the values themselves are consistently lower than the values measured when there was no defect present in the test-bearing. This can be seen clearly by comparing the results presented in Table 6.3 with the results in Table 6.2. For example, the mean dB value of sound pressure signal from a test-bearing with defect sample no.3, and with shaft-speed of 500rpm is 64.4dB as shown in Table 6.3. Whereas the mean dB value of sound pressure signal from a test-bearing with no defect is 66.0dB. This result indicates that the overall sound energy actually decreases in the presence of a line defect in the rolling element of the test-bearing. The reason for this is complex in nature, and it depends on the transfer function of the physical system. Thus the accepted norm that a quieter machine indicates that there is no defect presence could be misleading. The nature of the sound signal emitted needs to

be identified before the condition of the machine can be established. These results also show that whenever there was changes in the overall dB value of a measured signal, either it was lower or higher than the reference level, a more detailed study on the machine component must be performed in order to determine the cause.

The kurtosis values shown in Table 6.3 are used to indicate whether the defect signal is detectable from the measurement of sound pressure, air particle acceleration and vibration signals. The kurtosis values also indicate that the presence of defect sample no.3 is not detectable from the measurement of sound pressure signals. This finding is consistent with all the shaft-speeds tested in the study. In addition, Kurtosis values at shaft-speeds of 500rpm and 1500rpm reveal that air-particle acceleration signals are capable of indicating the presence of defect signal from defect sample no.3. However, when the shaft-speed was set to 3000rpm the Kurtosis value from air-particle acceleration signals failed to indicate the presence of defect in the test-bearing.

Another interesting finding from Table 6.3 is that the performance of air-particle acceleration signals to indicate the presence of a defect in the test-bearing is superior to the performance of vibration signal when the shaft rotates at low speed, i.e. 500rpm. On the other hand, the performance of the vibration method is slightly superior than the performance of air-particle acceleration signal when the shaft rotates at high speed, i.e. 1500rpm and 3000rpm. At low speed, the reading of vibration signals from an accelerometer were easily corrupted by the low-frequency vibration of the test-rig structure and also by the vibration of the test-bearing support structure. On the other hand, at high speed, the reading of the air-particle acceleration signals were easily corrupted by the high-frequency components from reflections of sound signals emitted by the other moving components in the test-rig. Although all the other moving components were placed in an enclosure, the high-level, high-frequency sound signal they produced can easily escape from tiny openings of the enclosure. Any reflections which were inline with the probe will be included in the air-particle signals that were being measured. This argument is supported by the evidence shown in Figure 6.3. Part(b) of the figure, shows a sample of air-particle acceleration signal when the shaft-speed was set to 500rpm. The impulsive nature of defect signals emitted by the defect sample no.3 are clearly indicated in the figure. It is also clear that most of the signals in

this figure consist of high frequency components, compared to Part (c) where a sample of vibration signal under similar situation is corrupted mostly by low-frequency vibration signal from the test-rig structure.

Results from the smallest size of defect tested in this study are shown in Table 6.4. The results from vibration signals show that the presence of defect sample no.4 in the test-bearing was not detected at the speeds tested in the study. Whereas, only a slight indication of the defect signal was indicated from the Kurtosis value of air-particle acceleration signal at 500rpm. This result confirm earlier findings that the air-particle acceleration signal is superior to vibration signal when the test-shaft was rotating at low speed, i.e. 500rpm. At other speeds tested, results from air-particle acceleration also failed to show any abnormality in the test-bearing.

Table 6.2 Results from analysis of bearing signals with no defect

Speed (rpm)	Type of Signals					
	Sound Pressure		Air-Particle Acceleration		Vibration	
	dB-Level	Kurtosis	dB-Level	Kurtosis	dB-Level	Kurtosis
500	66.0 (65.0 - 67.0)	2.9 (2.7 - 3.1)	7.9 (7.4 - 7.8)	3.1 (2.8 - 3.3)	27.7 (26.5 - 29.7)	3.0 (2.7 - 3.3)
1500	76.6 (76.2 - 77.0)	3.0 (2.7 - 3.3)	10.1 (9.7 - 10.3)	3.0 (2.7 - 3.3)	36.3 (35.5 - 36.8)	3.0 (2.9 - 3.2)
3000	79.6 (78.7 - 80.5)	2.9 (2.8 - 3.1)	13.1 (12.8 - 13.4)	3.0 (2.8 - 3.1)	61.4 (60.8 - 61.7)	2.9 (2.8 - 3.0)

Table 6.3 Results from analysis of bearing with defect sample no.3. (Nominal width of defect = 0.190mm).

Speed (rpm)	Type of Signals					
	Sound Pressure		Air-Particle Acceleration		Vibration	
	dB-Level	Kurtosis	dB-Level	Kurtosis	dB-Level	Kurtosis
500	64.4 (62.3 - 65.9)	3.1 (2.6 - 3.3)	6.0 (5.6 - 6.4)	5.1 (3.9 - 6.7)	11.2 (11.0 - 11.3)	3.4 (2.9 - 3.6)
1500	71.8 (70.5 - 73.9)	3.2 (2.8 - 3.3)	8.3 (7.8 - 9.3)	3.7 (3.1 - 4.1)	19.5 (19.3 - 19.7)	4.2 (3.4 - 6.1)
3000	77.3 (76.5 - 78.0)	2.9 (2.8 - 3.0)	13.2 (12.4 - 16.4)	3.1 (3.0 - 3.3)	25.0 (24.9 - 25.2)	3.9 (3.5 - 4.8)

Table 6.4 Results from analysis of bearing with defect sample no.4. (Nominal width of defect = 0.090mm).

Speed (rpm)	Type of Signals			
	Air-Particle Acceleration		Vibration	
	dB-Level	Kurtosis	dB-Level	Kurtosis
500	9.7 (9.4 - 9.9)	3.7 (3.2 - 4.2)	26.6 (26.0 - 27.3)	3.1 (2.9 - 3.3)
1500	10.2 (9.8 - 10.5)	2.8 (2.6 - 3.0)	35.0 (34.2 - 35.5)	2.9 (2.7 - 3.1)
3000	12.4 (12.3 - 12.6)	3.1 (2.9 - 3.3)	61.1 (60.8 - 61.4)	2.9 (2.6 - 3.2)

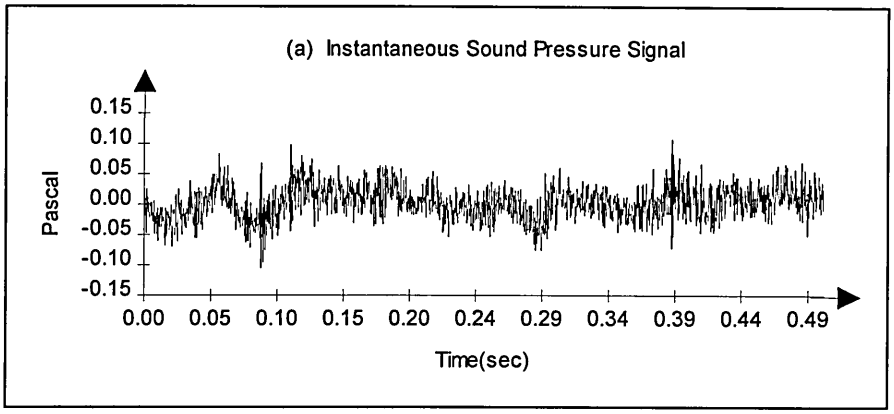

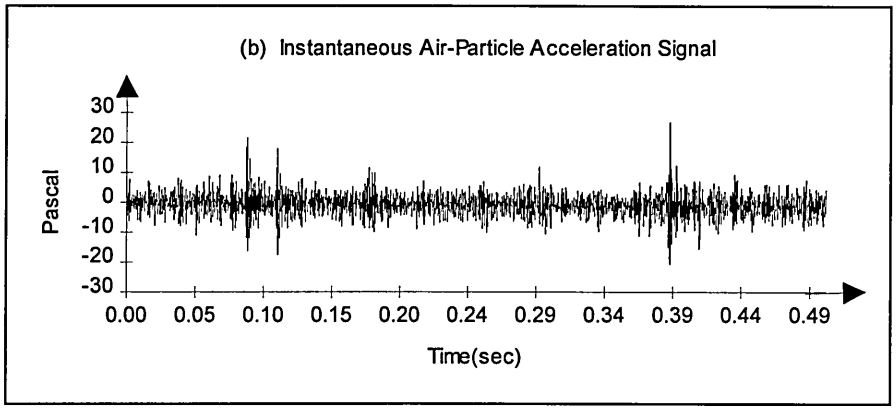

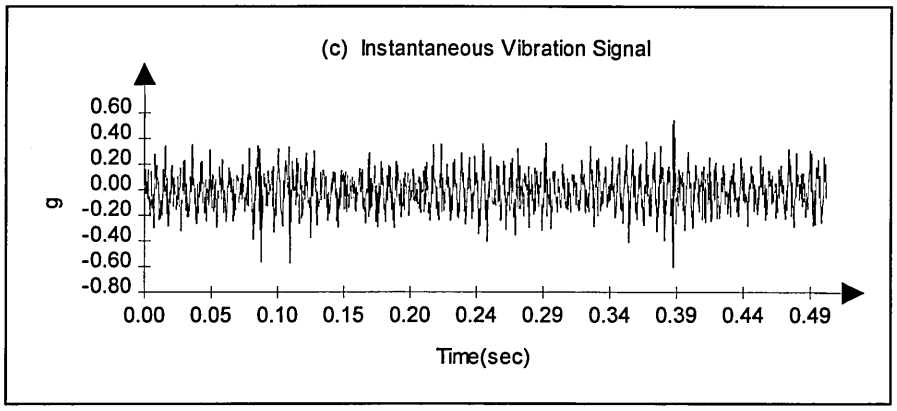

Figure 6.3 Samples of time domain signal measured from defect sample no.3 when the shaft-speed is set to 500rpm.

6.4.2 Effect of Background Noise

Experimental work to study the effect of high background noise on the performance of air-particle acceleration signals as carried out, and is presented in this section. The experiments were carried out using a cylindrical rolling element bearing with defect sample no.2 as shown in Plate 6.1. Data from the measurement of air-particle acceleration signals was analysed for three different speeds of the test-shaft: 500rpm, 1500rpm and 3000rpm. However, only results from shaft-speed of 1500rpm are presented in Table 6.5 because they show the limit of the effectiveness of air-particle acceleration signals in the presence of high background noise.

A white noise generator was connected to a loud speaker to produce high amplitude background sound signal which contain all the frequency range that were included in the study. A sound level meter was used to measure the overall dB levels of the background noise. A linear weight filter was used for the calculation of overall dB level, whereby all frequency components have equal contribution towards the overall value. For each scenario, eight samples of air-particle acceleration signals are recorded and analysed as indicated in Table 6.5. For each sample, the Kurtosis value was calculated and used to evaluate the effectiveness of using air-particle acceleration signal to indicate bearing defect in the presence of high background noise.

The second column in Table 6.5 presents Kurtosis values calculated from air-particle acceleration signals measured only from the test-rig with minimal background noise in the laboratory. A typical linear weight background sound level in the laboratory was measured between 54dB to 58dB. This was very low compared to the sound level measured from the test-rig alone at 72dB. Therefore, the effect of background noise level for this case was considered to be minimal.

The last row of the table presents the mean Kurtosis value calculated from all eight samples of the signals being measured for each scenario. For instance, the mean Kurtosis value measured from test-rig alone was calculated to be equal to 9.5. This shows a clear indication of the presence of defect sample no.2 in the test-bearing. Results shown in Table 6.5 also indicate that the presence of defect sample no.2 in the

test-bearing was detectable from measurement of air-particle acceleration signals even when the overall background noise level was 90dB. This background level was 14dB higher than the sound signal emitted by test-rig alone. This is a very good indication of one of the advantages derived from using air-particle acceleration signal to monitor the condition of a machine component.

A sample of time domain signals obtained from measurement of sound pressure and air-particle acceleration signals is shown in Figure 6.4. The signals in part (c) and (d) are obtained from the first sample of measurement when the overall background noise level is set to 90dB which is 14dB higher than the sound signal produced by the test-rig alone. The impulsive signals due to the presence of defect sample no.2 is clearly indicated in the air-particle acceleration signals. Whereas, measurement of sound pressure signals failed to indicate the presence of defect in the test-bearing as shown in part (c) of the figure.

This result shows that even if the background noise energy is much higher than the sound energy emitted by the defective bearing, air-particle acceleration signals are still able to pick up the signals emitted by the defective bearing. However, the efficiency of using air-particle acceleration signal is also dependent on the direction of the background noise. For this experiment the direction of background noise propagation is perpendicular to the axis of the measurement probe, therefore obviously, the effect of the high background noise on the measurement of air-particle acceleration signal is minimal. Nevertheless, these results show that a big improvement is achieved when using air-particle acceleration signals compared to the performance of using sound pressure signals.

The directionality characteristic of the two-microphone method can be used to search for a dominant sound source. A sound incident at ninety degrees angle with respect to the probe axis will show minimum amplitude display on the reading of air-particle acceleration signal, as shown in Figure 3.5. Therefore, the direction and location of a dominant sound source is easily indicated using this method.

Table 6.5 Kurtosis values of air-particle acceleration signal in the presence of high background noise. Shaft-speed = 1500rpm.

Defect Sample no.2	Test-Rig Alone: 76dB	Background Noise: 87dB	Background Noise: 90dB	Background Noise: 93dB	Background Noise: 97dB
Signal no.1	10.5	4.6	4.9	3.4	3.1
Signal no.2	10.8	3.7	6.0	3.1	3.1
Signal no.3	10.2	4.5	3.4	3.5	3.3
Signal no.4	11.9	4.3	5.7	4.6	3.0
Signal no.5	7.0	4.3	5.3	3.4	3.2
Signal no.6	12.7	4.0	3.7	2.9	3.0
Signal no.7	5.3	5.5	4.4	3.2	3.0
Signal no.8	7.3	6.1	4.6	3.7	3.0
MEAN	9.5	4.6	4.8	3.5	3.1

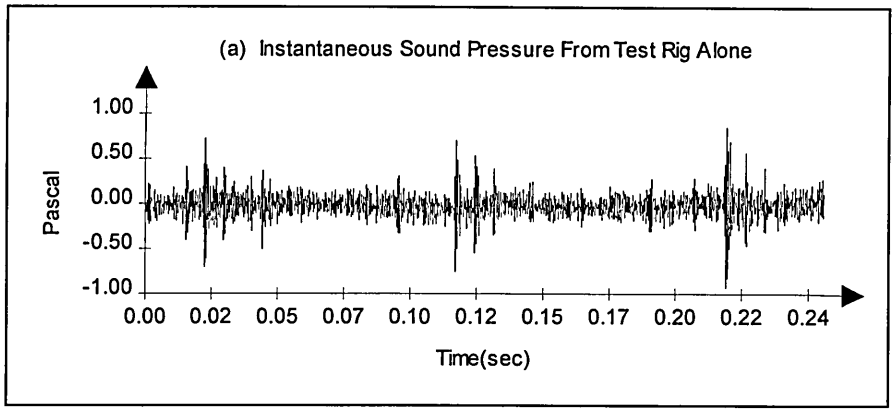

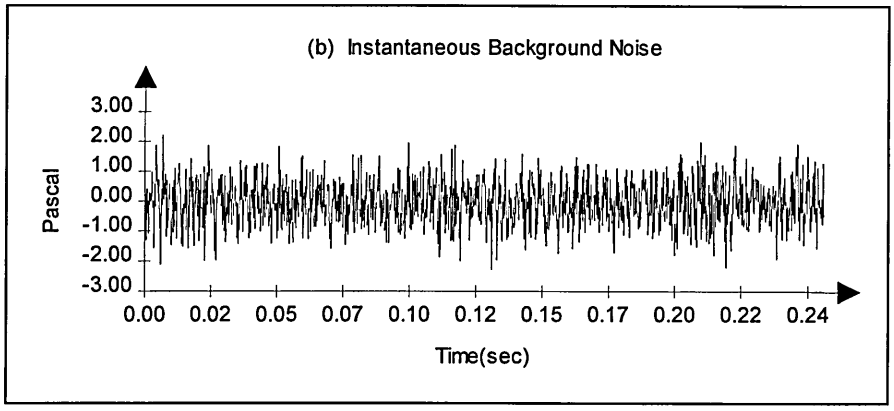

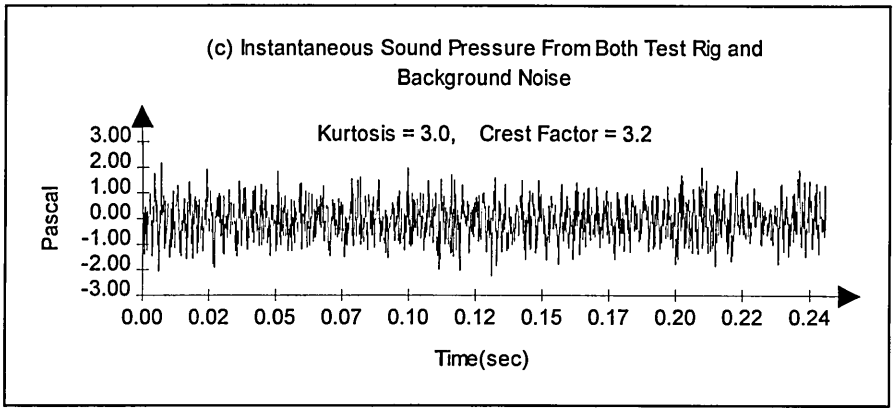

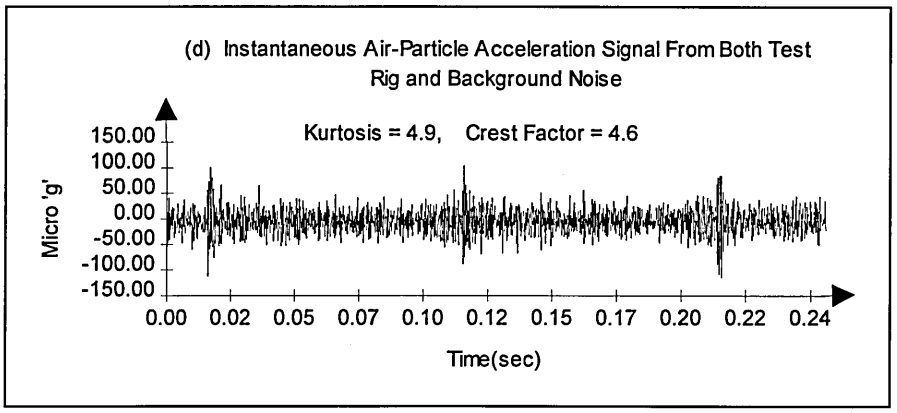

Figure 6.4 A sample of time-domain signals measured from test-rig with defect sample no.2 and a high background noise at 90dB.

6.5 Industrial Case Study

A four-channel tape recorder was used to carry out field measurement of sound and air-particle acceleration signals. Then, the recorded signals were brought into the laboratory to be analysed. This is the common method used to analyse field data if the analysis equipment is expensive, bulky and sensitive to mechanical shock. Although, robust and portable equipment can also perform the same task in the field if it is available. In this study a Store 4D Racal, four-channel tape recorder was used to record vibration, sound and air-particle acceleration signals in an industrial environment.

6.5.1 Calibration of Tape Recorder

Before the tape recorder was used in the industry, the performance of the tape recorder was checked and calibrated in the laboratory. The amplitude and phase responses in each channel of the tape recorder were also checked to make sure that they were within the acceptable limit for sound intensity measurement technique. Although, for the measurement of air-particle acceleration signals, only the amplitude response between each channel has to be identical. The overall set-up for the tape calibration procedure is shown in Figure 6.5 below.

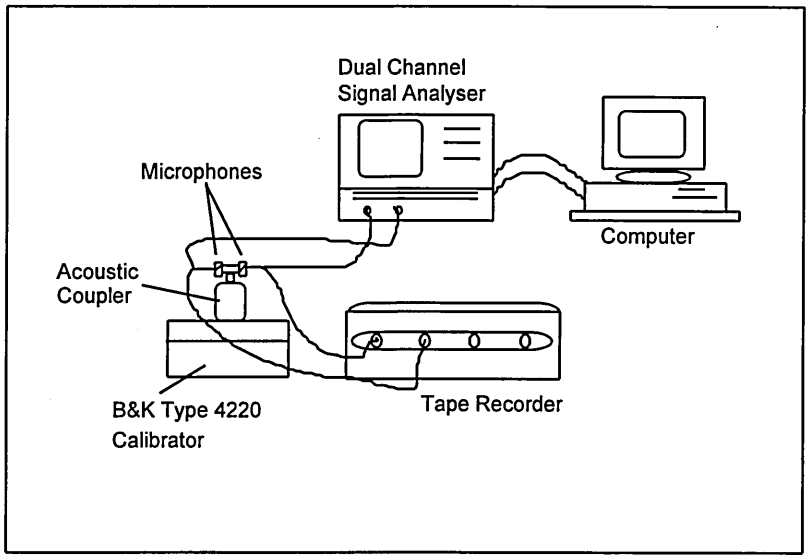

Figure 6.5 Overall set up of tape calibration procedure.

The results of phase calibration between two channels of the tape recorder is presented in this section. For this case, the calibrator was used to produce a sound signal at a particular frequency. The acoustic coupler will make sure that the sound signals recorded by the two microphones are at the same phase relative to each other. Phase mis-match in the two channels will cause a lower frequency limit in the sound intensity measurement technique. The signals measured from the two microphones were recorded onto the tape recorder, at the same time the signals were also recorded by the signal analyser. From the recorded signal of the tape recorder and the signal analyser, the accuracy of the tape-recorded signal were confirmed.

Calculation of phase mis-match between the two channels of the tape recorder used to record sound signals was carried out using the following equation:

$$\phi = \tau_{12} \times f \times \frac{360^o}{cycle} \qquad (6.6)$$

where

ϕ is the phase mis-match between the two channels.

τ_{12} is the time delay between the two channels calculated from the maximum value of cross-correlation function.

f is the frequency of the sound signal being measured in Hertz.

The phase mis-match at a frequency of 40Hz is calculated to be:

$$\begin{aligned} \phi &= 7.08\times10^{-7}\,\text{sec} \times 40\,\text{cycle/sec} \times 360\,\text{degree/cycle} \\ &= 0.01\,\text{degree} \end{aligned}$$

It shows that the worst scenario in the phase mismatch calculation is very small, and therefore, the effect of phase mis-match in tape measurement of sound signal was considered to be minimal.

6.5.2 Monitoring of Bearing Signals at Caparo Merchant Bar, Scunthorpe

The Caparo Merchant Bar (CMB) was officially opened in 1985 as a joint venture with British Steel. It produces popular sizes of flat plate, angle, channel and round steels for the volume sector market For the purpose of this study, measurement of vibration, sound pressure and air particle acceleration signals were carried out on the rear bearing of Rolling Stand 2 in the Light Section Mill. The instruments used for the measurements included: sound level meter, accelerometer, sound intensity probe, charge amplifier, dual channel signal analyser and a four-channel tape recorder. A set-up of the measuring transducer with the machine component is shown in Plate 6.2. All the signals were measured and recorded simultaneously, and the characteristics of the signals being measured represent a typical scenario of the operational activities of the plant. The background noise level measured during the study varied from 90dB up to 100dB measured on a linear-weighted scale, and the nominal speed of the shaft was measured to be 1062rpm. These measurements were carried out on Wednesday 26th June 1996. The data were recorded onto the tape recorder and brought to the laboratory for further analysis work.

Plate 6.2 Positions of the accelerometer and microphones for the measurement of industrial data.

6.5.2.1 Analysis of data

Because it is not possible to monitor a defective bearing component in the plant, only measurement of a normal bearing under typical operating condition was carried out. Comparison study on the performance of vibration, sound pressure and air-particle acceleration signals was performed to evaluate the effectiveness of using air-particle acceleration signal in an industrial environment. Basically, operation of the Roller Stand 2 can be separated into three parts:

(i) unloaded, where no steel bar was being rolled,

(ii) initial loading step, where the steel bar was being rolled into position, and

(iii) fully loaded, where the steel bar was already in position for rolling.

All of the three steps of operation can be seen clearly from the time domain measurement of vibration signals as shown in Figure 6.6. When the roller was not loaded the vibration signal shows a uniform high frequency oscillation of the bearing housing with relatively low amplitudes. However, at the instance when the bar was being fed to the roller a sudden increase in vibration amplitude was recorded as shown in Part (b) of the figure. The vibration signals of a loaded roller as shown in Part (c) indicates that the amplitude of the vibration signal was higher compared to the vibration level when the roller was not loaded. The vibration of a loaded roller mainly consists of lower frequency components due to the response of the whole machine structure being measured by the accelerometer. This can be seen by comparing the nominal period of oscillations of the vibration signals shown in Part (a) and (c) of the figure.

The instantaneous time domain of air-particle acceleration and sound pressure signals presented in Figures 6.7 and 6.8 can only indicate two modes of roller operation: loaded and unloaded. The high impulsive signals shown from measurement of vibration signal during the loading operation is not indicated from sound and air-particle acceleration signals. This is because the air-particle acceleration measurement technique is only sensitive to the local change of the air-particle motion. During the loading operation, the high impulsive nature of vibration and sound pressure signals were located at the roller itself which was far away from the rear bearing. Therefore, the local air-particle acceleration signals near the rear bearing were not affected by the loading process. Whereas, reading of sound pressure signals was easily corrupted by the presence of high background noise in the plant. Kurtosis values calculated from all the measured signals showed that the bearing being monitored was in good condition.

Measurement of vibration signals as shown in Figure 6.9 was dominated by frequency components ranging from 2.5KHz to 3.0KHz which can be associated with the transfer function of the bearing housing. The frequency spectrum of the air-particle acceleration

signal showed a uniform distribution of high frequency components between 3.5KHz up to 6.4KHz, although the amplitudes are slightly less than the low frequency components. Whereas, frequency averaging of sound pressure signals show that it is dominated by low frequency components at 144Hz and 472Hz which mostly come from background noise from other sources in the plant. This shows that the measurement of air particle acceleration signal is more sensitive towards the changes in high frequency components. This is the region which is most affected by the presence of a defect in a bearing due to metal-to-metal contact in the bearing components. This result is similar to the discussion presented in Section 6.3.1. The frequency spectra in Figure 6.9 are obtained from averaging fifty instantaneous spectrum of the signals being measured. The frequency averaging process was performed in order to minimise the effect of random noise on the measured signals.

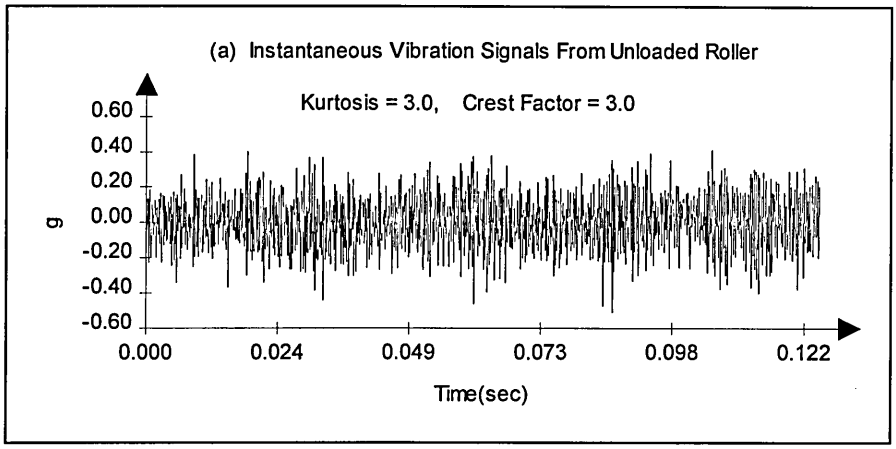

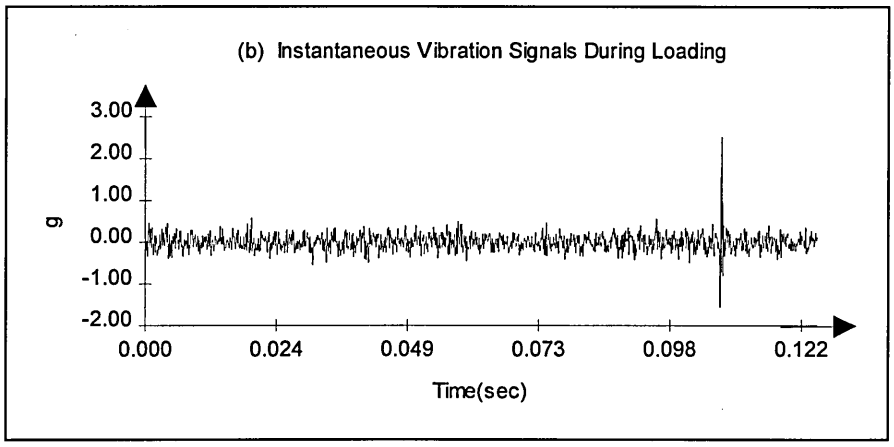

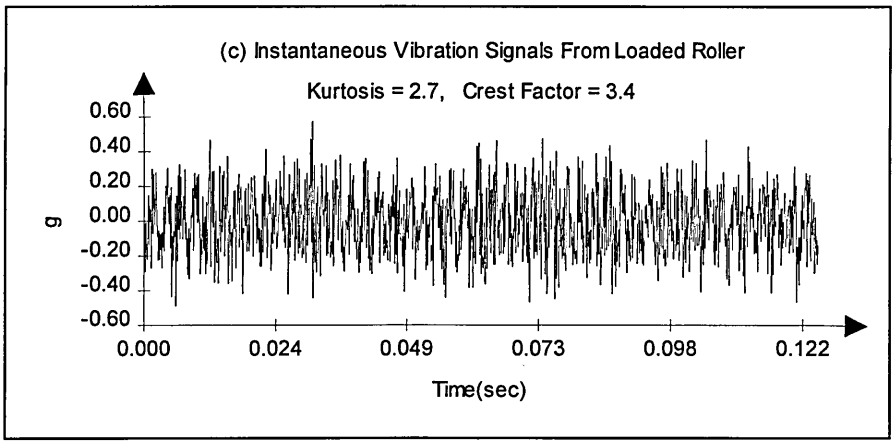

Figure 6.6 Instantaneous vibration signals from different operating conditions of Roller Stand 2.

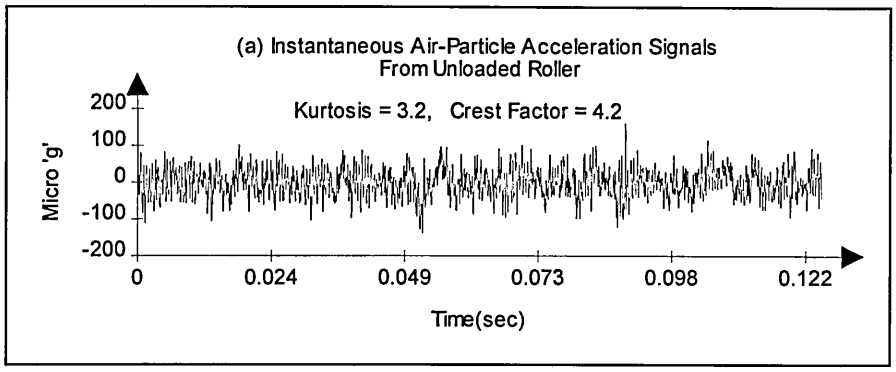

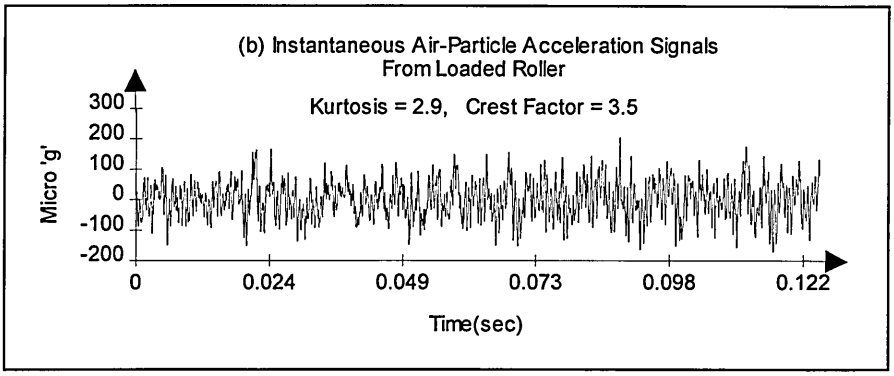

Figure 6.7 Instantaneous Air-Particle Acceleration signals from different operating conditions of Roller Stand 2.

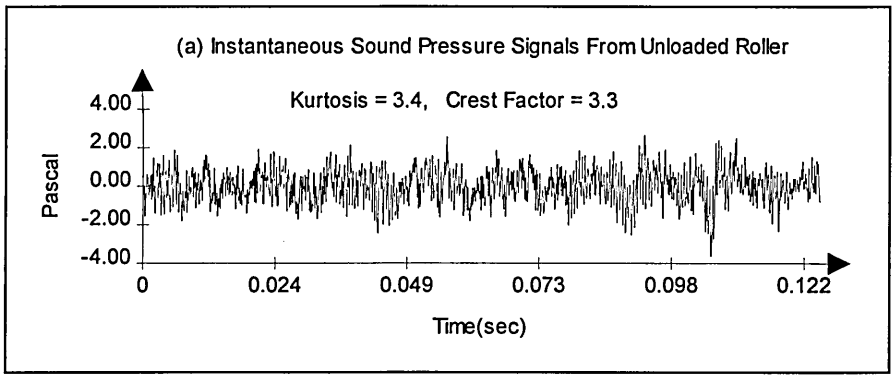

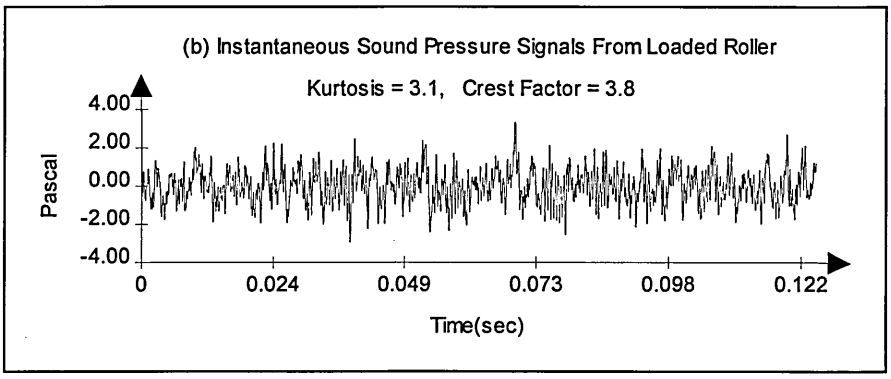

Figure 6.8 Instantaneous sound pressure signals from different operating conditions of Roller Stand 2.

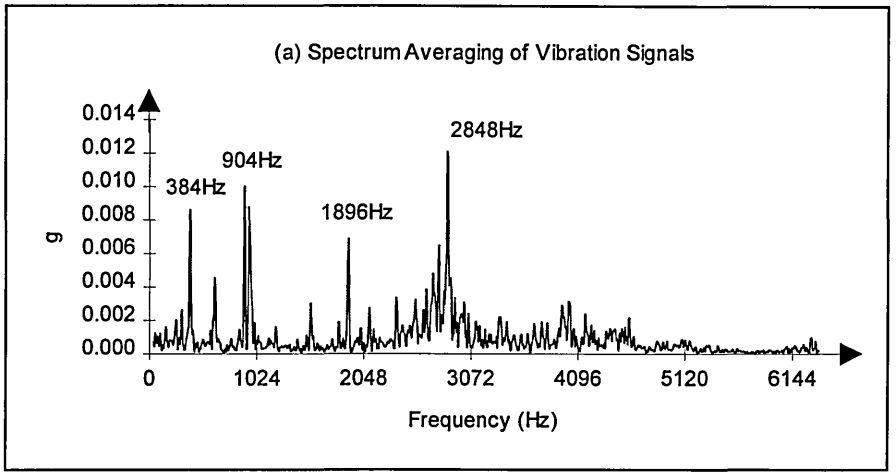

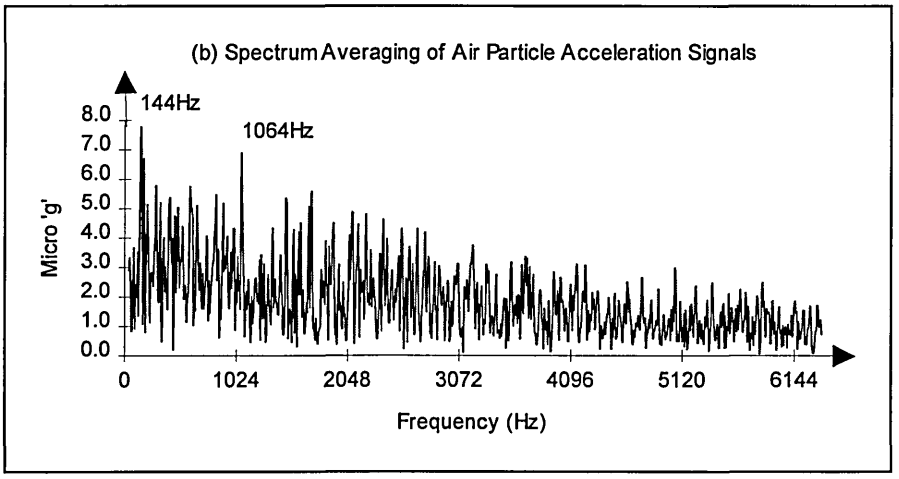

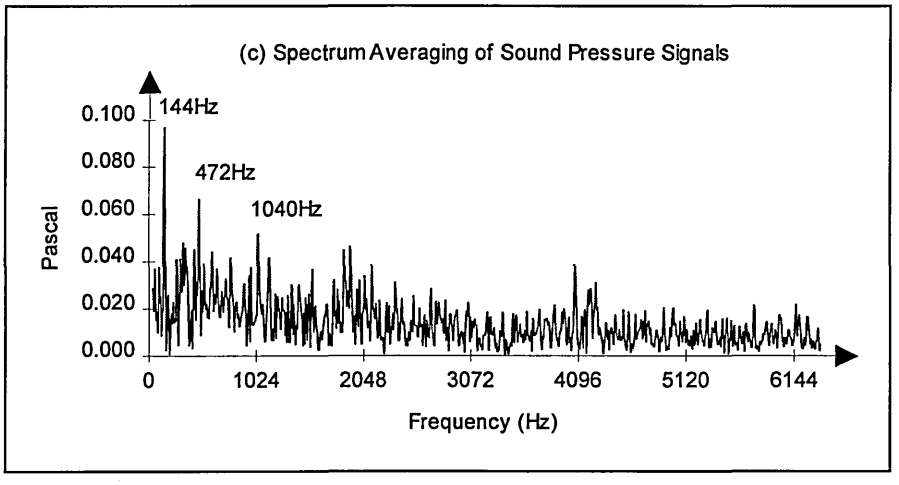

Figure 6.9 Frequency averages from fifty readings of measured signal from Roller Stand 2, Light Mill Section.

6.6 Summary

In this chapter the effectiveness of using air-particle acceleration signals for monitoring bearing condition is presented. The advantages and limitations of using air-particle acceleration signals are also identified. Results from the experimental works showed that the performance of the air-particle acceleration signal is better than the performance of sound pressure signal in the presence of high background noise. In fact, the indication of impulsive defect signals are shown clearly from the measurement of air-particle acceleration signals even when the background noise was 14dB higher than the overall sound level of the defective bearing signals. A 3dB increment of sound pressure level represents a double in power of the sound source.

The sensitivity of the air-particle acceleration signal to indicate very small defects in the bearing component is almost identical to the sensitivity of vibration signal. Moreover, at low bearing speed (i.e. 500rpm) the performance of air-particle acceleration signals are consistently better than the performance of vibration signals. This is because the vibration measurement at low speed was easily corrupted by the resonance vibration of the test-rig structure. Whereas the defect frequency mainly consists of high frequency components which is easily detectable from the measurement of air-particle acceleration signal. However at high speed tests (i.e. at 1500rpm and 3000rpm) the performance of vibration signals is slightly superior to the performance of air-particle acceleration signals.

The measurement of air-particle acceleration in the field was carried out using a four-channel tape recorder. A sample of results from measurements of sound pressure, air-particle acceleration and vibration signals to monitor bearing condition in an industrial environment is also presented in this chapter. Basically, this chapter presents the application of a new and novel method of monitoring bearing condition using air-particle acceleration signal. The method developed in this study can easily be incorporated with the hearing conservation program and the condition-based maintenance program which are already implemented in industry.

CHAPTER 7

APPLICATION OF ARTIFICIAL NEURAL NETWORKS

7.1 Introduction

The machine component monitoring system being developed in this study should be able to identify the condition of a test-bearing quickly and consistently. One way of achieving this is by incorporating artificial intelligence into the monitoring system. The development of artificial neural networks in recent years provides a powerful method that can be implemented to analyse a large amount of data and to deduce expert information from the data. As a result, artificial neural networks are included in the study and they are used to identify complex patterns produced by the test-bearing.

Artificial neural networks are parallel distributed signal processing systems that imitate the neuron structure of a biological brain. The application of this system is most appropriate when we have the input and output signals from a machine component, but the algorithm required to process the input signals is not precisely known. The artificial neural network was trained to learn the required "knowledge" from examples of input and output patterns acquired from the test bearing. The knowledge acquired from training is stored in the connection weights (synaptic weights) that link all the neurons. During the training process the weights are altered in response to the training data. When minimum root sum-squared error from the output is achieved, the training process is terminated and the networks were saved for future use. Basically, artificial neural networks are used for two purposes: classification and modeling. In this study, the application of artificial neural networks mainly falls in the classification category, where air-particle acceleration signals from bearings with different types of defect are fed into a network and the types of defect present in the bearing component are identified by a trained network.

7.2 Network Design

Nowadays, with rapid development of artificial neural networks, there are two main tasks left for a user to do: network design and data presentation. In this study, the multilayer perceptron network (MLP) was utilised. This type of network consists of an input layer, one or two hidden layers, and an output layer as shown in Figure 7.1 below.

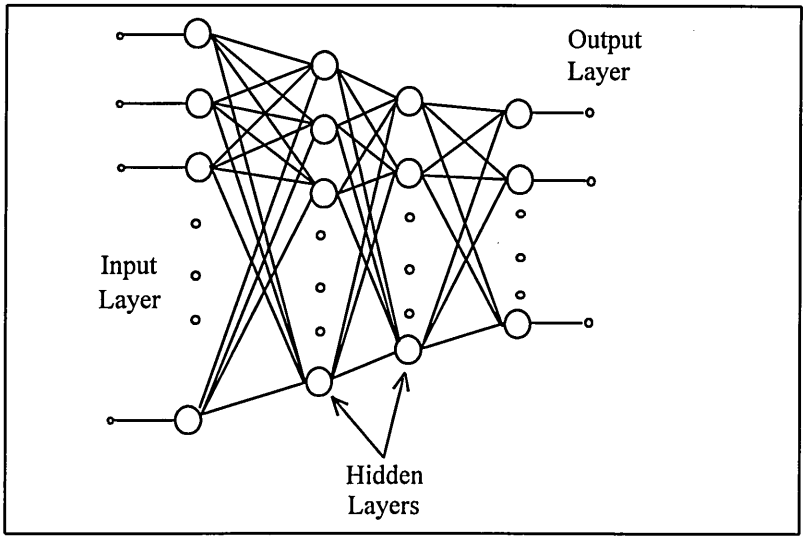

Figure 7.1 A schematic layout of a multilayer perceptron with two hidden layers.

There are three methods available to train an artificial neural networks: supervised, unsupervised and re-enforcement learning. Supervised learning can be implemented when samples of input patterns and their expected output patterns are readily available from previous data. In this method, a set of input pattern is fed into a network and the expected output pattern is also presented to calculate the error produced by the network. Once the training session is completed, the trained network can be tested with a new set of data that it has not seen before. This type of learning process was chosen for this study.

Unsupervised learning is implemented to classify data when no prior information is available about the data. In this type of learning, the network tries to group each input vector into a cluster in an output grid. The total number of clusters available are dependent on the number of neurons assigned to the output grid. This type of learning method is seldom used due to its complexity and unpredictable outcomes.

Re-enforcement learning is midway between supervised and unsupervised learning. In this type of learning, input data is fed into the network and a scalar value is given to evaluate the performance of the network. This value is used as a performance index to guide the network during a training process.

7.3 Utilisation of Back-Propagation Algorithm

The development of the back-propagation learning algorithm by Rumelhart, Hinton and Williams (1986) certainly put an end to the negative impression about learning in multilayer perceptrons that has been implied by the famous article written by Minsky and Papert (1969). With the development of the back-propagation algorithm, it proved that there was an efficient method available that can be used to train a multilayer perceptron. In a training process, it calculates the error and also the rate of change of error for a given set of weights and then modifies each of the weights in the network to minimise the error using the following equation:

$$WChange_t = -\eta \left(\frac{dE}{dW}\right)_t + \alpha * WChange_{t-1} \qquad (7.1)$$

where *WChange* is a change in the connection weight, η is the learning rate parameter, α is the momentum coefficient assigned for the network and $\frac{dE}{dW}$ is the rate of change of error with respect to a particular weight. This equation shows that as the gradient of the error surface becomes steeper the change in the weight becomes

larger. The inclusion of the momentum coefficient in the equation is to ensure that the error surface does not stop and get "trapped" in a local minima as shown in Figure 7.2.

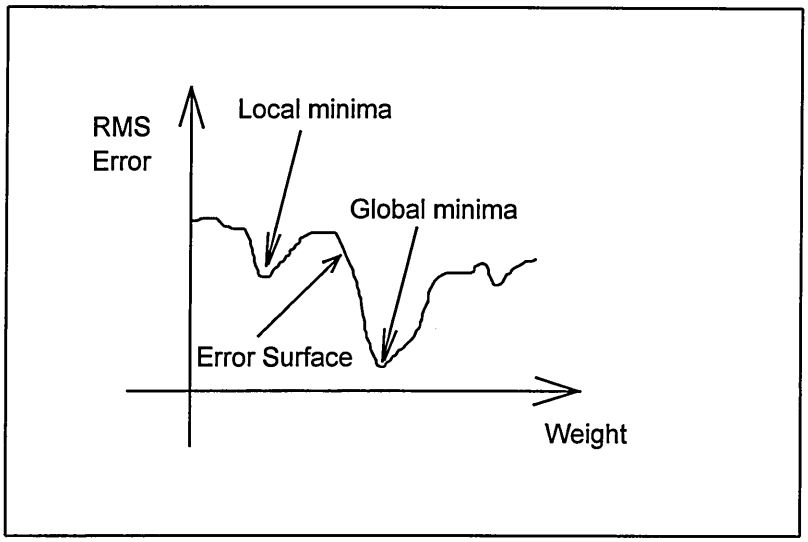

Figure 7.2 Illustration of an error surface for a single weight.

7.3.1 The Forward Pass

The input pattern used to train a chosen network design was fed to the network using the forward pass algorithm. The learning process for an MLP network with single hidden layer can be summarised by the following steps (Haykin 1994):

(i) Randomise all the weights in the connection of neurons in the network if necessary.

(ii) Present one of the pth training patterns to the input layer.

$$x_p = (x_{p1}, x_{p2}, \ldots, x_{pN}). \qquad (7.2)$$

(iii) Calculate net input to hidden layer neuron j.

$$y_j = \sum_{i=1}^{N} W_{ij}\, x_{pi}. \qquad (7.3)$$

W_{ij} is the weight of a connection between ith input node and jth hidden neuron, and N is the total number of nodes in the input layer.

(iv) Apply the net input to hidden neuron j to the transfer function to find a hidden neuron's output activation.

$$oh_j = f(y_j) = \frac{1}{1+e^{-y_j}}. \qquad (7.4)$$

The effect of this equation is to restrict the output of a neuron between 0 and 1. This equation is commonly known as the sigmoid function or the activation function.

(v) Feed forward the activations of the hidden neurons to the output neuron k to calculate its net input.

$$y_k = \sum_{j=1}^{L} W_{jk}\, oh_j \qquad (7.5)$$

W_{jk} is the weight of a connection between jth and kth neurons, and L is the total number of neurons in the hidden layer.

(vi) Apply the net input to the output layer neuron k to the transfer function to find the output neuron's activation value.

$$oo_k = f(y_k) = \frac{1}{1+e^{-y_k}}. \qquad (7.6)$$

The formulation in the previous steps are easier to be understood using the illustration in Figure 7.3. At this stage the actual output activations from the network are obtained. These activation values are the effect of supplying the network with the input pattern. Error from the network performance is obtained from the difference between the expected output pattern with the actual output activation pattern from the network.

Next, the weights in the connection of the neurons are modified to minimise the error using the back propagation algorithm.

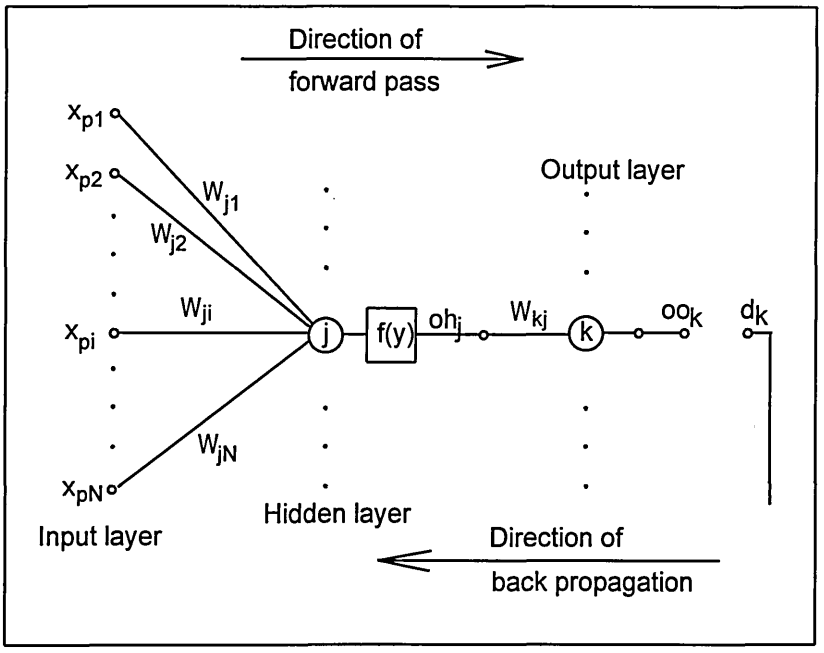

Figure 7.3 Graphical illustration of an internal structure of a multilayer perceptron with single hidden layer.

7.3.2 Back Propagation

The error function at each output neuron is defined as the difference between the desired output (d_k) pattern and the actual output activation from the network. Therefore, the error function at the output neuron can be written as

$$error_k = (d_k - oo_k) \tag{7.7}$$

Next, this error value is multiplied by the derivative of the activation function calculated for the output neuron to produce a delta term for that neuron.

$$\delta\, o_k = error_k \left(\frac{\partial f}{\partial y_k}\right) = error_k\, oo_k(1-oo_k) \tag{7.8}$$

The error signal is propagated backward and the error value of neuron j in the hidden layer is determined by the following equation

$$error_j = \sum_{k}^{M} \delta\, o_k\, W_{kj}. \tag{7.9}$$

Where M is the total number of nodes in the output layer. Similar to the output layer, the delta term for each hidden neuron is obtained from

$$\delta\, h_j = error_j\, oh_j(1-oh_j). \tag{7.10}$$

The weight error derivative $\left(\frac{dE}{dW}\right)$ defined earlier as the rate of change of error with respect to a particular weight is computed by multiplying the delta term at each neuron with the activation of other neuron that it is connected to. For a neuron connection between the hidden layer and the output layer

$$\left(\frac{dE}{dW}\right)_{jk} = \delta\, o_k\, (oh_j) \qquad (7.11)$$

Similarly, the weight error derivative for a connection between the input layer and the hidden layer is computed by the following equation:

$$\left(\frac{dE}{dW}\right)_{ij} = \delta\, h_j\, (x_{pi}). \qquad (7.12)$$

Finally, the weights are updated to minimise the error, a learning rate parameter and a momentum coefficient are incorporated in the equations. Initially, the weights between the hidden and output layer are updated

$$W_{jk}(t) = W_{jk}(t-1) - \eta \left(\frac{dE}{dW}\right)_{jk} + \alpha \left[W_{jk}(t-1) - W_{jk}(t-2)\right] \qquad (7.13)$$

Then, the weights for the connection between the input layer and the output layer are also updated.

$$W_{ij}(t) = W_{ij}(t-1) - \eta \left(\frac{dE}{dW}\right)_{ij} + \alpha \left[W_{ij}(t-1) - W_{ij}(t-2)\right]. \qquad (7.14)$$

A general form of equations (7.13) and (7.14) is already presented in equation (7.1). The training steps presented in this and the previous sections are repeated until the magnitude of the root sum-squared error at the output layer was lower than the maximum allowable value specified by the user.

7.4 Identification of Bearing Defects

The multilayer perceptron with single hidden layer has chosen for this study. The stochastic back propagation algorithm is used to train the network. With this algorithm, the weight changes in the network are made after each pattern presentation. Because the order of input pattern may influence the learning process, they are presented to the network in random order. Optimum values for the learning rate and the momentum coefficient are determined by a heuristic method. Once the network design has been resolved, the next task was to select the relevant features from raw data. The procedure for selecting these features is presented in the next section.

7.4.1 Feature Selection Using Wavelet Transform

In this study the different types of defect tested in a cylindrical roller bearing were identified using the artificial neural network algorithm. The type of test-bearing used for this study was the same as the test-bearing presented in Chapter 6. A test-bearing with four different conditions namely; normal bearing, rolling element line defect, outer race line defect and inner race line defect was tested in this study. The shaft speed for the initial study was maintained at 1500rpm, and only air-particle acceleration signal was utilised to train the network.

The main purpose of a feature selection algorithm is to pick up only the important parameters that can be used to represent a sample of measured signal. Since only a few parameters will be chosen as an input to the artificial neural networks software, the algorithm for selecting these parameters must be able to represent the raw signal effectively. For this reason, the wavelet transform method was selected as a feature selection algorithm in this study. Six features were chosen from a result of the wavelet transform method of air-particle acceleration signals. These features were obtained from the summation of the magnitudes of wavelet coefficient at different levels as shown in Figure 7.4. Each feature was normalised by the summation of wavelet coefficients from all levels of the wavelet transform result. Since these features represent the summation of wavelet coefficients at different frequency bins, the time

information of the signal is lost. The frequency range for each feature increases in an octave frequency band as indicated by the shaded region in the figure. The parameter *Fmax* shown in the figure is the maximum frequency component that was available from the measured signal. In this study, the Coifman wavelet (C12) was used to transform the measured signals since it is capable of representing time-frequency components of a signal with minimal phase shift. A diagram that shows the waveform of a Coifman wavelet is already shown in Chapter 5.

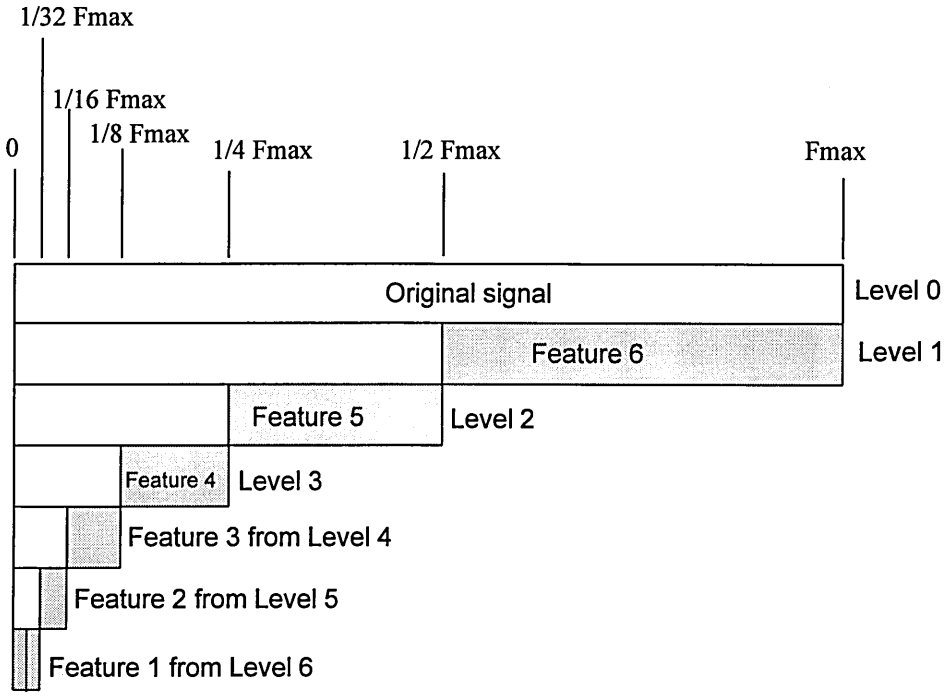

Figure 7.4 Representation of features from the frequency bins of a wavelet transform algorithm.

All of the features were calculated from the magnitude of wavelet transform coefficients. As indicated in Figure 7.4, only coefficients from the first six levels of the wavelet transform result were used for calculating these features. The mathematical formulation to calculate the features is presented below:

$$F_i = \frac{\sum_{j=1}^{N} MW_{(7-i,\,j)}}{\sum_{l=1}^{L}\sum_{j=1}^{N} MW_{(l,\,j)}} \quad . \qquad (7.15)$$

Where $MW_{(l,j)}$ is the magnitude of wavelet transform coefficient from level l, j is the index of wavelet coefficient in level l, N is the total number of coefficient in level l, L is the total number of levels from the wavelet transform process and i is an integer number which represent the feature's index, ranging from 1 to 6. All features were normalised with the summation of all of the wavelet transform coefficients available from a signal.

7.4.2 Experimental Determination of Optimal Network Design

There were three variables left to be decided to achieve an optimal design of the multilayer perceptron chosen in this study. These variables are:

(i) the number of neurons in the hidden layer,
(ii) the value for learning rate parameter (η), and
(iii) the value for momentum coefficient (α).

The ultimate objective of a pattern classifier in this study is to achieve an acceptable rate of correct classification of the different bearing conditions using air-particle acceleration signals. Therefore, the parameters that are used to evaluate the performance of the different network design included: (i) the percentage accuracy of the network to classify bearing signals, (ii) the minimum magnitude of error values, and (iii) the number of epochs when the training was terminated. An epoch is defined as a single pass of the entire input pattern into a network.

In this study, forty records of time domain signals were recorded at random for each bearing condition. Each sample contains 2048 data points which represent five revolutions of the test-bearing shaft. A set containing twenty data samples from each

case of bearing condition was selected to train a network, and another similar set was selected independently to evaluate the performance of the trained network. All work involving the artificial neural networks were performed using a window-based NeuralDesk(TM) software which was developed by Neural Computer Sciences company. A computer program was developed using C language to calculate all the features that are required. This program is used to calculate the features from the output of a wavelet transform algorithm. A listing of this program is shown in Appendix D.

Results from training of the artificial neural networks with different numbers of neuron in the hidden layer are shown in Table 7.1. For this study, the values for learning rate parameter (η) and momentum coefficient (α) were set to 0.1 and 0.9 respectively. Six neurons were specified in the input layer which is equal to the number of features calculated from the output of wavelet transform algorithm. Four neurons were set in the output layer which represent four different conditions of the test-bearing. Training of the network was terminated when the root sum-squared error during training fell below 0.0001.

Table 7.1 Performance of multilayer perceptron with different number of neurons in the hidden layer

Number of Neurons in Hidden Layer	Percentage of Correct Classification							
	Query Data				Training Data			
	ND*	OD	RD	ID	ND	OD	RD	ID
3	85	95	100	95	100	100	100	100
4	85	100	100	95	100	100	100	100
5	85	100	100	95	100	100	100	100
6	85	100	100	95	100	100	100	100

* ND ≡ No defect, OD ≡ Outer race defect,
RD ≡ Rolling element defect, and ID ≡ Inner race defect

The results show that the optimal number of hidden neurons was equal to four. Increasing the number of neurons more than four did not improve the performance of the artificial neural networks. The results also showed that fifteen percent of the query data measured from bearings without defect are misclassified as indicating the presence

of rolling element defect. Five percent of the data measured from bearings with inner race defect are misclassified as indicating the presence of outer race defect. One hundred percent correct classifications are achieved from the network when features from outer race defect and rolling element defect are tested. Finally, one hundred percent correct classification is indicated when the network was tested using the same set of data that are used for training.

The next study was carried out to determine the optimal values for the learning rate parameter (η) and momentum coefficient (α). An optimal network design as determined in the previous study was implemented for this experiment. Therefore, the network consisted of six neurons in the input layer, with a single hidden layer containing four neurons and another four neurons in the output layer. All training sessions were initiated using the same random values of weights in the neurons' connection. Training of the network was terminated when the total number of epochs reached 20,000 or when the error value fell below 0.001, which ever came first. Results from the experiment are presented in Table 7.2 and Figure 7.5 as shown below.

Table 7.2 Training results of multilayer perceptron using four hidden neurons

Momentum Coefficient (α)	Learning Rate (η)				
	0.10	0.25	0.50	0.75	0.90
0.10	0.0069[+] (20,000)*	0.367 (20,000)	0.444 (20,000)	0.458 (20,000)	0.462 (20,000)
0.25	0.0059 (20,000)	0.368 (20,000)	0.454 (20,000)	0.461 (20,000)	0.466 (20,000)
0.50	0.0027 (20,000)	0.001 (20,000)	0.001 (9465)	0.001 (5058)	0.001 (4366)
0.75	0.0015 (20,000)	0.001 (10,303)	0.001 (3443)	0.001 (1872)	0.001 (1546)
0.90	0.001 (9205)	0.404 (20,000)	0.317 (20,000)	0.001 (17,806)	0.001 (5268)

[+] This number represents the magnitude of error when training was terminated.

* The number in bracket shows the total number of epoch when training was terminated.

This table shows that when the value of the momentum coefficient is low (i.e. less than 0.5) the network is unable to learn from the training session. Therefore, the momentum coefficient must be set to a high value for the network to be able to search for the global minima on the error surface. However, the values for momentum coefficient and learning rate parameter must be limited between zero to one. In addition, as a rule-of-thumb, the summation of these two variables should be equal to one (NeuralDesk User's Guide, 1994). When the learning rate was set to a low value, the error surface plots show that the error surface converges to an asymptotic value in a smooth and gradual manner. This causes the network to learn at a very slow pace and it might take a very long time before the network was fully trained. On the other hand, when the learning rate was set to a high value it moved the error in a large step and the network may become unstable. This phenomenon was indicated by unsteady oscillations of the error surface plots. The goal of this study was to find a balance when setting the values for the learning rate parameter and the momentum coefficient so that the network is able to search for the global minima in a reasonable length of time. The results show that the optimal value for learning rate parameter is 0.10 and the optimal value for the momentum coefficient is 0.90. Once all the parameters for designing an optimal multilayer perceptron are identified, it is tested with another set of data. When air-particle acceleration data were obtained by setting the shaft speed to 3000rpm, one hundred percent correct defect-classification for all the different types of defect were achieved from this test.

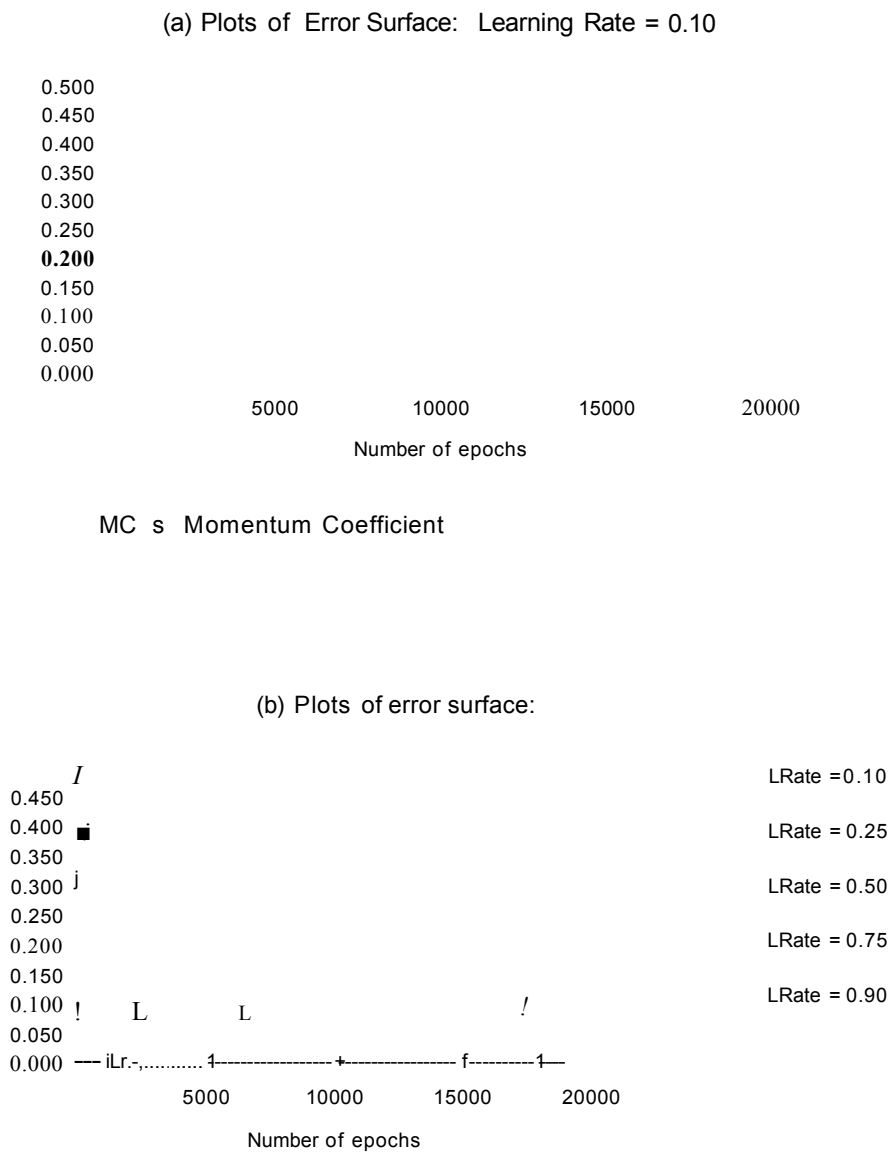

Figure 7.5 Plots of mean-squared error versus the number of epochs for different values of learning rate and momentum coefficient.

7.5 Discussion on the Experimental Results

The results shown in this study indicated that wavelet transform method can be used as a pre-processor for artificial neural networks applications. In addition, they also showed that features from the measurement of air-particle acceleration signals can be

as input to the neural network algorithm. When the shaft-speed was set to 1500rpm, measurement of the air-particle acceleration signals was corrupted by the natural vibration of the test-rig structure. As a result, fifteen percent false alarms were indicated from the response of the artificial neural networks when it was tested using signals from a normal bearing. In this case, all of the false alarm signals were classified as an indication of rolling element defect, where these data were actually obtained from a normal bearing.

However, when the shaft-speed was increased to 3000rpm, one hundred percent correct classification was performed by the network for all types of bearing defect tested in this study. Therefore, the artificial neural networks used in this study is capable of indicating the presence of defect in the test-bearing. In addition, the type of defect is also recognised by the network. The kind of pre-processing analysis method must be chosen carefully to make sure that the network can learn to classify the type of fault occurring in the test-bearing. An efficient feature extraction algorithm will ensure that the network can learn in a short time and the generalization capability of the trained network is improved. All of the parameters required to obtain an optimal network design such as the number of hidden layers, number of neurons in the hidden layer, number of neurons in the output layer, the learning rate parameter and the momentum coefficient were determined using a trial-and-error method.

CHAPTER 8

CONCLUSION AND SUGGESTIONS FOR FUTURE WORK

8.1 Conclusion

A new and novel method for monitoring rolling element bearings using air-particle acceleration signal is successfully developed in this study. This type of signal was derived using a two-microphone method based on the principles of sound intensity measurement technique. However, the requirement imposed on the measurement probe and on the analysing equipment for measuring air-particle acceleration signals is less demanding compared with the requirement for measuring sound intensity signals. For example, the amplitude-response and phase-response of the two microphones used to measure sound intensity signals must be identical. Whereas, for measuring air-particle acceleration signals only the amplitude response needs to be identical. As a result, the cost to set up a measurement system utilising air-particle acceleration signals is much cheaper than the cost of sound intensity measurement system. The most attractive feature of using air-particle acceleration signals is the non-contact and non-intrusive nature of the measurement transducer. This makes it a very attractive method that can be implemented in harsh industrial environment. Another important characteristic of air-particle acceleration signals is high signal-to-noise ratio. This is because air-particle acceleration is a vector quantity compared to the scalar quantity of sound pressure signals.

The performance from utilising air-particle acceleration signals to indicate bearing component defect has been compared with the performance from utilising sound pressure and vibration signals. The method developed in this study to utilise air-particle acceleration signals, has proven to be able to take advantage of the non-intrusive and non-contact nature of the measuring transducers and yet without the limitations of sound pressure measurement. The new method developed in this study is capable of indicating the presence of defective signals from a bearing component where the surrounding background noise was high. Experimental results from the study showed that even if the overall background sound level was 14dB higher than the sound level emitted by the

test-bearing, the impulsive signals from a defective bearing component were clearly indicated from the measurements of air-particle acceleration signals. The sensitivity of air-particle acceleration signals to indicate bearing defects are almost the same as the sensitivity of vibration signals. However, vibration measurements are dependent on the way the accelerometer is coupled to the vibrating surface, and the signal can easily be corrupted by the presence of power-supply-line frequency and its harmonics.

The measured signals were analysed using several different types of signal processing method including: statistical, spectral, cepstral and wavelet transform methods. Statistical variables such as kurtosis and crest factor are used successfully to indicate the presence of defective component in a test-bearing. However, the type of defect was not identifiable from the values of these variables. Frequency spectrum analysis method was used to detect the presence of defect in the test-bearing. It was difficult to determine the type of defect indicated from the frequency-spectrum plots because these plots were dependent on the transfer function of the bearing housing. Moreover, the frequency spectra were also affected by the modal vibration of the test-rig structure. Diagnosis works for identifying the type of defect in the test-bearing were successfully carried out using cepstrum and zoomed cepstrum analysis methods. Results from these two methods are accurate when compared with the calculated defect frequency of the test-bearing. Wavelet transform and wavelet packet transform methods were also implemented in the study. These methods are successfully utilised in the study for the following tasks:

(i) to capture the time-frequency signatures of bearing signals using the phase plane diagrams obtained from best basis, best level, and wavelet basis,

(ii) to perform denoising operation on a signal using multilayer analysis in wavelet packet transform method,

(iii) to perform multiscale analysis of a signal from the result of wavelet transform method,

(iv) to select important features that represent a signal

(v) to compress a signal.

The machine component monitoring system developed in this study is capable of identifying the condition of a test-bearing quickly and consistently. This is achieved by incorporating artificial neural networks in the monitoring system. A multilayer perceptron with back propagation training algorithm was tested in the study. Only air-particle acceleration signals were used for testing the network. Results from the experiment show that in a worst scenario when the shaft-speed was set to 1500rpm, fifteen percent false alarm (wrong classification of a normal bearing signals) were indicated by the network. One hundred percent correct classification has been achieved from outer race defect and rolling element defect signals, and ninety-five percent correct classification has been achieved from test-bearing with inner race defect at this speed. This is because at 1500rpm, the measurement of bearing signals were corrupted by the natural vibration of the test-rig structure. When the shaft-speed was set to 3000rpm, one hundred percent correct classification has been achieved for all the different types of defect tested in this study. Finally, the machine condition monitoring system developed in this study has been successfully applied in an industrial case study.

8.2 Contribution to the Field of Machine Condition Monitoring

A non-contact and non-intrusive machine condition monitoring system which utilised air-particle acceleration signals is firmly established in this research study. This is a very attractive method that can be used for monitoring the condition of a machine component in industry. Although only cylindrical rolling element bearings have been used in this study, this method can also be extended to monitor gears, pumps, motors and other machine components. The steps required for measuring air-particle acceleration signals are much easier to carry out than the steps required for measuring vibration signals. Moreover, the method developed in this research can be applied in combination with other established methods already available in the industry. This

method can also be incorporated into noise maintenance programme of machines in industry. The unwanted sound signals produced by these machines are now fully exploited to diagnose the faults that cause them.

A new method to capture a family of impulses that may occur randomly during the operation of a defective bearing is also developed in this study. This method is utilised to capture the impulsive signals with a high signal-to-noise ratio when other conventional methods failed to do so. It is called the correlated time averaging method. It is very good at indicating the presence of rolling element defect in the test-bearing where conventional time averaging method is not applicable. One of the advantages of using this new method is that it can be used to carry out time-domain averaging of bearing signals without using trigger mechanism.

8.3 Suggestions for Future Work

A dedicated system for on-line machine component monitoring system using air-particle acceleration signals can be developed in the future. Real-time application of air-particle acceleration signal to monitor machine components will make it an attractive method to be implemented in industry.

It has been shown from this study that at low speed (i.e. at 500rpm) the performance of air-particle acceleration signals was slightly superior to the performance of vibration signals. Therefore, a detailed study of the application of air-particle acceleration signals for low speed bearings is proposed. Other types of artificial neural networks algorithm such as a Kohonen network, and a hybrid neural networks can also be incorporated in the future.

REFERENCES

Anderson, J. S. and Anderson, M. B., (1993), *Noise - Its Measurement, Analysis, Rating and Control*, Ashgate Publishing Company.

Badi, M. N. Dell, M. D. Fellows, J. A. E., (1990), "Alternative Methods of Diagnosing Gear Box Faults," Proceedings of 2nd International Congress on Condition Monitoring and Diagnostic Engineering Management (COMADEM '90), pp. 214-250.

Baker, S., (1955), "An Acoustic Intensity Meter", Journal of Acoustic Society of America, Vol. 27, pp. 269-273.

Bannister, R. H., (1985), "A Review of Rolling Element Bearing Monitoring Technique," In Condition Monitoring of Machinery and Plant, Institution of Mechanical Engineers, Paper presented at a seminar organised by the Fluid Committee of Mechanical Engineers, pp. 11-24.

Barwell, F. T., (1979), *BEARING SYSTEMS: Principles and Practice*, Oxford University Press.

Better Accuracy Means Less Noise, (1994), Professional Engineering, July, pp. 18 - 38.

Boashash, B., (1991), "Time-Frequency Signal Analysis," *Advances in Spectrum Analysis and Array Processing, Volume I*, Haykin, Simon, Eds., Prentice Hall, Englewood Cliffs, NJ, pp. 418 - 517.

Brito, J. D. (1979), "Machinery Noise Source Analysis Using Surface Intensity", Proceedings of Noise-Conference, pp. 137-42.

Brown, N. D. and Jensen, T., "Machine-Condition Monitoring using Vibration Analysis: The use of Crest Factor and Cepstrum Analysis for Bearing Fault Detection," Bruel & Kjaer Application Notes, 11p.

Chapman, R. M., (1967), "Vibration Analysis Applied to Machinery Maintenance," Naval Engineers Journal, Vol.79, no.3, pp. 431-437.

Chaturvedi, G. K., Thomas, D. W., (1982), Bearing Fault Detection Using Adaptive Noise Cancelling," Transaction of the ASME - Journal of Mechanical Design, Vol. 104, pp. 280-289.

Clapp, C. W. and Firestone, F. A., (1941), "The Acoustic Wattmeter, An Instrument for Measuring Sound Energy Flow", Journal of Acoustical Society of America, Vol. 13, pp. 124-136.

Cody, M. A., (1992), "The Fast Wavelet Transform - Beyond Fourier Transforms," Dr. Dobb's Journal, April '92, pp. 16-8, 24, 26, 28, 100-1.

Cody, M. A., (1993), "A Wavelet Analyser - An Alternative to the FFT-based spectrum analyser," Dr. Dobb's Journal, April '93, pp. 44 - 54.

Cohen, L., (1989), "Time-Frequency Distribution - A Review," Proceedings of the IEEE, Vol. 77, no. 7, pp. 941-981.

Coifman, R. R., and Wickerhauser, M. V., (1993), "Theoretical Manual: Wavelets and Adapted Waveform Analysis - A Toolkit for Signal Processing and Numerical Analysis," A. K. Peters, Massachusetts, ISBN 1-56881-035-0, 43p.

Cooley, J. W. et al., (1969), "Fast Fourier Transform and Its Applications," IEEE Transaction on Education, Vol. E-12, no. 1, pp. 27-34.

Cooper, R. A. and Weekes, A. J., (1983), *Data, Models and Statistical Analysis*, Allan Publisher Ltd, Oxford, pp. 116 - 120.

Cory, W. T. W., (1991), "Overview of condition monitoring methods with emphasis on industrial fans," Proceedings of the Institution of Mechanical Engineers, 205 A, pp. 225 - 240.

Crocker, M. J., (1981), "Determination of Noise Sources and Sound Power Using the Surface Intensity and Acoustic Intensity Approaches," Proceedings of Inter-Noise '81, pp.895 - 898.

Daadbin, A. and Yuen, W. K., (1990), "Design of a test rig to demonstrate vibration monitoring," International Journal of Mechanical Engineering Education, Vol. 1 8, no. 3, pp. 201-209.

Daadbin, A., and Wong, J. C. H., (1991), "Different Vibration Monitoring Techniques and Their Application to Rolling Element Bearings", International Journal of Mechanical Engineering Education, Vol. 19, no. 4, pp. 295-304.

Dai, et al., (1994), "Introduction to Wavelet Transformation and Time Frequency Analysis", *Wavelet Application in Chemical Engineering,* Motard and Joseph, Eds., Kluwer Academic Publishers, London, pp. 1 - 26.

Daubechies, I., (1988), "Orthonormal Bases of Compactly Supported Wavelets", Comm. Pure and Applied Maths, Vol. XLI, pp. 909 - 996.

Deckert, J. C. et al., (1992), "Wavelet Features for Failure Detection and Identification in Vibrating Systems," Report no. TR-567, Alphatech Inc., Burlington, MA., 51p.

Diehl, G. M., (1973), *Machinery Acoustics*, John Wiley & Sons, New York, ISBN 0-471-21360-8, pp. 107 - 136.

Diniz, A. E. Liu, J . J., and Dornfield, D. A., (1992), "Correlating Tool Life, Tool Wear and Surface Roughness by Monitoring Acoustic Emission in Finish Turning, WEAR, Vol. 152, pp. 395-407.

Dyer, D., Stewart, R. M., (1978), "Detection of Rolling Element Bearing Damage by Statistical Vibration Analysis," Journal of Mechanical Design, Vol. 100, pp. 229 - 235.

Fahy, F. J., (1989), *Sound Intensity*, Elsevier Applied Science, Essex, , U.K.

Ford, R. A. J., (1990), "A Rig for Demonstrating Vibration-based Condition Monitoring of Rolling Bearings," Institution of Engineers Australia Vibration and Noise Conference, pp. 37-40.

Ford, R. D., (1970), *Introduction to Acoustics*, Elsevier Publishing Co., London, , p. 5.

Fuchs, E. A. et al., (1991), "Thermal Diagnostic for Monitoring Welding parameters in Real Time," Proceedings of SPIE 1991; Vol. 1467, pp.136-149.

Gabor, D., (1946), "Theory of Communication," Journal of the Institute of Electrical Engineers, Vol. 93, pp. 429 - 441.

Gade, S., (1985), "Validity of Intensity Measurements in Partially Diffuse Sound Field," Bruel and Kjaer Technical Review, Vol. 4, pp. 3-31.

Gargano, E. and Bartolini, A., (1991), "Use of Correlation Between Noise and Vibration For Diagnosing Rolling Element Bearings," Proceedings of Inter-noise '91, pp. 997-1000.

Geng, Z. and Qu, L., (1994), "Vibrational Diagnosis of Machine Parts Using the Wavelet Packet Technique," British Journal of NDT, Vol. 36, no. 1, pp. 11-15.

Grossmann, A., (1988), "Wavelet Transforms and Edge Detection," in Stochastic Processes in Physics and Engineering, (S. Abeveto, ed.), pp. 149-157,

Haddad, R. A., and Parsons, T. W., (1991), *DIGITAL SIGNAL PROCESSING: Theory, Applications, and Hardware*, W. H. Freeman and Co., New York, pp. 348-353 and pp. 535-546.

Hanna, A. J., (1974), "Predictive Maintenance Via Vibration Analysis," TAPPI, Vol. 57, no. 5, pp. 153-157.

Harris, J. H., (1967), *The Lubrication of Rolling Bearings*, Shell-Mex and B. P. Ltd., London

Harris, T., (1993), "Neural Networks in Machine Health Monitoring," Professional Engineering, July/August '93, p. 8.

Haykin, S., (1994), *Neural Networks - A Comprehensive Foundation*, Macmillan Publishing Co., ISBN 0-02-352761-7, pp. 121 - 201, 397 - 434.

Hodgson, T. H., (1977), "Investigation of the surface acoustical intensity method for determining the noise sound power of a large machine in situ," Journal of Acoustical Society of America, Vol. 61, no. 2, pp. 487-493.

Ibrahim Nur Tansel et al., (1993), "Detection of Tool Failure in End Milling With Wavelet Transformations and Neural Networks (WT-NN)", Manufacturing Science and Engineering, ASME, PED-Vol. 64, pp. 369 - 374.

Igarashi, T., and Yabe, S., (1983), "Studies on the Vibration and Sound on Defective Rolling Bearings," Bulletin of Japan Society of Mechanical Engineers, Vol. 26, pp. 1791-1798.

Igarashi, T., (1964), "Noise of Ball Bearing in Electric Motor," Bulletin of Japan Society of Mechanical Engineers, Vol. 7, no. 25, pp. 200-208.

Igarashi, T., (1962), "Noise of Ball Bearing: 2nd. Report," Bulletin of Japan Society of Mechanical Engineers, Vol. 5, no. 17, pp. 184-194.

Igarashi, T., (1960), "Noise of Ball Bearing: 1st. Report," Bulletin of Japan Society of Mechanical Engineers, Vol. 3, no. 10, pp. 220 - 227.

Jacobsen, F. et al., (1996), "A Sound Intensity Probe Measuring From 50Hz to 10KHz," Proceedings of Internoise '96, pp. 3357 - 3362.

Jacobsen, F., (1990), "Active and Reactive Sound Intensity in a Reverberant Sound Field," Journal of Sound and Vibration, Vol. 143, no. 2, pp. 231-240.

Jacobsen, F., (1989), "Active and Reactive Coherent and Incoherent Sound Fields," Journal of Sound and Vibration, Vol. 130, no. 3, pp. 493-507.

James, C. et. al., (1991), "Pattern Recognition Based Bicoherence Analysis of Vibration for Bearing Condition Monitoring," Sensors, Controls and Quality Issues in Manufacturing, ASME, pp. 1 - 11.

Jayaram, V. D. and Jarchow, F., (1978), "Experimental Studies on Ball Bearing Noise," Wear, Vol. 46, pp. 321-326.

Kadambe, S., (1991), "The Application of Time-Frequency and Time-Scale Representation in Speech Analysis," PhD Thesis, The University of Rhode Island, Department of Electrical Engineering.

Kannatay-Asibu, Jr E., (1982), A Study of Tool Wear Using Statistical Analysis of Metal-Cutting Acoustic Emission, Wear, Vol. 76, pp. 247-261.

Khan, A. F., Williams, E. J., (1992), "Predicting the Remaining Life of Rolling Element Bearings," Proceedings of the Institution of Mechanical Engineers, pp. 403 - 408.

Kim, P. Y., (1984), "A Review of Rolling Element Bearing Health Monitoring (II) Preliminary Test Results on Current Technologies," Proceedings of Machinery Vibration Monitoring, pp. 127 - 137.

Kohonen, T., (1982), "Self-Organised Formation of Topologically Correct Feature Maps," Biological Cybernetics, Vol. 43, pp. 59-69.

Kohonen, T., (1990), "The Self-Organising Map," Proceedings of the IEEE, Vol. 78, no. 9, pp. 1464 - 1480.

Konig, W. et. al., (1992), "Tool Monitoring of Small Drills With Acoustic Emission," International Journal of Machine Tools Manufacturing, Vol. 32, no. 4, pp. 487-493.

Kronland-Martinet, R., and Grossmann, A., (1991), "Application of Time-Frequency and Time-Scale Methods (Wavelet Transforms) to the Analysis, Synthesis, and Transformation of Natural Sounds," in *Representations of Musical Signals*, (Kronland-Martinet, R. ed.), MIT Press, pp .45-85,

Kronland-Martinet, R., Morlet, J., and Grossmann, A., (199?), "Analysis of Sound Patterns Through Wavelet Transforms," International Journal of Pattern Recognition and Artificial Intelligence, Vol. 1, no. 2, pp. 274-302

Lahti, T., (1990), "Analysis Methods For Acoustical System Based On The FFT and Intensity Techniques," PhD Thesis - Espoo, Technical Research Centre of Finland, Publication 67, 288p.

Larson, H. J., (1982), *Introduction to Probability Theory and Statistical Influence,* 3rd Edition, J. Wiley.

Li, C. J., and Ma, J., (1992), "Bearing Localized Defect Detection Through Wavelet Decomposition of Vibration," Proceedings of the 46th Meeting of the Mechanical Failure Prevention; pp. 53 - 62.

Lippman, R. P., (1987), "An Introduction to Computing with Neural Nets," IEEE ASSP Magazine, Vol. 4, pp. 4 - 22.

Liu, T. I., Mengel J. M., (1991), "Detection of Ball Bearing Conditions by an A. I. Approach," Sensors, Controls and Quality Issues in Manufacturing, ASME, pp. 13-21.

Lopez, J. E. et al., (1994), "Fault Detection and Identification Using Real-Time Wavelet Feature Extraction," Journal of Vibration and Acoustics, Vol. 116, pp. 409-416.

Mallat, S. G., and Zhong, S., (1989), "Complete signal representation with multiscale edges," Technical Report RRT-483-RR-219, Courant Institute of Mathematical Sciences.

Mallat, S., (1989), "A Theory for Multiresolution Signal Decomposition: The Wavelet Representation," IEEE Transaction on Pattern Analysis and Machine Intelligence, Vol. 11, pp. 674-93.

Martin, H. R. and Honarvar, F., (1995), "Application of Statistical Moments to Bearing Failure Detection," Applied Acoustics, pp. 67 - 77.

Martin, H. R., (1992), "Detection of Gear Damage by Statistical Vibration Analysis", Proceedings of the Institution of Mechanical Engineers, pp. 395 - 401.

Milne, R., (1988), "The Role of Artificial Intelligence in Condition Monitoring and Diagnosis," Proceedings of COMADEM '88, pp. 371-375.

Milne, R., Aylett, J., (1991), "Portable Bearing Diagnostics Using Enveloping and Expert Systems," Proceedings of 3rd International Congress on Condition Monitoring and Diagnostic Engineering Management (COMADEM '91), pp. 75-79.

Minsky, M. L. and Papert, S. A., (1969), Perceptrons, Cambridge, MA, MIT Press.

Mohd Nor, M. J., Sopian, K., Abdullah, R., (1991), "Environmental Impact Assessment of Power Plants: Proposal of Noise Assessment Guideline for Malaysia", in H. Ibrahim et. al. (eds) Energy: Issues, Options, and Opportunities, Proceedings of the First International Energy Conference, 5-7 August '91, Shah Alam, (a publication of the Malaysian Institute of Energy), pp. 379-385. ISBN 983-99948-0-8.

Mohd Nor, M. J., Sopian, K., and Shamsuddin, A. H., (1992), "Preliminary Studies on the Noise Emitted by the UKM Fluidised Bed Boiler", in A.H. Shamsuddin and K. Sopian (eds), Proceedings of the Seminar on Fluidized Bed Combustion of Low Rank Coal, February '92, Kuching, Sarawak, ASEAN Sub-Committee on Non-Conventional Energy Research, pp. 49-56.

Morlet, J. et. al., (1982), "Wave Propagation and Sampling Theory, Part II: Sampling Theory and Complex Waves," Geophysics, Vol. 47, no. 2.

NeuralDesk Users Guide, (1994), Neural Computer Sciences, pp.-3.

Newland, D. E., (1993*), An Introduction to Random Vibrations, Spectral & Wavelet Analysis*, Longman Scientific & Technical, Essex, pp. 19 - 20.

Newland, D. E., (1994), "Wavelet Analysis of Vibration, Part 1: Theory," Journal of Vibration and Acoustics, Vol. 116, pp. 409-416.

Newland, D. E., (1994), "Wavelet Analysis of Vibration, Part 2: Wavelet Maps," Journal of Vibration and Acoustics, Vol.116, pp. 417-425.

Nicholas, J. R., (1991), "Instruments of Predictive Maintenance," Advancement in Instrumentation and Control, Vol. 46, pp. 489-498.

O'Brien, J. C et. al., "Neural Networks for Early Prediction of Machine Failure," IEE Colloquium on Advanced Vibration Measurement Technic and Instrumentation, 1992, Digest no. 105, pp. 2/1-4.

Page, C. H., (1952), "Instantaneous Power Spectra," Journal of Applied Physics, Vol. 23, pp. 103 - 106.

Palmgren, A., (1946), *Ball and Roller Bearing Engineering,* SKF Ind. Inc.

Pelton, H. K., (1993), *Noise Control Management*, Van Nostrand Reinhold, New York, pp. 13 - 21.

Richards, E. J., Westcott, M. E. and Jeyapalan, R. K., (1979), "On the Prediction of Impact of Noise Source, I: Acceleration Noise," Journal of Sound and Vibration, Vol. 62, no. 4, pp. 547 - 575.

Rolling Bearings, Motion and Control NSK Catalogue, (1989), Cat. no. A140a, NSK Ltd.

Rumelhart, D. E., Hinton, G. E. and Williams, R. J., (1986), "Learning Internal Representation by Error Propagation," In Parallel Distributed Processing: Explorations in the Microstructure of Cognition (Rumelhart, D. E. and McClelland, J. L. eds.), Vol. 1, Chapter 8, Cambridge, MA, MIT Press.

Scheithe, W., (1992), "Better Bearing Vibration Analysis," Hydrocarbon Processing, July '92, pp. 57-64.

Shultz, T. J., (1956), "Acoustic Wattmeter," Journal of Acoustics Society of America, Vol. 28, no. 4, pp. 693-699.

SKF General Catalogue, (1989), Printed by Carl Gerber GMBH, p.519.

Smith, R. L., (1992), "Rolling Element Bearing Diagnostics With Lasers, Microphones and Accelerometers," Proceedings of the 46th Meeting of the Mechanical Failures Prevention Group, (H. C. Pusey and S. C. Pusey Eds.), pp. 43-52.

Staszewski, W. J. and Tomlinson, G. R., (1994), "Application of the Wavelet Transform to Fault Detection in a Spur Gear," Mechanical Systems and Signal Processing, Vol. 8, no. 3, pp. 289-307.

Steele, N. C., Reeves, C. R., Hart, A., "Some Issues in the Use of Neural Networks," Proceedings of the Tenth IASTED International Conference on Applied Informatics, 1992, pp. 277-280.

Strang, G. and Fix, G., (1973), "A Fourier Analysis of the Finite Element Variational Method", in *Constructive Aspects of Functional Analysis*, Edizioni Cremonese, Rome.

Strang, G., (1989), "Wavelets and Dilation Equations: A Brief Introduction", SIAM Review, Vol. 31, no. 4, pp. 614 - 627.

Su, Y. T., Lin, M. H. and Lee, M. S., (1993), "The Effects of Surface Irregularities on Roller Bearing Vibrations," Journal of Sound and Vibration, Vol. 165, no. 3, pp. 455-466.

Tamura, A., (1968), "On the Vibrations Caused by Ball Diameter Differences in a Ball Bearing," Bulletin of Japan Society of Mechanical Engineers, Vol. 11, no. 44, pp. 229-234.

Tamura, H. and Shimizu, H., (1968), "Vibration of Rotor due to Ball Bearing (3rd Report, Spring Property of Bearing Containing a Large Number of Balls)," Bulletin of Japan Society of Mechanical Engineers, Vol. 11, no. 47, pp. 825-837.

Tandon, N. and Nakra, B. C, (1990), "The Application of the sound-intensity Technique to Defect Detection rolling -element bearings," Applied Acoustics, Vol. 29, pp. 207 - 217.

Taylor, J. I., (1992), "State-of-the-art Predictive Maintenance Programs," Tappi Journal, August '92, pp. 75-78.

Trmal G. J., and Johnson, D. E., (1993), "Reliability of Gear Fault Detection Using Acoustic Noise Signature", Proceedings of 5th International Congress on Condition Monitoring and Diagnostic Engineering Management (COMADEM '93), pp. 73 - 78.

Trujillo, M. et al., (1994), "Inspection of Micro-Tools at High Rotational Speeds," International Journal of Machine Tools Manufacture, Vol. 34, no. 8, pp. 1059-1077.

Tuteur, F. B., (1988), "Wavelet Transformations in Signal Detection," Proceedings of the International Conference on ASSP, pp. 1435-1438.

Whitehouse, D. J., (1978), "Beta Functions for Surface Typology?", Annals of the CIRP, Vol. 27, pp. 491-497.

Wickerhauser, M. V, (1991), "Adapted Wavelet Analysis From Theory to Software," ISBN 1-56881-041-5, pp. 153-175.

Wickerhauser, M. V., (1992), "Acoustic signal Compression With Wavelet Packets", *Wavelets - A Tutorial in Theory and Applications*, C. K. Chui Ed., Academic Press, pp. 679 - 700.

Wigner, E. P., (1932), "On the Quantum Correction for Thermodynamic Equilibrium," Phys. Rev., Vol. 40, pp. 749 - 759.

Wilhelm, M., Spessert, B., (1992), "Vibration and Noise Excitation in the Timing Gear Train of Diesel Engines," Proceedings of the Institution of Mechanical Engineers, C432/122, pp. 155-172.

Appendix A

Derivation of Air-Particle Acceleration Formula Using a Two-Microphone Method

Euler's equation is used to relate the air-particle acceleration and the pressure gradient between the two closely spaced sound pressure microphones.

$$-\nabla p = \rho_o \left[\frac{\partial \boldsymbol{v}}{\partial t} + (\boldsymbol{v} \cdot \nabla)\boldsymbol{v} \right] \qquad (1)$$

where ∇p is the sound pressure gradient between the two microphones, ρ_o is the standard atmospheric air density and $\boldsymbol{v}$ is the vector quantity of the air-particle velocity. With the assumption of small pertubation, no mean flow and neglecting higher order terms, the above equation can be simplified as:

$$\frac{\partial \boldsymbol{v}}{\partial t} = -\frac{1}{\rho_o} \nabla p . \qquad (2)$$

Subtitute the equation $\boldsymbol{ap} = \frac{d\boldsymbol{v}}{dt}$ into equation (2), to obtain the following equation:

$$\boldsymbol{ap} = -\frac{1}{\rho_o} \nabla p . \qquad (3)$$

where $\boldsymbol{ap}$ is the variable that represent the air-particle acceleration signals.

If the measurement of sound pressure signal propagation is carried out along the probe axis, the above equation can be simplified further to obtain the equation below.

$$\boldsymbol{ap} = -\frac{1}{\rho_o} \frac{dp}{dr} . \qquad (4)$$

Furthermore,

$$\frac{dp}{dr} = \lim_{\Delta r \to 0} \left(\frac{\Delta p}{\Delta r}\right) \approx \frac{(p_2 - p_1)}{\Delta r}, \qquad (5)$$

where p_1 is the pressure signal from the first microphone, p_2 is the pressure signal from the second microphone and Δr is the space between the two sound pressure microphones.

Subtitute equation (5) into equation (4), and include the time variable in the resulting equation to get the final formula for representing the air-particle acceleration signals.

$$\boldsymbol{a}\boldsymbol{p}(t) = \left(\frac{1}{\rho_o \Delta r}\right) [\, p_1(t) - p_2(t)] \qquad (6)$$

Appendix B

Listing of Command and Micro Files

(i)Listings of Command Files

```
---------------------------------------------------------------------------------------
! A command file named inb&k800.dsp to create a start up window
! for importing the frequency domain data from B&K 2032 Analyser.
!
! This file is used to automatically
! import 800 data-points of frequency spectrum  from B&K2032 Analyser.
!
!begin

CONFIG(21,0,16,"EOI") @cr                    !configuring B&K equipment....
OUTPUT(26,"AF 0,800") @cr
ENTERA(26,800) @cr                           !importing the 800 points of data
@MESSAGE("800 DATA POINTS IMPORTED: .....")

! Display message on the screen
!end

---------------------------------------------------------------------------------------

! This is a  command file  named in2048.dsp to create a start up window
! for importing the time domain data from B&K 2032 analyser.
!
! This file is used to automatically
! import 2048 data-points of time domain signals from B&K 2032 analyser
!
!begin

INIT @cr                                     !initialising the ieee card
HELLO @cr                                    !check on operational ieee
@MESSAGE("IEEE card is initiated .....")
! Display message on the screen, and waiting for  RETURN key to be pressed
! Note: This file must be used with the appropriate window in Dadisp's software

@CNTL_HOME                                   ! Go to the first window
CONFIG(21,0,16,"EOI") @cr                    ! Configuring B&K equipment....
OUTPUT(26,"AF 0,1024") @cr                   ! to import data from 0 to 1024 pts.
ENTERA(26,1024) @cr                          ! Importing the data
@MESSAGE("THE FIRST 1024 DATA POINTS IMPORTED: .....")

@CNTL_HOME
```

```
@SP                                  ! Go to the second window
CONFIG(21,0,16,"EOI") @cr            ! Configuring B&K equipment....
OUTPUT(26,"AF 1024,2047") @cr              ! to import data from 1024 to 2047 pts.
ENTERA(26,1024) @cr                        ! Importing the next data
@MESSAGE("2048 DATA POINTS IMPORTED: .....")
                                           ! Display message on the screen
@CNTL_HOME                                 ! Send cursor to the first window
                                           !end
```

(ii) Listing of Macros command

```
svdb setvunits("dB")                 ! Set vertical units to "dB"
svg  setvunits("g")                  ! Set vertical units to "g"
svp  setvunits("Pa")                 ! Set vertical units to "Pa"
shhz sethunits("Hz")                 ! Set horizontal units to "Hz"
sdx8 setdeltax(8)                    ! Set deltax to 8
sdx16 setdeltax(16)                  ! Set deltax to 16
sdx2 setdeltax(2)                    ! Set deltax to 2
sdx4 setdeltax(4)                    ! Set deltax to 4

c clear                              ! To clear a window
ca clearall                          ! To clear all window
ln linecur(-1,1)                     ! To draw line on a worksheet
tx textcur(1,-1,-1,1)                ! To input text with small font

aa load("ascdira.dsp")               ! To write ascii file to A directory
ac load("ascdirc.dsp")               ! To write ascii file to C directory
ra load("rdasci.dsp")                ! To read ascii file from A directory
ld load("loadset.dsp")               ! To load entire dataset into worksheet
tc load("TC.DSP")                    ! To run Turbo C program from Dadisp software
ms menufile("m_stat.men")            ! To load the pop up menu for statistical
                                     ! analysis

sv setvunits("Volts")|sethunits("Hz")|setdeltax(1/8)
sg setvunits("G")|sethunits("Hz")|setdeltax(1/8)
sy setvunits("(x100) Percent")
lp1 label("Prob. Distribution Function")
lp2 label("Prob. Dens. of Beta Function")
yc setvunits("Counts")
x1 sethunits("No Units")
y1 setvunits("Y (Units)")
y2 setvunits("No Units")
```

Appendix C

Listing of C Program to Calculate Statistical Parameters

```
/*****************************************************************/

#include <stdio.h>
#include <stdlib.h>
#include <math.h>

double sum, y, min, max, mean;
double power(double, int);
double Rv, Rp, Rq, Rt;

int i;
char infile[30];
FILE *ifp = infile

main()
{
void  stat1(void), stat2(void), beta(void);
void  prn_info(void);

prn_info();

printf("\n\nEnter the name of the input file: ");
scanf("%s", infile);
ifp = fopen(infile, "r");

stat1();                /* Function to calculate mean, max, min, .... */

ifp = fopen(infile,"r");

stat2();                /* Function to calculate R's and other statistical variables */

beta();                 /* Function to calculate beta func. statistical analysis */

fclose(ifp);

}

/************** Functions Used in the Main Program ************/
void prn_info(void)
{
 printf("\n*********************************************");
 printf("\n*   This program reads the time history data from a file     *");
 printf("\n*   and calculates the statistical parameters for the data    *");
 printf("\n*   such as the mean, max, min, rms, standard deviation,      *");
```

```
 printf("\n*   skew, and kurtosis. In addition, this program will also    *");
 printf("\n*   calculates the statistical parameters of a beta function   *");
 printf("\n*   such as Rv, Rp, Rt, Rq, 'a', 'b', Skew_beta, and           *");
 printf("\n*   kurtosis_beta.   *");
 printf("\n*       ----------------------------------------------------   *");
 printf("\n*                      written by:                             *");
 printf("\n*                   Mohd Jailani Mohd-Nor                      *");
 printf("\n*                   School of Engineering                      *");
 printf("\n*                 Sheffield Hallam University                  *");
 printf("\n*                 Pond Street, Sheffield S1 1WB                *");
 printf("\n*                                                              *");
 printf("\n***************************************************");

}

/*****************************************************************/
void stat1(void)
{

if (fscanf(ifp,"%lf", &y) !=1) {
 printf("\n\nNo data found - bye! ");
 printf("\n\nHit any key to continue...");
 getch();
 exit(1);
 }

min = max = sum = mean = y;
i = 1;

while (fscanf(ifp,"%lf", &y) == 1)  {
 ++i;
 if (y < min)
   min = y;
 else if (y > max)
   max = y;
 sum += y;
 mean = sum  / i;
 }
}

/*****************************************************************/
void stat2(void)
{
double crest, rms, std, kutosi, skew;
double sumstd, sumsqr, sumskew, sumkurt;
int j;

Rv = mean - min;
```

```
 if (Rv < 0.0) Rv = Rv*(-1);

Rp = max - mean;
 if (Rp < 0.0) Rp = Rp*(-1);
Rt = max - min;

sumstd = sumsqr = sumskew = sumkurt = 0.0;
j = 0;

while (fscanf(ifp,"%lf", &y) == 1)  {
  ++j;
  sumsqr = sumsqr + power(y,2);
  sumstd = sumstd + power((y-mean), 2);
  sumskew = sumskew + power((y-mean), 3);
  sumkurt = sumkurt + power((y-mean), 4);

}

rms = sqrt(sumsqr/i);
Rq = std = sqrt(sumstd/i);
skew = (sumskew/i)/(power(std,3));
kutosi = (sumkurt/i)/(power(std,4));
crest = max/rms;

printf("\n%s%5d\n%s%12.3f\n%s%12.3f\n%s%12.3f\n%s%12.3f\n%s%12.3f\n%s%12.
3f\n%s%12.3f\n%s%12.3f",
    "No. of Item:   ",i,
    "Mean:         ",mean,
    "Min:          ",min,
    "Max:          ",max,
    "Std Dev.:      ",std,
    "Skew:         ",skew,
    "Kurtosis:      ",kutosi,
    "RMS:          ",rms,
    "Crest Factor:  ",crest);

printf("\n\n%s%12.3f\n%s%12.3f\n%s%12.3f\n%s%12.3f",
    "Rq:  ",Rq,
    "Rp   ",Rp,
    "Rv:  ",Rv,
    "Rt:  ",Rt);
}

/*****************************************************************/
void beta(void)
{
double  a,b,skb,ktb;
double  skew(double, double), kurtosis(double, double);
```

```
a = Rv*(Rv*Rp - power(Rq,2)) / (Rt*(power(Rq,2)));
b = Rp*(Rv*Rp - power(Rq,2)) / (Rt*(power(Rq,2)));
skb = skew(a,b);
ktb = kurtosis(a,b);
printf("\n\n%s%12.3f\n%s%12.3f\n%s%12.3f\n%s%12.3f",
    "Value of 'a':    ",a,
    "Value of 'b':    ",b,
    "Skew_beta:       ",skb,
    "Kurtosis_beta:   ",ktb);
printf("\n\n Hit any key to continue..... ");
getch();

}

/*****************************************************************/
double skew(double aa, double bb)
{
double ss, s1;
double s2, s3;

        s1 = 2*(bb-aa)/(aa+bb+2);
        s2 = (aa+bb+1)/(aa*bb);
        s3 = sqrt(s2);
        ss = s1*s3;
        return ss;
}

/*****************************************************************/
double kurtosis(double a2, double b2)
{
double kk, k1, k2;

        k1 = 6*((a2-b2)*(a2-b2)*(a2+b2+1)-a2*b2*(a2+b2+2));
        k2 = a2*b2*(a2+b2+3)*(a2+b2+2);
        kk = k1/k2;
        return kk;
}
/*****************************************************************/
double power(double z, int n)
{
double pp = 1.0;
int k;
for (k = 1; k <= n; ++k) {
pp = pp * z;          }

return pp;
}
/*****************************************************************/
```

Appendix D

Listing of C Program to Calculate Features For Neural Network Applications

```
#include  <stdio.h>
#include  <stdlib.h>
#include  <math.h>

double y,inpvec[2049];
double sumtot, sum1,sum2,sum3,sum4,sum5,sum6;
double smfeat1,smfeat2,smfeat3,smfeat4,smfeat5,smfeat6;
int l,m,i,limit = 2048;
char  ans = 'y', infile[30], outfile[30];
FILE *ifp = infile;
FILE *ofp = outfile;

main()
{
void   prn_info(void);

prn_info();
 printf("\n\nEnter the name of the output file:  ");
 scanf("%s", outfile);
 ofp = fopen(outfile, "w");

 for (l=0; l <= 2048; ++l) {
  inpvec[m] = 0.0;
  }  /* bracket for the for loop */

 while(ans == 'y' || ans == 'Y' ){
  printf("\n\nEnter the name of the input file:  ");
  scanf("%s", infile);
  ifp = fopen(infile, "r");

  if (fscanf(ifp,"%lf", &y) !=1) {
   printf("\n\nNo data found - bye! ");
   printf("\n\nHit any key to continue...");
   getch();
   exit(1);
  }  /* close bracket for the if statement */

 sumtot = 0.0;
 for (m=1; m <= 2048; ++m) {
  fscanf(ifp,"%lf", &inpvec[m]);
  if (inpvec[m] < 0.0) {
       inpvec[m] = inpvec[m]*(-1);
```

```
        sumtot += inpvec[m];
        }
    else

    sumtot += inpvec[m];
  }
  printf("\n The total magnitude sum of wavelet coefficients  = %7.3lf\n", sumtot);
  printf("\n\nHit any key to continue...");
  getch();

  sum1 = sum2 = sum3 = sum4 = sum5 = sum6 = 0.0;
  smfeat1 = smfeat2 = smfeat3 = 0.0;
  smfeat4 = smfeat5 = smfeat6 = 0.0;
  for (i=1; i <= 64; ++i) sum1 += inpvec[i];
  for (i=65; i <= 128; ++i) sum2 += inpvec[i];
  for (i=129; i <= 256; ++i) sum3 += inpvec[i];
  for (i=257; i <= 512; ++i) sum4 += inpvec[i];
  for (i=513; i <= 1024; ++i) sum5 += inpvec[i];
  for (i=1025; i <= 2048; ++i) sum6 += inpvec[i];

  smfeat1 = sum1/sumtot;
  smfeat2 = sum2/sumtot;
  smfeat3 = sum3/sumtot;
  smfeat4 = sum4/sumtot;
  smfeat5 = sum5/sumtot;
  smfeat6 = sum6/sumtot;

  fprintf(ofp,"\n%8.2lf%8.2lf%8.2lf%8.2lf%8.2lf%8.2lf\n",
          smfeat1,smfeat2,smfeat3,smfeat4,smfeat5,smfeat6);


printf("\n\n%s%12.3f\n%s%12.3f\n%s%12.3f\n%s%12.3f\n%s%12.3f\n%s%12.3f\n\n",
    "Feature 1:  ",smfeat1,
    "Feature 2:  ",smfeat2,
    "Feature 3:  ",smfeat3,
    "Feature 4:  ",smfeat4,
    "Feature 5:  ",smfeat5,
    "Feature 6:  ",smfeat6);

  fclose(ifp);
  printf("\nDo you want to read another data file? .....\n");
  printf("\nPlease enter Y or N \n");
  ans = getchar();
 }  /* close bracket for the while loop */

fclose(ofp);
return 0;
}  /* close bracket for the main function */
```

```
/*
%%%%%%%%%%%%%%%%%%%%%%%%%%%%%%%%%%%%%%%%%%%%%%%%%%%%%%%%%%%%%%%%%%%%%%%
*/

void prn_info(void)
{
 printf("\n*************************************************************");
 printf("\n*   This program reads an output file from a wavelet         *");
 printf("\n*   transform method and calculates the features needed      *");
 printf("\n*   for neural network applications. Six features are        *");
 printf("\n*   calculated from each file which represents the           *");
 printf("\n*   strength of the wavelet ceofficients at different        *");
 printf("\n*   levels of the wavelet transform method.                  *");
 printf("\n*   ---------------------------------------------------------*");
 printf("\n*                                                            *");
 printf("\n*                written by:                                 *");
 printf("\n*              Jailani Mohd-Nor                              *");
 printf("\n*            School of Engineering                           *");
 printf("\n*           Sheffield Hallam University                      *");
 printf("\n*          Pond street, Sheffield S1 1WB                     *");
 printf("\n*                                                            *");
 printf("\n*                                                            *");
 printf("\n*************************************************************\n");

}
/*
&&&&&&&&&&&&&&&&&&&&&&&&&&&&&&&&&&&&&&&&&&&&&&&&&&&&&&&&&&&&&&&&&&&&&&&
*/
```